VIBRATIONAL RAMAN OPTICAL ACTIVITY OF CARBOHYDRATES

By Alasdair Fraser Bell

A Thesis presented in
partial fulfilment for
the degree of Doctor of Philosophy
in the
Faculty of Science of the
University of Glasgow.

Chemistry Department
October 1994

ProQuest LLC.
789 East Eisenhower Parkway
P.O. Box 1346
Ann Arbor, MI 48106 – 1346

Acknowledgements

Firstly, I would like to thank my supervisor Professor Laurence Barron to whom I am deeply indebted for his patient guidance and encouragement throughout the period of this research.

In addition, I am grateful to Dr. Lutz Hecht for his excellent advice on the finer points of both experimental and theoretical matters.

I would also like to thank Zai Wen, Steven Ford and Gary Wilson for many helpful discussions during the course of this research.

Also I would like to take this opportunity to thank all my family and friends for their support throughout the period of this research.

Finally, I would like to thank the Science and Engineering Research Council for providing the funding for this research.

Contents

Abstract

Vibrational Raman optical activity (ROA), measured as a small differential Raman scattering of right and left circularly polarized incident light from chiral molecules, is emerging as a powerful new chiroptical probe of the solution stereochemistry of biopolymers. Only recently with the advent of CCD detection combined with a backscattering configuration has ROA achieved the sensitivity required for the acquisition of high quality biopolymer spectra. The work presented in this thesis represents the first concerted effort to acquire, assign and interpret the ROA spectra of carbohydrates ranging from monosaccharides to polysaccharides.

The opening chapter of this thesis introduces the concept of optical activity as well as describing some conventional chiroptical techniques and contrasting the two complementary forms of vibrational optical activity: vibrational circular dichroism (VCD) and ROA. The following two chapters then deal with the fundamentals of the theory of ROA and the instrumentation required to measure it. Chapter 4 concentrates on the description of those aspects of carbohydrate stereochemistry that are required to appreciate the subsequent discussion of the ROA spectra. In addition, the main conventional physical methods of establishing carbohydrate conformation are briefly reviewed and the strength and weaknesses of each method noted.

The next two chapters deal exclusively with the ROA of monosaccharides. Chapter 5 consists of a detailed study of D-glucose employing deuterated analogues to assign the ROA signals to particular vibrational coordinates where possible and to relate them to stereochemical features such as anomeric configuration, hydroxymethyl

group conformation and relative disposition of hydroxyl groups around the ring. Chapter 6 extends the work on the monosaccharides to the ketose sugars and the results are combined with earlier ROA studies to clarify some of the old assignments and establish new ones.

In chapter 7 the ROA spectra of seven disaccharides of D-glucose with a range of different linkage types and configurations are presented. It is demonstrated that their ROA spectra contain a number of new signals sensitive to the conformation of the glycosidic link as well as many signals similar to those found in D-glucose itself.

The final chapter concentrates on the ROA spectra of a number of cyclodextrins and polysaccharides as well as a single glycoprotein. The interpretation of these spectra emphasise the influence of the secondary structure through ROA signals that were identified in the preceding chapter as originating in the coordinates of the glycosidic link.

Chapter 1

Introduction

This first chapter will begin with an introduction to the concept of optical activity and a brief survey of some conventional chiroptical techniques before introducing the newer technique of vibrational optical activity, the main subject of this thesis.

1.1 Optical Activity

Natural optical activity refers to the differential response to right and left circularly polarized light from chiral molecules. For an isotropic sample in the absence of any external magnetic or electric fields the determinant of chirality is the non-superposability of the constituent molecules with their mirror images. From a symmetry point of view this means that, although a chiral molecule may posess rotation axes, it must lack all improper rotations i.e. a centre of inversion, reflection planes and rotation-reflection axes. The differential interaction of chiral molecules with right and left circularly polarized light has a subtle dependence on the molecular properties, especially the geometrical aspects, with the result that chiroptical techniques provide highly sensitive methods of probing molecular structure. The importance of such methods in biology is clear as not only are the functions of biological molecules intimately related to their three-dimensional structure but chirality is also built into all the key molecules of life.

The study of optical activity has had a long and enduring history. Since the beginning of the last century it has provided the impetus for researchers in a number of fields to make important discoveries. Early

examples of this include the recognition that molecules must adopt three dimensional shapes,[1] and the connection between electromagnetism and light.[2] In more recent times, the unification of the weak and electromagnetic forces showed that parity violation in the weak force infiltrates into electromagnetic phenomena to some extent leading to new insights into chirality through the small optical rotations of free atoms and the tiny energy differences predicted between enantiomers.[3] Also advances in the past two decades in both the theoretical description[4-7] and experimental acquisition[8-12] of vibrational optical activity have opened up a new realm of optical activity phenomena.

1.2 Electronic Optical Activity

The first measurement of optical activity was performed by Arago in 1811 who noticed colours in sunlight that had passed along the optic axis of a quartz crystal placed between crossed polarizers.[13] It was later established by Biot[14] that this effect originates in a rotation of the plane of polarization of linearly polarized light accompanied by a wavelength dependence of this optical rotation. Biot extended this work to certain organic liquids and aqueous solutions as well as discovering a second form of quartz that rotated the plane of polarization in the opposite sense.[15] The fact that randomly oriented fluids were able to sustain optical rotation led to the conclusion that optical activity originated in the individual molecules; whereas in quartz it was a consequence of the crystal structure.

The discovery of right and left circularly polarized light by Fresnel in 1824 was followed by the realization that linearly polarized light could be decomposed into coherent right and left circularly polarized components[16] as depicted in Figure 1.1(a). Once this discovery had been

appreciated the origin of optical rotation was ascribed to a difference in the propagation velocities, and thus the refractive indices, for right and left circularly polarized light through a chiral medium (Figure 1.1(b)). This difference in the refractive indices is known as the circular birefringence of the medium. The dependence of optical rotation on the wavelength of the incident light is known as optical rotatory dispersion (ORD).[17]

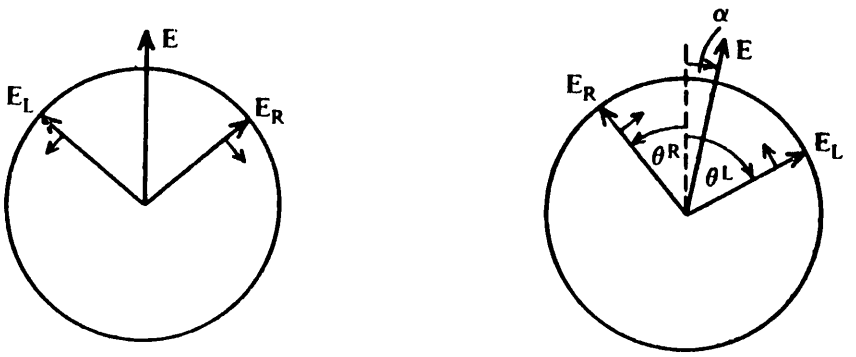

Figure 1.1 (a) The electric field vector of a linearly polarized light beam decomposed into coherent right and left circularly polarized components. (b) The phase difference introduced by the differential refractive indices for right and left circularly polarized light causes a rotation, α, in the plane of polarization.

When the frequency of the incident polarized light coincides with an electronic transition frequency the result is a differential absorption of the right and left circularly polarized states, known as electronic circular dichroism (ECD).[17] This phenomenon was first observed in quartz crystals in 1847 by Haidinger[18] and later in solutions of transition metal complexes by Cotton.[19] The differential absorption leads not only to a difference in the intensity of the right and left circularly polarized light transmitted but also, as shown in Figure 1.2, to an elliptical polarization. Both are a measure of circular dichroism but for technical reasons the intensity difference is easier to measure.

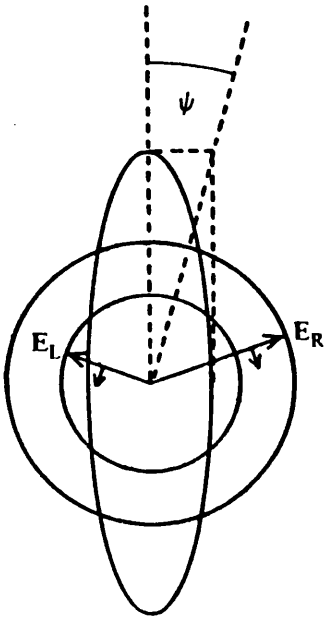

Figure 1.2 Elliptical polarization resolved into coherent right and left circular polarizations of different amplitudes.

The field of optical activity received an enormous boost in the 1950's and 60's when, as a result of leaps in electronic technology, in particular in the development of photomultiplier tubes and electro-optic modulators, it became possible to measure ORD and CD routinely. Until that time the majority of optical activity studies had relied on optical rotation measurements at a single wavelength. Although the two measurements are connected by the Kramers-Kronig transformation,[20] CD has in recent times come to be favoured over ORD as it detects the properties of single electron transitions simplyfing the theoretical analysis considerably. Furthermore, superior instrumentation is commercially available for CD measurements and better resolution can be achieved as the CD bands fall to zero quicker outside the absorption region.

In 1846, Faraday discovered that optical rotation could be induced in an otherwise optically inactive sample by a magnetic field but only in the direction of the magnetic field.[2] The sense of rotation depends on the relative orientations of the magnetic field and the light beam. This became known as the Faraday effect and provided experimental evidence for the connection between electromagnetism and light. A similar effect, known as magnetic circular dichroism, can also be observed when the CD of an achiral sample consisting of otherwise optically inactive molecules is measured in the direction of a magnetic field.

1.3 Vibrational Optical Activity

The conventional chiroptical techniques discussed in the previous section are all based on electronic optical activity. It has long been appreciated that vibrational optical activity measurements could provide a portal into a new realm of chiroptical studies but only in the past two decades has the optical and electronic technology become available to measure the small optical activity inherent in vibrational transitions. The most obvious way to achieve this is to extend circular dichroism in the visible and ultraviolet regions, where it originates in electronic transitions, into the infra-red where molecular vibrations absorb electromagnetic radiation. This gives rise to the technique of vibrational circular dichroism (VCD), which is defined as the small differential absorption of left and right circularly polarized infra-red light by a chiral medium. (Optical rotation in the infra-red has long been known but is unpromising in this context as electronic transitions are mainly responsible and the rotatory power decreases with increasing wavelength.[5]) Perhaps not so obvious is the use of Raman scattered light which is frequency shifted from the visible incident light by an amount corresponding to molecular vibrational transitions. Thus, Raman

optical activity (ROA) can be defined as a small differential Raman scattering of right and left circularly polarized visible light from chiral molecules.

Vibrational optical activity can be thought of as a hybrid of the two established fields of electronic optical activity and vibrational spectroscopy. Both techniques represent powerful methods of probing molecular structure but certain advantages can accrue from their combination. Electronic circular dichroism, although very sensitive to molecular conformation, is restricted to probing chromophores and their immediate molecular environments and cannot be used at all when no chromophores are present. Vibrational optical activity on the other hand is associated with all the 3N-6 normal modes of a chiral molecule. Each of these modes embraces a different part of the molecule which acts as a "vibrational chromophore" for that particular vibrational transition. The mechanism by which vibrational optical activity is generated is different to that of electronic optical activity so it should provide a new perspective on optical activity.[5] Usually, electronic optical activity arises indirectly through the chiral perturbation of an achiral chromophore by its immediate environment; whereas vibrational optical activity probes the chirality directly. From the viewpoint of vibrational spectroscopy, the combination with optical activity provides a sensitivity to absolute configuration plus an increased conformational sensitivity to a method that is already highly structure sensitive. To summarise: vibrational optical activity should provide a new probe of chiral molecules with the resolution of a vibrational spectroscopic technique but with the configurational and conformational sensitivity of a chiroptical technique.

The two distinct techniques of VCD and ROA exhibit a high degree of complementarity. The mechanisms by which the two phenomena are generated are different so each provides an unique perspective on vibrational optical activity.[5,6] ROA can be measured down to ~ 50 cm^{-1} with a right-angle scattering geometry[10] but is more difficult to measure in the C-H stretch region between ~ 2850 and 3050 cm^{-1} as the signals are an order of magnitude weaker than those normally observed and the strong polarization of many of the bands makes the elimination of artifacts difficult. In contrast, VCD was first recorded in the C-H stretch region but can only provide high quality spectra down to about ~ 700 cm^{-1}.[11,12] For ROA the whole wavenumber range can be acquired without any alterations to the instrument;[9,10] however, this is not the case for VCD where changes in the detector material and the optical layout are required to make measurements in different wavelength regions. Another important difference is the wavelength of the incident light. VCD employs infra-red radiation which is more difficult to manipulate than the visible light used in ROA. According to the λ^{-1} dependence of optical activity, VCD signals will be approximately an order of magnitude weaker than those generated by ROA. However, this inherent disadvantage is balanced to some degree by the fact that Raman scattering gives much weaker signals than infra-red absorption. In addition, the sources of artifacts in vibrational optical activity also display a wavelength dependence this time in favour of VCD.[21] Finally, one important consideration for biological studies is the strong infra-red absorption of water, the natural solvent for biological activity, which obscures large sections of the VCD spectrum and so gives ROA a natural advantage because water has few Raman bands.

The first observation of vibrational optical activity in an isotropic sample came in 1973 through the measurement of the ROA of

1-phenylethylamine by Barron, Bogaard and Buckingham using a depolarized right-angle scattering configuration.[22] One year later the first VCD measurement on an isotropic sample, in the C-H stretching region of 2,2,2 trifluoro-1-phenylethanol, was reported.[23] In 1975, Barron demonstrated that even for achiral molecules a magnetic field parallel to the incident light beam could induce a circular intensity difference. The first example was found in the resonance Raman spectrum of ferrocytochrome c.[24] Similarly, an electric field will also induce a circular intensity difference and this effect was first observed in 1980 by Buckingham and Shatwell[25] in the Rayleigh optical activity of gaseous methyl chloride. On symmetry grounds there is no electric analogue of VCD but magnetic VCD is possible and was first reported in 1981 by Keiderling.[26] Since the first observation of ROA a whole range of different scattering geometries have been employed and three distinct experimental strategies have been developed which will be discussed in more detail in the next chapter.

References

1. L. Pasteur, *Ann. Chim.*, **24** (1848) 457.
2. M. Faraday, *Phil. Trans. Roy. Soc.*, **136** (1846) 1.
3. T. D. Lee and C. N. Yang, *Phys. Rev.*, **104** (1956) 254-258.
4. L. D. Barron and A. D. Buckingham, *Mol. Phys.*, **20** (1971) 1111.
5. L. D. Barron in *Molecular Light Scattering and Optical Activity*, Cambridge University Press, Cambridge, 1982.
6. L. Nafie and M. Diem, *Acc. Chem. Res.*, **12** (1979) 296.
7. P. L. Polavarapu, *J. Chem. Phys.*, **94** (1990) 8106-8112.
8. L. D. Barron and L. Hecht in *Advances in Spectroscopy*, Vol 21, *Biomolecular Spectroscopy, Part B*, R. J. H. Clark and R. E. Hester (Eds.), Wiley, Chichester, 1993, 235-266.
9. L. Hecht, L. D. Barron, A. R. Gargaro, Z. Q. Wen and W. Hug, *J. Raman Spectrosc.*, **23** (1992) 401-411.
10. L. Hecht and L. D. Barron, *J. Raman Spectrosc.*, **25** (1994) 443-451.
11. T. A. Keiderling and P. Pancoska in *Advances in Spectroscopy*, Vol. 21, *Biomolecular Spectroscopy, Part B*, R. J. H. Clark and R. E. Hester (Eds.), Wiley, Chichester, 1993, 267-315.
12. T. A. Keiderling in *Practical Fourier Transform Infrared Spectroscopy*, K. Krishnan and J. R. Ferraro (Eds.), Academic Press, San Diego, 1990, 203-284.
13. D. F. J. Arago, *Mém. de l'Inst.*, **12** (1811) 93.
14. J. B. Biot, *Mém de l'Inst.*, **13** (1812) 218.
15. J. B. Biot, *Bull. Soc. Philomath.*, (1815) 190.
16. A. Fresnel, *Bull. Soc. Philomath.*, (1824) 147.
17. P. Crabbe in *Optical Rotatory Dispersion and Circular Dichroism in Organic Chemistry*, G. Snatzke (Ed.), Heyden, London, 1967, 1-14.
18. W. Haidinger, *Ann. Phys.*, **70** (1847) 531.

19. A. Cotton, *Compt. Rend.*, **120** (1895) 989 and 1044.

20. A. Moscowitz, *Adv. Chem. Phys.*, **4** (1962) 67.

21. W. Hug, *Appl. Spectrosc.*, **35** (1981) 115-124.

22. L. D. Barron, M. P. Boogard and A. D. Buckingham, *J. Am. Chem. Soc.*, **95** (1973) 603.

23. G. Holzwarth, C. E. Hsu, H. S. Mosher, J. R. Faulkner and A. Moscowitz, *J. Am. Chem. Soc.*, **96** (1974) 251.

24. L. D. Barron, *Nature*, **57** (1975) 372.

25. A. D. Buckingham and R. A. Shatwell, *Phys. Rev. Letts.*, **45** (1980) 21.

26. T. A. Keiderling, *J. Phys. Chem.*, **75** (1981) 3639.

Chapter 2

Basic ROA Theory

In this section a broad outline of the basic theory of ROA is presented at a level sufficient to follow the interpretation of carbohydrate ROA spectra, the instrumental strategy employed in the measurements and the *ab initio* intensity calculations that appear to be the most promising method of predicting ROA spectra. Details of simple models for ROA generation, such as the bond polarizability or inertial models, along with the theoretical background for magnetic ROA can be found in ref. 1. SI units have been employed throughout and extensive use has been made of cartesian tensor notation.

2.1 The Polarizability and Optical Activity Tensors

The fundamental scattering mechanism responsible for ROA was first formulated by Atkins and Barron in 1969 who based their development on the interference between waves scattered via the polarizability and optical activity tensors of a chiral molecule.[2,3] Later Barron and Buckingham[4] developed a more definitive theory in which the scattered light responsible for Rayleigh and Raman optical activity is generated through the interaction of the electric and magnetic fields of the incident light wave and the electric and magnetic multipole moments of the molecule. The incident light wave sets the multipoles oscillating which in turn produces secondary light waves scattered in all directions. These secondary light waves are treated using classical electrodynamics and the molecules are treated as quantum-mechanical objects. Three kinds of dynamic molecular property tensor are requried to describe this interaction; the electric dipole-electric dipole polarizability tensor $\alpha_{\alpha\beta}$,

the electric dipole-magnetic dipole optical activity tensor $G'_{\alpha\beta}$, and the electric dipole-electric quadrupole optical activity tensor $A_{\alpha\beta\gamma}$, which are derived from time dependent perturbation theory[1] and appear later in the dimensionless circular intensity difference (CID) expressions. The quantum-mechanical expressions for these property tensors are

$$\alpha_{\alpha\beta} = \frac{2}{\hbar} \sum_{j \neq n} (\omega_{jn}/\omega_{jn}^2-\omega^2)\ \mathrm{Re}(\langle n|\mu_\alpha|j\rangle\langle j|\mu_\beta|n\rangle) \qquad \ldots\ 2.1(a)$$

$$G'_{\alpha\beta} = -\frac{2}{\hbar} \sum_{j \neq n} (\omega/\omega_{jn}^2-\omega^2)\ \mathrm{Im}(\langle n|\mu_\alpha|j\rangle\langle j|m_\beta|n\rangle) \qquad \ldots\ 2.1(b)$$

$$A_{\alpha\beta\gamma} = \frac{2}{\hbar} \sum_{j \neq n} (\omega_{jn}/\omega_{jn}^2-\omega^2)\ \mathrm{Re}(\langle n|\mu_\alpha|j\rangle\langle j|\Theta_{\beta\gamma}|n\rangle) \qquad \ldots\ 2.1(c)$$

where $\hbar = h/2\pi$ and $\omega = 2\pi c/\lambda$ is the angular frequency of the incident light and $\omega_{jn} \equiv \omega_j - \omega_n$ is the angular frequency separation between the initial and virtual intermediate states $|n\rangle$ and $|j\rangle$ of the molecule. The electric dipole, magnetic dipole and traceless quadrupole moment operators appearing in equations 2.1(a-c) are defined as

$$\mu_\alpha = \sum_i e_i r_{i\alpha} \qquad \ldots\ 2.2(a)$$

$$m_\alpha = \sum_i (e_i/2m_i)\,\varepsilon_{\alpha\beta\gamma} r_{i\beta} p_{i\gamma} \qquad \ldots\ 2.2(b)$$

$$\Theta_{\alpha\beta} = \frac{1}{2} \sum_i e_i(3r_{i\alpha}r_{i\beta} - r_i^2\delta_{\alpha\beta}) \qquad \ldots\ 2.2(c)$$

where particle i with a position vector $\mathbf{r}_i$ has a charge e_i, mass m_i and momentum $\mathbf{p}_i$. The greek subscripts denote vector or tensor components and can be equal to x, y or z; a repeated greek suffix in a product denotes summation over the three components; $\delta_{\alpha\beta}$ is the unit second rank symmetric tensor, and $\varepsilon_{\alpha\beta\gamma}$ is the unit third rank antisymmetric tensor.

The real induced oscillating multipole moments can be written in terms of the real parts of the electric vector **E**, the associated magnetic vector **B** and the electric field gradient $\nabla_\alpha E_\beta$ of the incident light wave:

$$\mu_\alpha = \alpha_{\alpha\beta} E_\beta + (1/\omega) G'_{\alpha\beta} \dot{B}_\beta + 1/3 A_{\alpha\beta\gamma} \nabla_\beta E_\gamma + \ldots \quad \ldots 2.3(a)$$

$$m_\alpha = -(1/\omega) G'_{\alpha\beta} \dot{E}_\beta + \ldots \quad \ldots 2.3(b)$$

$$\Theta_{\alpha\beta} = A_{\alpha\beta\gamma} E_\gamma + \ldots \quad \ldots 2.3(c)$$

where dotted electromagnetic field components represent time derivatives and the del operator spatial derivatives. Thus, the polarizability tensor $\alpha_{\alpha\beta}$ describes the oscillating electric dipole moments induced by the electric field; the magnetic dipole optical activity tensor $G'_{\alpha\beta}$ describes the oscillating electric and magnetic dipole moments induced by the time derivatives of the magnetic and electric fields, respectively; and the electric quadrupole optical activity tensor $A_{\alpha\beta\gamma}$ describes the oscillating electric dipole moments induced by the electric field gradient and the oscillating electric quadrupole moments induced by the electric field.

2.2 The ROA Observables

Three distinct circular polarization modulation strategies have now been developed for measuring Raman optical activity. In Glasgow, the incident circular polarization (ICP) approach is employed which involves measuring the differential Raman scattered intensities in right and left circularly polarized incident light.[5] In addition, the Syracuse group has recently pioneered the measurement of scattered circular polarization

(SCP) ROA[6-8] and dual circular polarization (DCP) ROA.[9,10] SCP ROA is defined as the difference in intensities associated with right and left circular polarization states in the scattered radiation excited by linearly polarized incident light. DCP ROA is the combination of the ICP and SCP modulation techniques where the incident light is switched between right and left circular and the difference in intensities of the right and left circularly polarized scattered light are measured. There are two ways in which they can be combined: in-phase (DCP_I) where the left circularly polarized component of the scattered intensity generated by the left circularly polarized incident light is subtracted from the right circularly polarized component of the scattered intensity generated by the right circularly polarized incident light, and out-of-phase (DCP_{II}) where the left circularly polarized scattered light excited by the right circularly polarized light is subtracted from the right circularly polarized scattered light excited by the left circularly polarized incident light.

For comparison with theoretical calculations the following dimensionless CID's for the three modulation strategies are employed:

$$\Delta_{ICP} = (I^R - I^L)/(I^R + I^L) \quad \text{... 2.4(a)}$$

$$\Delta_{SCP} = (I_R - I_L)/(I_R + I_L) \quad \text{... 2.4(b)}$$

$$\Delta_{DCP_I} = (I^R_R - I^L_L)/(I^R_R + I^L_L) \quad \text{... 2.4(c)}$$

$$\Delta_{DCP_{II}} = (I^R_L - I^L_R)/(I^R_L + I^L_R) \quad \text{... 2.4(d)}$$

where superscripts represent the circular polarization state of the incident light and subscripts the circular polarization state of the

scattered light. The denominator, which is equivalent to the conventional Raman intensity, serves to normalise the experimental measurement which is useful as it removes the need to consider absolute Raman intensities which may vary from one instrument to another. However, the raw Raman and ROA intensities are generally displayed separately because in certain circumstances coupled normal modes having different Raman intensities often yield conservative ROA couplets. These represent an interesting special case and if the dimensionless CID's were plotted directly the couplet would no longer appear to be conservative.

The ICP approach is preferred over SCP because, although the two are equivalent within the far-from-resonance approximation at transparent frequencies,[6] a dead time of ~ 9 seconds is required to move the quarter-wave plate in the detection system between a position that can measure right and left circularly polarized intensity in the SCP approach.[7,8] Similarly, although in-phase DCP_I measurements should yield a slightly improved signal-to-noise ratio (SNR), theoretical analysis indicates that as well as the dead time problem artifact control is more difficult with this approach.[11]

2.3 The ICP CID Expressions

Light scattering occurs in all directions which means that Rayleigh and Raman optical activity can be measured in a number of different experimental configurations. The most common configuration for conventional Raman measurements is right-angle (90^O) scattering; indeed the first ROA measurements employed this geometry.[12] In right-angle scattering two distinct measurements, polarized and depolarized, can be made depending on whether a linear polaroid analyser is placed in the scattered beam with its axis perpendicular or parallel to the scattering

plane, respectively. In addition to right-angle scattering both backscattering (180^{O}) and forward scattering (0^{O}) are of prime importance for ROA as we shall see later.

Expressions for the dimensionless ICP CID's for all possible scattering geometries can now be obtained by the method outlined below. From classical electrodynamics an expression for the electric field vector radiated by the oscillating electric dipole, magnetic dipole and electric quadrupole moments induced by right and left circularly polarized incident light waves in terms of polarizability and optical activity tensors can be formulated for any scattering direction. The intensity of the scattered light, which is proportional to the squared modulus of the electric field vector, is then used to develop the sum ($I^{R}+I^{L}$) and difference ($I^{R}-I^{L}$) terms of the dimensionless ICP CID's for any scattering angle of interest. An explicit derivation for polarized right-angle scattering can be found in ref. 1.

The expressions found by the method outlined above are simplified by averaging over all possible orientations of the molecule so that they apply to isotropic samples such as neat liquids and solutions. The averaging procedure generates the following tensor component products that are invariant to axis rotation:

$$\alpha = 1/3\alpha_{\alpha\alpha} = 1/3(\alpha_{xx} + \alpha_{yy} + \alpha_{zz}) \qquad \ldots 2.5(a)$$

$$G' = 1/3G'_{\alpha\alpha} = 1/3(G'_{xx} + G'_{yy} + G'_{zz}) \qquad \ldots 2.5(b)$$

$$\begin{aligned}\beta(\alpha)^2 &= 1/2(3\alpha_{\alpha\beta}\alpha_{\alpha\beta} - \alpha_{\alpha\alpha}\alpha_{\beta\beta}) \\ &= 1/2\,[(\alpha_{xx} - \alpha_{yy})^2 + (\alpha_{xx} - \alpha_{zz})^2 + (\alpha_{yy} - \alpha_{zz})^2 \\ &\quad + 6(\alpha_{xy}^2 + \alpha_{xz}^2 + \alpha_{yz}^2)\,] \qquad \ldots 2.5(c)\end{aligned}$$

$$\beta(G')^2 = 1/2(3\alpha_{\alpha\beta}G'_{\alpha\beta} - \alpha_{\alpha\alpha}G'_{\beta\beta})$$
$$= 1/2\{[(\alpha_{xx} - \alpha_{yy})(G'_{xx} - G'_{yy}) + (\alpha_{xx} - \alpha_{zz})(G'_{xx} - G'_{zz})$$
$$+ (\alpha_{yy} - \alpha_{zz})(G'_{yy} - G'_{zz})] + 3[\alpha_{xy}(G'_{xy} + G'_{yx})$$
$$+ \alpha_{xz}(G'_{xz} + G'_{zx}) + \alpha_{yz}(G'_{yz} + G'_{zy})]\} \quad \ldots 2.5(d)$$

$$\beta(A)^2 = 1/2\,\omega\alpha_{\alpha\beta}\varepsilon_{\alpha\gamma\delta}A_{\gamma\delta\beta}$$
$$= 1/2\;\omega[(\alpha_{yy} - \alpha_{xx})A_{zxy} + (\alpha_{xx} - \alpha_{zz})A_{yzx}$$
$$+ (\alpha_{zz} - \alpha_{yy})A_{xyz} + \alpha_{xy}(A_{yyz} - A_{zyy} + A_{zxx} - A_{xzz})$$
$$+ \alpha_{xz}(A_{yzz} - A_{zzy} + A_{xxy} - A_{yxx})$$
$$+ \alpha_{yz}(A_{zzx} - A_{xzz} + A_{xyy} - A_{yxx}) \quad \ldots 2.5(e)$$

where α and G' are the isotropic invariants and $\beta(\alpha)^2$, $\beta(G')^2$ and $\beta(A)^2$ are the anisotropic invariants. (Note that there is no isotropic tensor invariant for $\varepsilon_{\alpha\gamma\delta}A_{\gamma\delta\beta}$ because it is traceless). Thus, the following dimensionless ICP CID observables are generated in terms of the molecular polarizability and optical activity tensors

$$\Delta(0^O) = \frac{4[45\alpha G' + \beta(G')^2 - \beta(A)^2]}{c[45\alpha^2 + 7\beta(\alpha)^2]} \quad \ldots 2.6(a)$$

$$\Delta(180^O) = \frac{48[\beta(G')^2 + 1/3\beta(A)^2]}{2c[45\alpha^2 + 7\beta(\alpha)^2]} \quad \ldots 2.6(b)$$

$$\Delta_x(90^O) = \frac{2[45\alpha G' + 7\beta(G')^2 + \beta(A)^2]}{c[45\alpha^2 + 7\beta(\alpha)^2]} \quad \ldots 2.6(c)$$

$$\Delta_z(90^O) = \frac{12[\beta(G') - 1/3\beta(A)^2]}{6c\beta(\alpha)^2} \quad \ldots 2.6(d)$$

where x and z correspond to polarized and depolarized right-angle scattering configurations, respectively. Note that common factors in the numerators and denominators have not been cancelled so that the relative sums and differences can be compared directly. It is clear from inspection of the numerators in equations 2.6(a-d) that the ROA

intensity is generated through the terms in $\alpha G'$, $\beta(G')^2$ and $\beta(A)^2$. These terms have a sign dependence on the sense of circular polarization and represent the interference between light scattered via the polarizability and the two optical activity tensors. Other interference terms, such as G'^2 and A^2 also contribute but do not show a sign dependence on the sense of circular polarization and are in any case expected to be approximately three orders of magnitude weaker.

The CID expressions developed in equation 2.6(a-d) deal only with the special case of Rayleigh scattering, i.e. when the initial and final vibrational states are the same. For Raman scattering the initial and final vibrational states are different, so the following *transition* polarizability and optical activity tensors must be invoked to describe vibrational Raman optical activity.

$$\alpha_{\alpha\beta} \rightarrow \langle m_v|\alpha_{\alpha\beta}(Q)|n_v\rangle \qquad \ldots 2.7(a)$$

$$G'_{\alpha\beta} \rightarrow \langle m_v|G'_{\alpha\beta}(Q)|n_v\rangle \qquad \ldots 2.7(b)$$

$$A_{\alpha\beta\gamma} \rightarrow \langle m_v|A_{\alpha\beta\gamma}(Q)|n_v\rangle \qquad \ldots 2.7(c)$$

where $|n_v\rangle$ and $|m_v\rangle$ represent the initial and final vibrational states and $\alpha_{\alpha\beta}(Q)$, $G'_{\alpha\beta}(Q)$ and $A_{\alpha\beta\gamma}(Q)$ are the effective polarizability and optical activity tensors that depend on the normal vibrational coordinate Q. Developing these transition tensors using the Placzek approximation[1] yields the following expression

$$\langle m_v|\alpha_{\alpha\beta}(Q)|n_v\rangle = (\alpha_{\alpha\beta})_0\delta_{m_v n_v} + \sum \left(\frac{\partial\alpha_{\alpha\beta}}{\partial Q_p}\right)_0\langle m_v|Q_p|n_v\rangle \qquad \ldots 2.8$$

The first term describes Rayleigh scattering and the second term represents the vibrational Raman scattering. The subscript zero indicates that the function is taken at the equilibrium nuclear configuration. Applying this expression to a fundamental transition 1←0 the interference terms appearing in the dimensionless CID's can now be written as

$$\langle 0|\alpha_{\alpha\beta}|1_p\rangle\langle 1_p|\alpha_{\alpha\beta}|0\rangle = \left(\frac{\hbar}{2\omega_p}\right)\left(\frac{\partial\alpha_{\alpha\beta}}{\partial Q_p}\right)_0\left(\frac{\partial\alpha_{\alpha\beta}}{\partial Q_p}\right)_0 \quad \ldots 2.9(a)$$

$$\langle 0|\alpha_{\alpha\beta}|1_p\rangle\langle 1_p|G'_{\alpha\beta}|0\rangle = \left(\frac{\hbar}{2\omega_p}\right)\left(\frac{\partial\alpha_{\alpha\beta}}{\partial Q_p}\right)_0\left(\frac{\partial G'_{\alpha\beta}}{\partial Q_p}\right)_0 \quad \ldots 2.9(b)$$

$$\langle 0|\alpha_{\alpha\beta}|1_p\rangle\langle 1_p|\varepsilon_{\alpha\gamma\delta}A_{\gamma\delta\beta}|0\rangle = \left(\frac{\hbar}{2\omega_p}\right)\left(\frac{\partial\alpha_{\alpha\beta}}{\partial Q_p}\right)_0\varepsilon_{\alpha\gamma\delta}\left(\frac{\partial A_{\gamma\delta\beta}}{\partial Q_p}\right)_0 \quad \ldots 2.9(c)$$

From basic symmetry arguments Rayleigh optical activity requires that the same components of $\alpha_{\alpha\beta}$, $G'_{\alpha\beta}$ and $A_{\alpha\beta\gamma}$ must span the totally symmetric representation. Similarly, for vibrational Raman optical activity the components must span the same representation as the normal coordinate of vibration Q. This can only happen in the chiral point groups in which polar and axial tensors of the same rank, such as $\alpha_{\alpha\beta}$ and $G'_{\alpha\beta}$, transform in the same way. Furthermore, the second rank axial tensor $\varepsilon_{\alpha\beta\gamma}A_{\gamma\delta\beta}$ that combines with $\alpha_{\alpha\beta}$ has the same transformation properties as $G'_{\alpha\beta}$. Thus, all the Raman active bands in a chiral molecule could exhibit ROA.

2.4 ICP ROA in Backscattering

The determination of the optimum scattering geometry for ROA measurements of biological samples is based on the two group model of ROA generation. The basic premise of this model is that two waves scattered independently from two groups held in a chiral arrangement

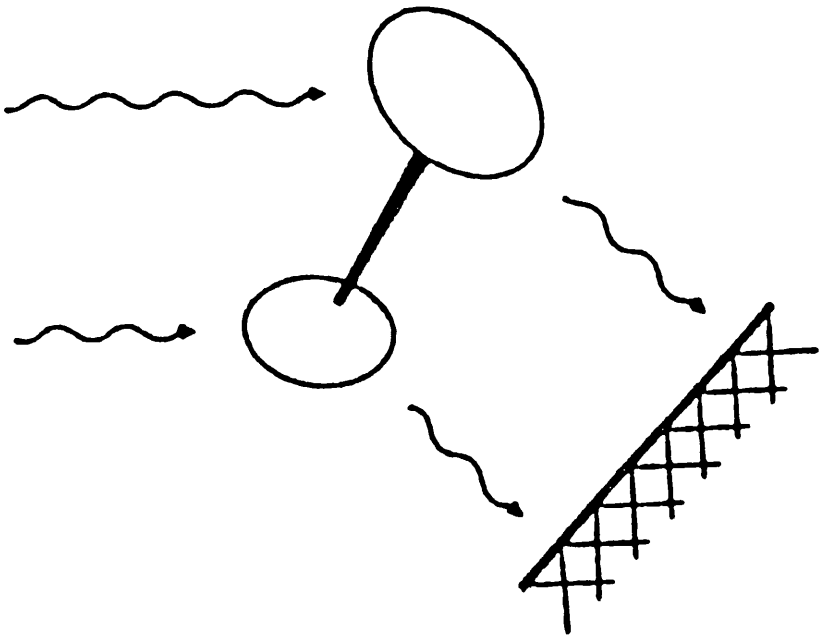

Figure 2.1 The photon scattering picture of the generation of Rayleigh and Raman optical activity by a simple chiral two-group model.

as depicted in Figure 2.1 is sufficient to generate ROA.[1] If axial bond symmetry is assumed the following useful simplifications can be developed

$$\alpha G' = 0 \qquad \ldots 2.10(a)$$

$$\beta(G')^2 = \beta(A)^2 = -3/4\,\omega\varepsilon_{\beta\gamma\delta}R_{21_\gamma}\alpha_{1_{\alpha\beta}}\alpha_{2_{\alpha\beta}} \qquad \ldots 2.10(b)$$

where $\alpha_{1_{\alpha\beta}}$ and $\alpha_{2_{\alpha\beta}}$ are the polarizability tensors referred to the local origins on group 1 and 2, respectively, and $\mathbf{R}_{21}$ is the vector from the local origin of group 1 to that on group 2. These results mean that within the two group approximation the electric dipole-magnetic dipole isotropic contribution, $\alpha G'$, vanishes and the electric dipole-magnetic dipole and electric dipole-electric quadrupole anisotropic contributions are equal. The expression in equation 2.10(b) expresses the dependence

of the ROA on the molecular geometry in concise tensor notation. Using these results the dimensionless CID expressions reduce to

$$\Delta(0^{o}) = 0 \qquad \ldots 2.11(a)$$

$$\Delta(180^{o}) = \frac{64\beta(G')^{2}}{2c[45\alpha^{2} + 7\beta(\alpha)^{2}]} \qquad \ldots 2.11(b)$$

$$\Delta_{x}(90^{o}) = \frac{16\beta(G')^{2}}{c[45\alpha^{2} + 7\beta(\alpha)^{2}]} \qquad \ldots 2.11(c)$$

$$\Delta_{z}(90^{o}) = \frac{8\beta(G')^{2}}{6c\beta(\alpha)^{2}} \qquad \ldots 2.11(d)$$

Probably the most striking prediction is the disappearance of ROA in the forward scattering direction. It was found that when this prediction was tested on trans-pinane, a molecule which is thought to provide a good approximation to axial bond symmetry, almost all the ROA signals had either vanished or were extremely weak.[13] From a closer inspection of equations 2.11(a-d) it is evident that a direct comparison can be made between polarized right-angle and backscattering Raman and ROA measurements. In the backscattering geometry there is four-fold increase in the ROA intensity and a two-fold increase in the Raman intensity over the corresponding polarized right-angle intensities. Combining these two results leads to the conclusion that implementing a backscattering geometry can result in an eight-fold reduction in the time taken to achieve a given SNR. Furthermore, the fact that the overall dimensionless CID is two times larger in backscattering means that the ROA receives an extra boost which is crucial when studying biological samples where the high backgrounds encountered can mean that ROA signals remain buried in the noise.[14,15] In addition to this obvious advantage, backscattered ROA is also easier to deal with theoretically as it contains no isotropic contribution, $\alpha G'$.

2.5 Ab initio ROA Calculations

Currently the most promising method for interpreting ROA spectra appears to be from *ab initio* ROA intensity calculations.[16] Such calculations take advantage of advances in quantum-mechanical methods for evaluating the polarizability and optical activity tensors that appear in the dimensionless CID expressions.[17] The calculations rely on the Placzek approximation, given above, to provide a description of the interference terms found in the CID expressions in terms of the derivatives of the polarizability and optical activity tensors with respect to the normal coordinate of vibration at the equilibrium nuclear configuration. Also, the $\omega_{jn}^2 - \omega^2$ term found in equations 2.1(a-c) for the polarizability and optical activity tensors is set to ω^2 where ω_{jn} is the transition frequency and ω is the excitation frequency. For transparent Raman scattering this is a reasonable approximation as the exciting frequency is much greater than the frequency shifts induced by the vibrational transitions of the molecule.

The required derivatives are calculated numerically at their static limits and at geometries displaced 0.005Å along each atomic coordinate. These calculations are carried out using the CADPAC program.[18] In principle, the polarizability and electric dipole-electric quadrupole optical activity tensors can be calculated analytically but no method has been developed for doing the same with the electric dipole-magnetic dipole optical activity tensor. Thus, because the calculations are done numerically, limits are placed on both the size of the molecule and the basis set. Furthermore, before the ROA can be calculated the starting geometry must also be calculated by *ab initio* methods.

The accuracy in calculating both the sign and intensity of ROA signals from *ab initio* methods has been tested over the past couple of years against experimental results on a number of relatively simple chiral model compounds. These include three membered rings containing heteroatoms such as methyl oxirane, tartaric acid, L-alanine, methylcyclopentanone and methylcyclohexanone.[19-23] The results obtained so far have been encouraging although a scaling factor usually has to be introduced to match the calculated and experimental frequencies.[16] The closest agreement is usually found for normal modes involving the vibrational coordinates most directly sampling the chirality, such as C-C or C-O stretching coordinates of the backbone of molecules, found between ~ 500 and 1100 cm^{-1}. Although at the present level of development wide variations from the predicted intensities are sometimes observed, the matching of predicted signs to those observed provides an excellent method of assigning absolute configuration. Furthermore, *ab initio* calculations automatically yield data on the relative contributions of the three interference terms. This information can be isolated experimentally but requires at least three different experiments with linearly independent ROA intensities. Finally, the sensitivity of ROA also provides a more stringent test of the force field than conventional vibrational spectroscopy.

No *ab initio* ROA intensity calculations have yet been performed on a carbohydrate so it is difficult to assess the impact they will have in this area. However, calculations on L-alanine provided an important first step in the understanding of the ROA spectra of the amino-acids and peptides[21] and similar calculations on a standard monosaccharide, such as D-glucose, may prove equally as useful. The study of complete disaccharides is probably a long way off. As shown later a number of ROA signals in di- and polysaccharides are assigned to the glycosidic

link and interesting results may be forthcoming from *ab initio* calculations of disaccharide fragments containing the linkage atoms.

References

1. L. D. Barron in *Molecular Light Scattering and Optical Activity,* Cambridge University Press, Cambridge, 1982.
2. P. W. Atkins and L. D. Barron, *Molec. Phys.,* **16** (1969) 453.
3. L. D. Barron, Doctoral Thesis, Oxford University, 1969.
4. L. D. Barron and A. D. Buckingham, *Molec. Phys.,* **20** (1971) 1111.
5. L. Hecht, L. D. Barron, A. R. Gargaro, Z. Q. Wen and W. Hug, *J. Raman Spectrosc.,* **23** (1992) 401-411.
6. K. M. Spencer, T. B. Freedman and L. A. Nafie, *Chem. Phys. Letts.,* **149** (1988) 367-374.
7. L. Hecht, D. Che and L. A. Nafie, *Appl. Spectrosc.,* **45** (1991) 18-25.
8. L. Hecht, D. Che and L. A. Nafie, *J. Phys. Chem.,* **96** (1992) 4266-4270.
9. L. A. Nafie and T. B. Freedman, *Chem. Phys. Letts.,* **154** (1989) 260-266.
10. D. Che, L. Hecht and L. A. Nafie, *Chem. Phys. Letts.,* **180** (1991) 182.
11. L. Hecht and L. D. Barron, *Appl. Spectrosc.,* **44** (1990) 483.
12. L. D. Barron, M. P. Boogard and A. D. Buckingham, *J. Am. Chem. Soc.,* **95** (1973) 603.
13. L. D. Barron, L. Hecht, A. R. Gargaro and W. Hug, *J. Raman Spectrosc.,* **21** (1990) 375-379.
14. L. Hecht, L. D. Barron and W. Hug, *Chem. Phys. Letts.,* **158** (1989) 341-344.
15. L. D. Barron, L. Hecht, W. Hug, and M. J. MacIntosh, *J. Am. Chem. Soc.,* **111** (1989) 8731.
16. P. L. Polavarapu, *J. Phys. Chem.,* **94** (1990) 8106-8112.
17. R. D. Amos, *Chem. Phys. Letts.,* **87** (1982) 23.

18. R. D. Amos and J. E. Rice, *The Cambridge Analytical Derivatives Package*, Issue 4.0, Cambridge, 1987.

19. P. K. Bose, P. L. Polavarapu, L. D. Barron and L. Hecht, *J. Phys. Chem.*, **94** (1990) 1734-1740.

20. L. D. Barron, A. R. Gargaro, L. Hecht, P. L. Polavarapu and H. Sugeta, *Spectrochim. Acta.*, **48A** (1992) 1051-1066.

21. L. D. Barron, A. R. Gargaro, L. Hecht and P. L. Polavarapu, *Spectrochim. Acta.*, **47A** (1991) 1001-1016.

22. P. L. Polavarapu, P. K. Bose, L. Hecht and L. D. Barron, *J. Phys. Chem.*, **97** (1993) 11211-11215.

23. P. L. Polavarapu, T. M. Black, L. D. Barron and L. Hecht, *J. Am. Chem. Soc.*, **115** (1993) 7736-7742.

Chapter 3

Instrumentation

In this chapter the basic design and performance of the backscattering ICP ROA instrument GUROAS1 (Glasgow University ROA Spectrometer No. 1) is described on which all the carbohydrate ROA measurements discussed later have been performed. The experimental set-up is based on the "mirror with a hole" idea commonly employed for conventional Raman measurements with this scattering geometry.[1] The ICP ROA approach is used for the reasons discussed in chapter 2 and polarization modulation spectroscopy is employed to overcome short-term instabilities until an acceptable signal-to-noise ratio (SNR) is achieved. The most important components are the electro-optic modulator, the thick Lyot depolarizer, the holographic notch filter, the fast single grating spectrometer and the cooled back-thinned charge coupled device (CCD) detector. The layout of this instrument is sketched in Figure 3.1.

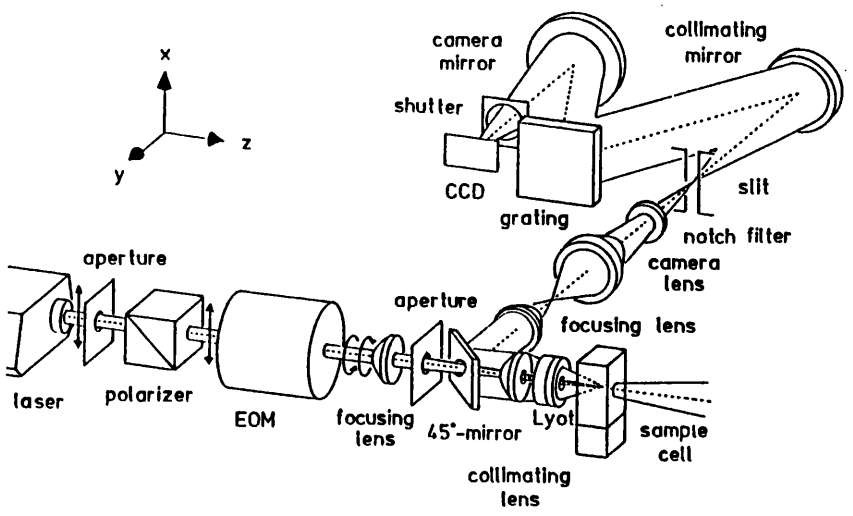

Figure 3.1 The optical layout of the backscattering Glasgow University ICP ROA spectrometer (adapted from ref. 1).

3.1 The Optical Design

The continuous wave, single line argon ion laser employed generates a coherent beam of up to 2 W of power at 514.5 nm. The choice of excitation wavelength is important as a balance must be struck between the λ^{-4} dependence of the Raman intensity and the increased fluorescence encountered at lower wavelength, especially in biological samples. The already good linear polarization of the laser beam is improved with a calcite Glan Taylor type prism polarizer,[2] positioned at the laser head which is anti-reflection coated to ensure at least 95% transmittance at 514.5 nm.

For successful ICP ROA measurements the accurate modulation between right and left circular polarization states is crucial.[3] The conversion from linear to circular polarization is achieved using an electro-optic modulator (EOM). The birefringence required to produce circularly polarized light is induced in the EOM by a high voltage applied across a uniaxial crystal. By reversing the direction of the electric field applied to the crystal it is possible to produce both right and left circularly polarized light. The EOM employed in Glasgow is based on a potassium dideuterium phosphate crystal and is temperature stabilised at 25 ± 0.1^{0}C to eliminate birefringence drifts. The voltage across the crystal is supplied by a high voltage linear differential amplifier which generates a precise square-wave causing the EOM to switch accurately between the right and left circular states. The dead time introduced by this switching is on the millisecond timescale.

The circularly polarized light is focussed into the sample using a lens which produces a cylindrical laser focal region ~ 14.7 mm in length and ~ 49 μm in diameter. The sample cell itself is placed in a 6×6×12.5

mm quartz microfluorescence cell which has a maximum capacity of ~ 300 μl. The mounting on which the cell is placed has controls which allow accurate variations to be made to the vertical and horizontal position through which the laser beam enters the sample and also the angle of tilt of the cell relative to the laser beam. These controls are necessary for the precise alignment of the cell so that reflections from the cell surfaces return directly back down the central axis and not into the collection optics. The backscattered Raman light is effectively depolarized by a thick Lyot depolarizer consisting of two calcite plates oriented with their optical axes at 45^{o} to one another.[2] The Lyot depolarizer is mounted to allow rotation to locate the optimum depolarization position. The backscattered light then passes through a collimating lens and is reflected at right angles by an aluminium mirror tilted at 45^{o}. The Lyot depolarizer, collimating lens and aluminium mirror are housed in a mounting block which must be precisely aligned. The three components within the block are anti-reflection coated and have holes drilled in their centres to allow the incident light to reach the sample.

The collimated and reflected light leaves the block perpendicular to the incident beam through a focussing lens. A second camera lens picks up light from the focal point produced by the first focussing lens and focusses the light through the entrance slit of the spectrograph magnifying the image by a factor of approximately two to match the f-number of the spectrograph. Positioned in front of the entrance slit is a holographic notch filter without which stray light from the Rayleigh line, which has a degrading effect on the SNR and can introduce sloping baselines into the ROA spectrum, would enter the spectrograph.[4-6] Holographic notch filters are constructed by recording the interference pattern formed between two mutually coherent laser

beams within a gelatin emulsion. The recorded image of the interference pattern is then chemically converted into a holographic diffraction grating. Only light of the wavelength fulfilling the Bragg condition, in this case the Rayleigh light at 514.5 nm, will be diffracted by the grating. The transmission of these filters is greater than 80% outside the blocked region and is nearly constant throughout the wavelength range studied, as shown in Figure 3.2 for the latest generation of filter, so no intensity calibration is necessary. The other main features of holographic notch filters include the narrow bandwidth and extremely sharp edges of the blocked region, which allow measurement close to the Rayleigh line, and their high optical density of greater than 6 in the blocked region, which almost completely supresses the Rayleigh line.[6]

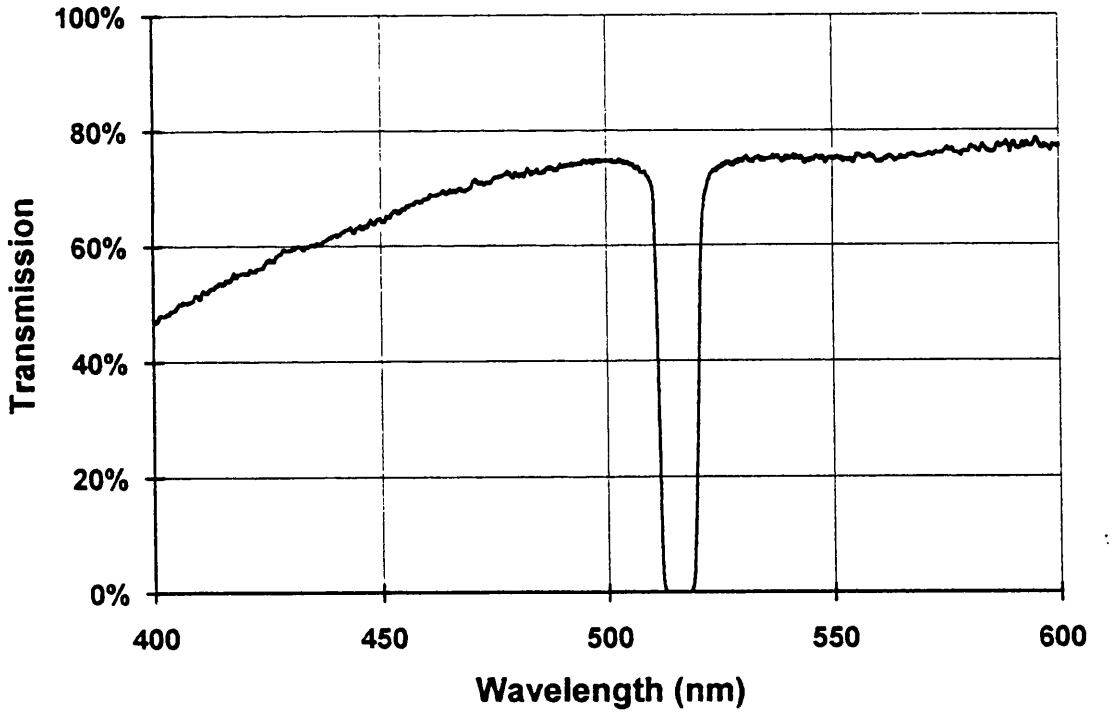

Figure 3.2 Plot of transmission against wavelength for the 'super notch plus' holographic filter.

The excellent stray light rejection provided by holographic notch filters make it possible to employ a single grating spectrograph with its

associated high throughput instead of using slow double or triple grating spectrographs previously required.[7] Indeed, earlier ROA instruments incorporating single grating spectrographs sacrificed low wavenumber capability for high throughput.[8,9] In Glasgow, a 245.671 mm focal length f/4.1 single grating spectrograph is used. The scattered light enters through an adjustable slit and is collimated and deflected at an angle of 20^{o} onto a plane reflecting holographic grating. This grating has 1200 grooves per mm and disperses the scattered light onto a camera mirror which focusses the dispersed light into the detection system. The reflective efficiency of the grating is ~ 60% at the 514.5 nm.

The detection system is based upon a cooled, back-thinned back-illuminated CCD detector.[10-12] The use of a CCD detector represents an improvement on earlier multichannel detectors, such as intensified diode arrays, for a number of reasons. A CCD detector is based upon a two-dimensional array that measures both the intensity against wavelength and against slit height; whereas earlier multichannel detectors only measure intensity against wavelength since they only have a single line of elements. This advantage is realized by the process of binning. Binning simply involves selectively combining all the detector elements in a given row into a single charge packet and works because although the signal is proportional to the number of pixels in a row the noise is only proportional to the square root of that number.[10] Furthermore, the CCD camera has extremely low readout noise and, unlike other detectors, requires no intensification stage which degrades the SNR. By back-thinning the CCD chip and utilizing back-illumination a quantum efficiency of ~ 80% can be achieved at 514.5 nm compared with only 20% of conventional CCD's, as depicted in Figure 3.3, and over the wavelength measured in an ROA experiment this value is almost constant so no intensity calibration is required.[10-12] The CCD is cooled

to 200 K reducing the thermally generated dark current to only 0.14 electrons per second making this source of noise almost negligible. To maximise the spectral coverage the CCD is oriented with its long axis parallel to the direction of dispersion of the spectrometer. Thus, for the CCD camera of 385 by 578 pixels used in Glasgow a spectral coverage of ~ 1150 cm^{-1} is possible for a 1200 grooves per mm grating.

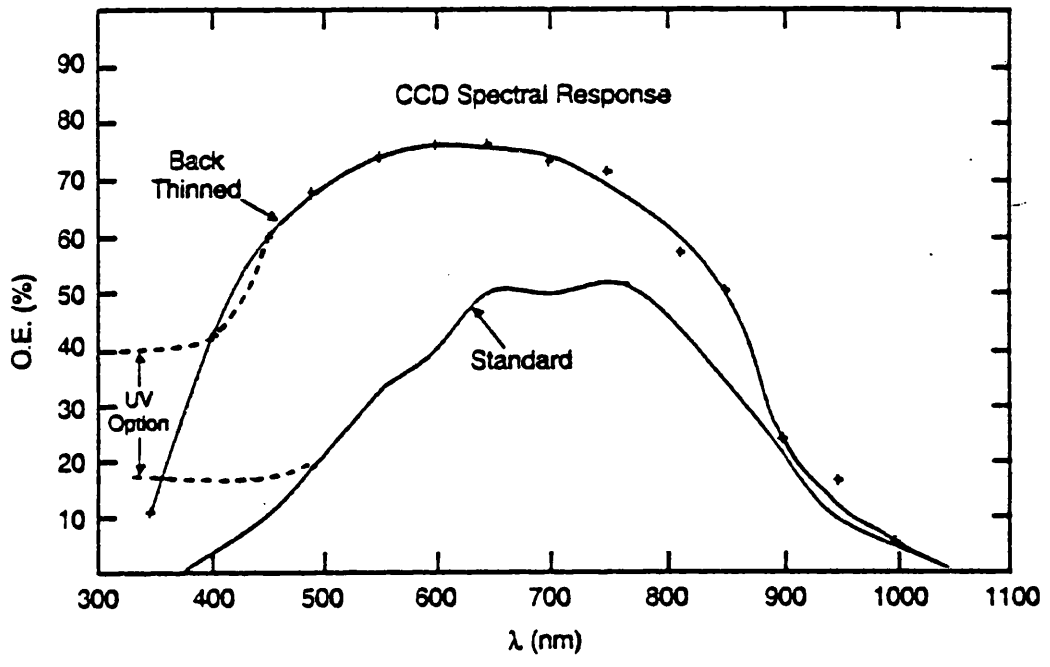

Figure 3.3 Typical response curves for standard and back-thinned CCD detectors

3.2 Computer Control and Spectral Acquistion

The whole process of spectral acquisition is driven by a high speed Dell personal computer. It controls the synchronisation of the EOM and CCD detector and is linked to a high resolution monitor and laser printer. A customised version of Lab Calc is used for data acquistion and any spectral manipulations.

The sequence of acquisition begins with the resetting of the EOM and the amplifier. A signal is then sent from the computer to the modulator telling it to produce right circularly polarized light. At the same instant the CCD camera chip is cleared and the shutter opened to permit the detection of the right circularly polarized scattered light. The shutter remains open for a predetermined exposure time before the rows of data are vertically binned. This exposure time is chosen so that the chip is nearly saturated to maximise the SNR obtained. The data from the CCD are sent to the computer and stored in the memory in a specially created file for the right circularly polarized Raman spectra. The chip is cleared again and a signal sent to the modulator initiating a switch to left circular polarization. Again after the preset exposure time has elapsed the shutter closes and the data are binned and transferred this time to a specially created file for left circularly polarized Raman spectra in the computer memory. The left and right circularly polarized Raman spectra are then subtracted from one another, stored in the memory and the difference displayed on the computer screen. This sequence is repeated with each additional acquisition pair being added to those previously stored in the memory. The ROA spectrum appears on screen throughout the spectral acquisition so that small offset adjustments can be made to the amplifier to correct for any inaccuracies in the incident polarization states.

3.3 Artifact Control

Since ROA is such a weak phenomenon, typically three to four orders of magnitude smaller than the associated Raman effect which is itself weak, its measurement tends to be prone to artifacts.[3] Artifacts are spurious scattering differences for right and left circularly polarized light that are not due to the chirality of the sample, usually taking the

form of sharp S-shaped signals on strongly polarized Raman bands in the ROA spectrum. The elimination or reduction of artifacts is one of the main goals for ROA instrumentation. Indeed, it was only after the origin of the major sources of artifacts were understood in terms of the polarization dependence of the molecular polarizability contributions, which revealed that strongly polarized Raman bands were the most susceptible to artifacts, that the first genuine ROA measurement was made.[13]

The main sources of artifact generation are the deviation of the polarization of the incident light from precisely right and left circularity which introduces an elliptical polarization and the differences between the degree of ellipticity introduced into the two circular states.[3,14] These problems arise mainly as a result of incorrect alignment of the EOM, residual linear birefringence in the optical elements especially the modulator and the refraction that occurs at all angled surfaces. The EOM as discussed in section 3.1 is both temperature stabilised and supplied with an extremely stable and accurate voltage in an attempt to improve the degree of circular polarization. The problem of residual linear birefringence, the retardation of one linearly polarized component with respect to its orthogonal component,[2] is reduced by employing high quality strain-free quartz throughout the optical train, except for the Lyot depolarizer and the collection lens.

A number of other mechanisms for the generation of artifacts have also been proposed.[3,14] Backreflected incident light from the walls of the sample and other optical elements can travel back into the laser cavity causing a deterioration in the degree of linear polarization of the laser light. This problem is combatted by coating all the optical elements except the samples cell with anti-reflection coatings and

placing two aperatures in the optical train. Another problem is that an optically active sample will rotate the plane of polarization and subsequently generate artifacts although this problem can be reduced by using a smaller pathlength sample cell. Dust particles in the sample can introduce baseline offsets or slopes into the ROA spectrum due to excessive stray light. For backscattering ROA artifacts are greatly reduced compared to right-angle scattering as the cone of collection displays rotational symmetry cancelling out some of the sources of artifact generation.[15]

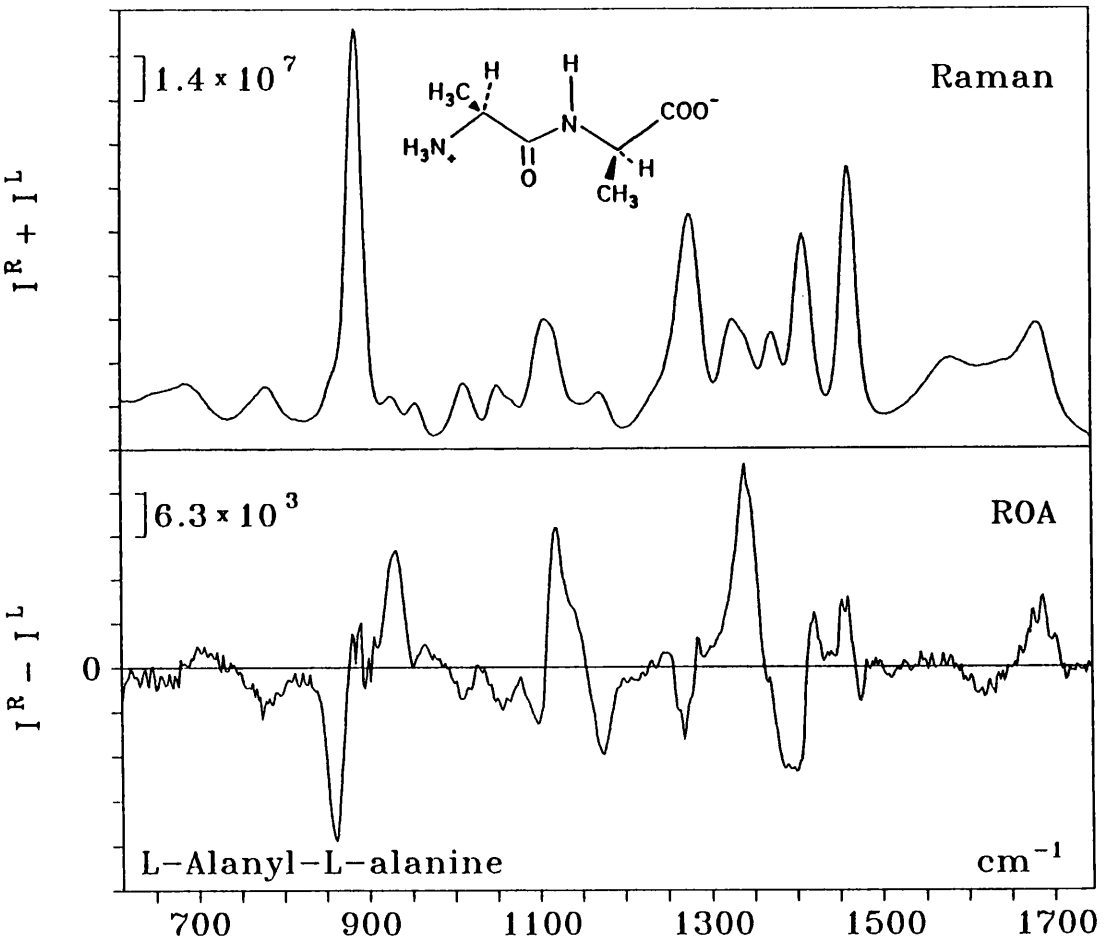

Figure 3.4 Backscattered Raman ($I^R + I^L$) and ROA ($I^R - I^L$) spectra of L-alanyl-L-alanine in water.

Despite the precautions mentioned above the backscattered cone of light will still contain some linear contaminants and without the Lyot depolarizer and collimating lens the ROA spectrum would be swamped with artifacts. The Lyot depolarizer is mounted on a rotating block and the optimum depolarization position is found by testing against a strongly polarized band at ~ 886 cm^{-1} in L-alanyl-L-alanine until the artifact is appropriately suppressed as shown in Figure 3.4. Certain depolarizer positions may introduce slopes and baseline offsets so care must be taken to avoid this.

3.5 Calibration

The spectrometer employed in Glasgow scans through the spectrum in units of wavelength (nm) but Raman and ROA spectra are conventionally presented in terms of wavenumber shifts (cm^{-1}) from the exciting wavelength. Thus, the following expression is required to convert between the two units and calibrate the instrument.

$$\Delta\tilde{\nu} = 10^7\left[\frac{1}{\lambda_0} - \frac{1}{(c-a)d + \lambda_c}\right]$$

where $\Delta\tilde{\nu}$ is the wavenumber shift of the Raman band from the exciting line. The first term in the bracket converts λ_0, the exciting wavelength, from nanometers into wavenumbers. The second term converts λ_c, the wavelength setting of the spectrograph, into wavenumbers and is combined with a correction term, (c-a)d, which is used to calibrate the instrument. In this correction term c is the pixel on the CCD camera that corresponds to the wavelength setting on the spectrograph, a is the actual pixel that is measuring light of that wavelength and d is the dispersion across the chip in nm per pixel. The dispersion is calculated by measuring the number of pixels between two

widely spaced bands occurring at known wavenumber. The actual calibration is achieved, with α-pinene as a standard, by making small variations to d, c and λ_c until good agreement is obtained with the reference spectrum. This process is repeated for a number of different spectrograph settings and provides an accuracy of ±2 cm^{-1} for the peak wavenumber of Raman bands.

3.6 Instrument Performance

There are five main criteria that determine the performance of a ROA instrument. These are the sensitivity, the speed of acquisition, the spectral resolution, the wavenumber range covered and finally the control of artifacts already discussed in section 3.4. It is possible with the current experimental set-up to detect signals with Δ_{ICP}-values as small as ~ 10^{-5}. This degree of sensitivity is certainly adequate for studying carbohydrates which typically give rise to signals with Δ_{ICP}-values of ~ 10^{-4}.

The acquisition times for ROA spectra depend upon the concentration of the sample, the strength of the signals and the SNR required. An example of the speed and reliability of the current backscattering ROA instrument is shown in Figure 3.5 where the ROA spectra of the two enantiomers of trans-pinane are displayed after 10 minutes along with the spectra acquired after only 20 seconds of one enantiomer. Most of the prominent ROA signals are already identifiable after this short time. Note also the excellent mirror symmetry between the spectra of the two enantiomers which reflects the reliability of the measurement. A typical mono- or disaccharide ROA spectrum can be obtained in one or two hours with all the key features identifiable after about 10 minutes. However, for polysaccharides which are measured at much lower

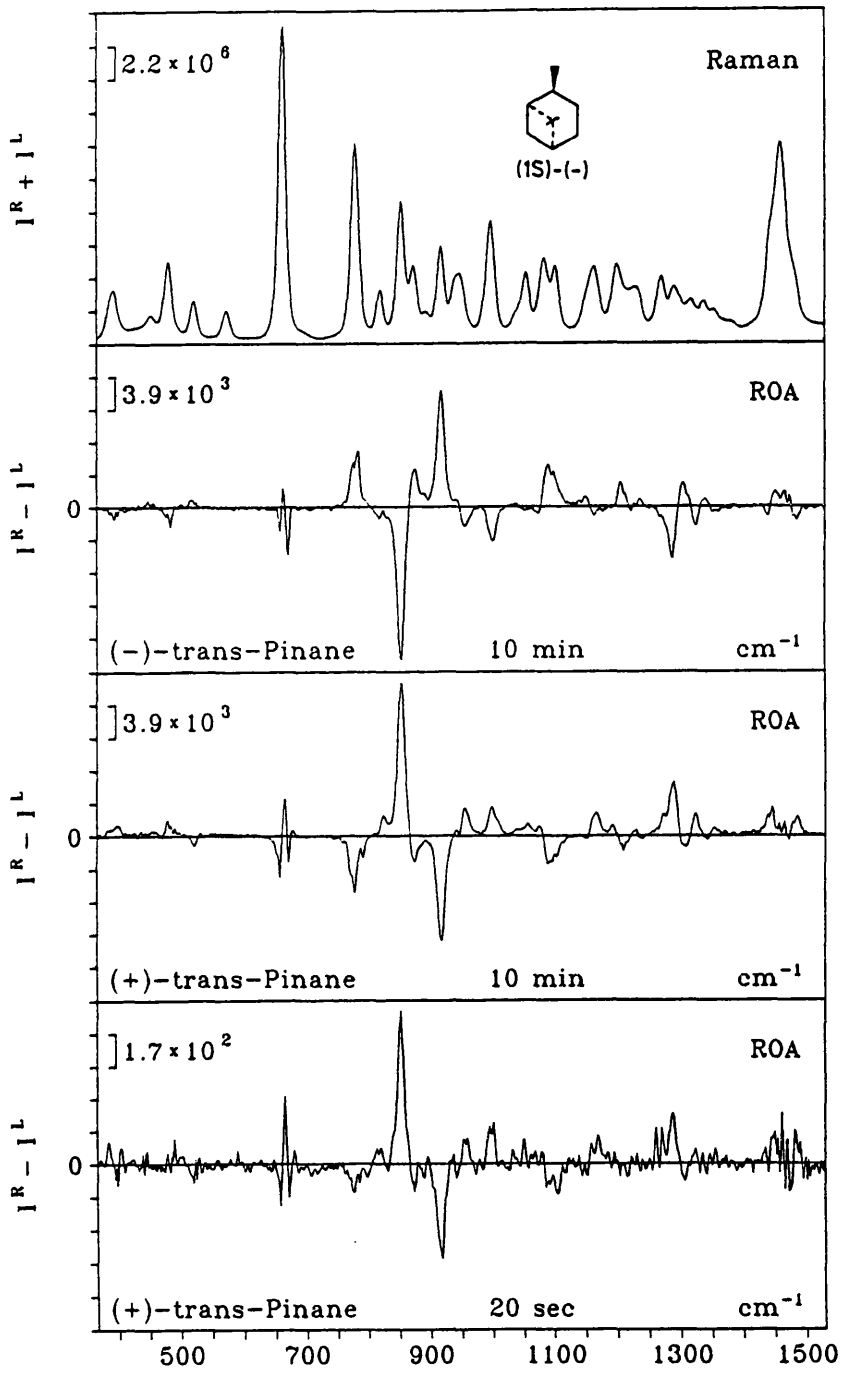

Figure 3.5 Backscattered Raman ($I^R + I^L$) and ROA ($I^R - I^L$) spectra of neat (1S)-(-)-trans-pinane recorded in 10 min (top) and backscattered ROA spectra of (1R)-(+)-trans-pinane acquired in 10 min (middle) and 20 s (bottom).

concentrations, it can take upto 24 hours to achieve an acceptable SNR. The dead time of the instrument is only ~ 0.55 seconds per modulation cycle.

The spectral resolution is determined principally by the dispersion of the grating and the width of the spectrograph entance slit. With the 1200 grooves per mm grating currently in use in Glasgow a resolution of ~ 2.8 cm^{-1} is possible for a slit width of 10 μm at 500 nm.[1] Widening the entrance slit increases the amount of light entering the spectrograph, and thus the Raman intensity, but degrades the resolution. Therefore, a suitable balance between Raman intensity and spectral resolution must be struck. For carbohydrates a slit width of 120 μm is employed which corresponds to a spectral band pass of 12.3 cm^{-1} at 540 nm. The slit height is also variable between 1 mm and 8 mm although in principle it should not effect the resolution, opening the slit height does increase the Raman intensity while at the same time allowing more stray light to enter the spectrograph.

One of the difficulties encountered in backscattering ROA measurements is the large amount of stray light that is present as a consequence of the scattering geometry. Until recently high levels of stray light have restricted backscattering ROA measurements to a lower limit of ~ 600 cm^{-1} for biological samples.[16] However, improvements in holographic filter technology have led to the replacement of edge filters with notch filters. These notch filters have a higher optical density in the blocked region so providing better suppression of the Rayleigh line and cut-off closer to the Rayleigh line and with a sharper edge.[4-6] Thus, incorporating new models of holographic notch filters the lower limit on backscattering ROA measurements has been successfully lowered over the course of this project first to ~ 350 cm^{-1} and then

~ 250 cm^{-1} on typical biological samples such as carbohydrates and amino-acids.[17,18] To date only preliminary backscattering ROA measurements have been made in the region above 2000 cm^{-1} due to the difficulties encountered with weak signals and strongly polarized bands.[19]

References

1. L. Hecht, L. D. Barron, A. R. Gargaro, Z. Q. Wen and W. Hug, *J. Raman Spectrosc.*, **23** (1992) 401-411.
2. D. S. Klinger, J. S. Lewis and C. E. Randall in *Polarized Light in Optics and Spectroscopy*, Academic Press, London, 1990.
3. W. Hug, *Appl. Spectrosc.*, **35** (1981) 115-124.
4. B. Yang, M. D. Morris and H. Owen, *Appl. Spectrosc.*, **45** (1991) 1533-1536.
5. H. Owen in *Computer and Optically Generated Holographic Optics*, SPIE Vol. 1555.
6. J. M. Tedesco, H. Owen, D. M. Pallister and M. D. Morris, *Anal. Chem.*, **65** (1993) 441A.
7. L. D. Barron, J. F. Torrance and D. J. Cutler, *J. Raman Spectrosc.*, **18** (1987) 281-287.
8. P. L. Polavarapu, *Appl. Spectrosc.*, **37** (1983) 447.
9. M. R. Oboodi, M. A. Davies, U. Gunnia, M. B. Blackburn and M. Diem, *J. Raman Spectrosc.*, **16** (1985) 366.
10. P. M. Epperson and M. B. Dentor, *Anal. Chem.*, **61** (1989) 1513-1519.
11. R. B. Bilhorn, J. V. Sweedler, P. M. Epperson and M. B. Denton, *Appl. Spectrosc.*, **41** (1987) 1114 and 1125.
12. D. Falkin and M. Vosloo, *Spectroscopy Europe*, **5** (1993) 16-21.
13. L. D. Barron, M. P. Boogard and A. D. Buckingham, *J. Am. Chem. Soc.*, **95** (1973) 603-605.
14. L. Hecht and L. D. Barron, *Appl. Spectroscopy*, **44** (1990) 483-491.
15. J. R. Escribano, *Chem. Phys. Letts.*, **121** (1986) 191-193.
16. L. D. Barron in *Advances in Spectroscopy Vol. 21, Biomolecular Spectroscopy, Part B*, R. J. H. Clark and R. E. Hester (Eds.), Wiley, Chichester, 1993, 235-266.

17. A. F. Bell, L. Hecht and L. D. Barron, *J. Raman Spectrosc.*, **24** (1993) 633-635.

18. A. F. Bell and S. J. Ford, unpublished results.

19. A. R. Gargaro, unpublished results.

Chapter 4

Carbohydrate Stereochemistry

In this chapter those aspects of carbohydrate stereochemistry relevant to the ROA studies in the following chapters will be introduced together with some of the physical methods available for studying saccharide structural systems.

4.1 Monosaccharides

The monosaccharides are regarded as the simplest carbohydrate units as they cannot be hydrolysed into smaller carbohydrate molecules. They have the general empirical formula $(CH_2O)_n$, although substituents containing nitrogen, sulphur and phosphorous atoms often appear in nature. The smallest molecules that exhibit the typical physical properties usually associated with carbohydrates are glyceraldehyde and dihydroxyacetone shown in Figure 4.1. Both contain three carbon atoms and for this reason are known as trioses. Glyceraldehyde contains an aldehyde functionality and belongs to the general class of monosaccharides known as the aldoses. Dihydroxyacetone contains a ketone functionality and is therefore called a ketose. Furthermore, glyceraldehyde has a chiral centre at carbon atom 2 so it can exist in two enantiomeric forms. These two forms are designated D and L referring to the absolute configuration of the chiral centre. In general, the designators D and L refer to the absolute configuration of the chiral centre furthest from the aldehyde or ketone group with D referring to structures with the hydroxyl group at this position on the right hand side of the Fischer projection and L on the left. Almost all naturally occurring carbohydrates have the D configuration.

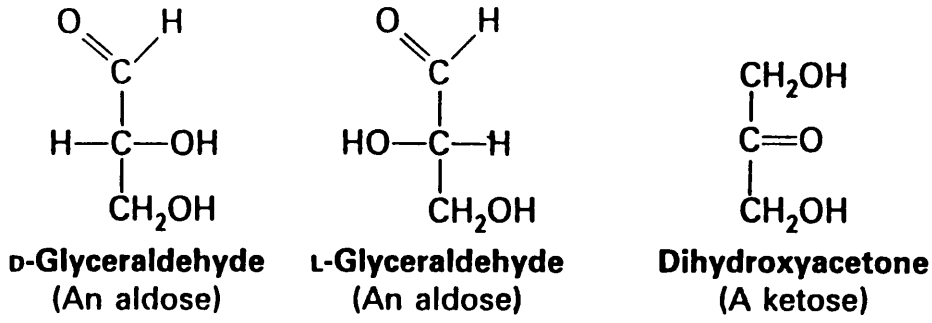

Figure 4.1 Structural formulae of D- and L-glyceraldehyde and dihydroxyacetone.

Sugars with four, five or six carbon atoms are known as tetroses, pentoses and hexoses, respectively. For aldose sugars with four carbon atoms there are two chiral centres resulting in four possible stereoisomers, two belonging to the D-series and two belonging to the L-series. Likewise, for the aldose sugars with five and six carbon atoms there are a total of eight and sixteen possible stereoisomers, respectively. The structures and numbering system employed for the stereoisomers of aldose sugars belonging to the D-series are depicted in Figure 4.2. (Note that the other stereoisomers belonging to the L-series are simply mirror images of those shown in Figure 4.2.) The ketose sugars have one fewer chiral centre which means that there is only half the number of possible stereoisomers as shown in Figure 4.3.

The monosaccharides that have been studied by ROA and which are discussed in detail later fall into three general categories: the aldohexoses, the aldopentoses and the ketohexoses. The pyranose forms of these monosaccharides differ from one another in the presence and position of substitution of an exocyclic hydroxymethyl group. The aldohexoses have an exocyclic hydroxymethyl group substituted at carbon atom 5, the aldopentoses lack any such group and for the ketohexoses this group is found on the anomeric carbon as depicted in

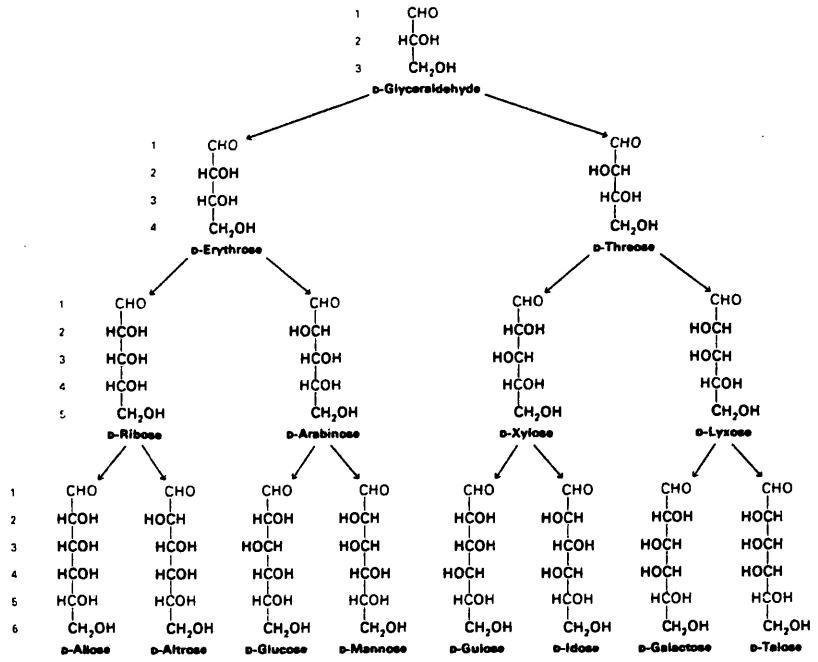

Figure 4.2 The structure and numbering system employed for the stereo-isomers of the aldose sugars belonging to the D-series.

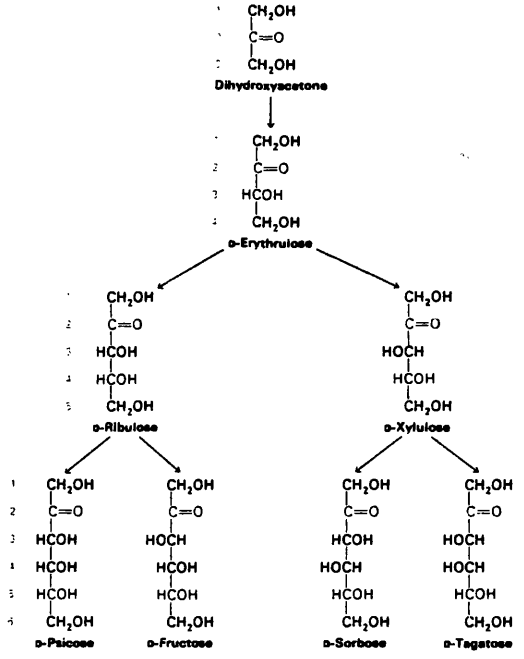

Figure 4.3 The structure and numbering system employed for the stereo-isomers of the ketose sugars belonging to the D-series.

Figure 4.4. These structural differences can have a major influence on the anomeric populations, the chair conformations and the pyranose-furanose equilibria adopted by monosaccharides falling into these three different categories. In addition, it is worth noting that the ketohexoses have a different atom numbering scheme to the aldohexoses and aldopentoses (Figure 4.4).

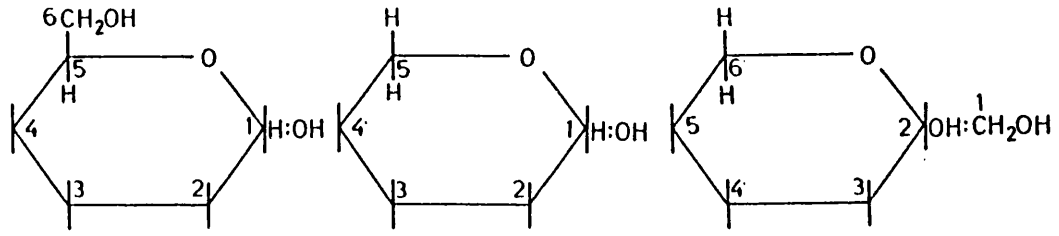

Figure 4.4 The basic structural formulae of the aldohexoses, aldopentoses and ketohexoses.

4.1.1 Ring Conformations

In solution, the predominant form of the pentose and hexose sugars is not an open-chain, rather the sugars cyclise into five or six membered rings *via* intramolecular hemiacetal or hemiketal formation between either an aldehyde or ketone functional group, respectively, and an alcohol functional group.[1] On cyclisation a new chiral centre is created so that two epimeric sugars, called anomers, can be formed. For the D-sugars which form six membered rings one of the anomers has the hydroxyl group at the newly created chiral centre in an axial orientation and is known as the α-anomeric form while the other has this group in an equatorial orientation and is known as the β-anomeric form. (Note that these anomeric designators are reversed for the L-sugars.) The properties of the anomeric centre is an important feature

of carbohydrate stereochemistry and will be discussed in more detail later.

In carbohydrate nomenclature six membered rings are given the suffix 'pyranose' reflecting their similarity to the heterocyclic compound pyran. It is well known that for almost all monosaccharides the chair conformation of the pyranose ring has the lowest energy.[1,2] In this particular conformation bonds may have either an axial orientation, approximately perpendicular to the plane of the ring, or an equatorial orientation, approximately in the plane of the ring. Bulky substituents will preferentially adopt an equatorial over an axial orientation as this relieves unfavourable 1,3 diaxial interactions.[1] The two types of bond are interconverted, without the cleavage of any bonds, by the process of pseudorotation[1,2] so for each monosaccharide two distinct chair forms with different energies are possible as depicted in Figure 4.5.

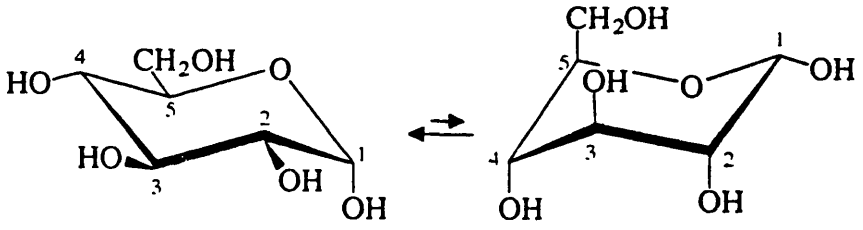

Figure 4.5 The two chair conformations of α-D-glucose.

When classifying pyranose ring conformations the letter C is used to designate a chair form. To fully specify the conformation two numbers representing the atoms that lie above and below the best plane defined by the remaining ring atoms are written as super- and subscripts, respectively. The best plane is chosen so that the lowest numbered ring carbon atoms are displaced from the plane. Thus, for an aldohexose

such as α-D-glucose (Figure 4.5) the two chair forms are designated $^4C_1$ and $^1C_4$ with the former predominating as smaller substituents will be involved in 1,3 diaxial interactions.

Five membered carbohydrate rings are given the suffix 'furanose' reflecting the similarity to the heterocyclic compound furan. Furanose rings exhibit a much greater degree of conformational flexibility than pyranose rings as the barriers to rotation are substantially lower.[2] The most important conformations of the furanose rings are the envelope and twist forms. The envelope forms have one atom removed from the best plane and are named according to whether this atom lies above or below the best plane by using a super- or a subscript, respectively. The twist conformations have two atoms removed from the best plane and are named in a similar manner to the pyranose chair conformations except that only three atoms lie in the best plane. Bulky substituents on furanose rings will preferentially adopt a pseudo-equatorial orientation, in which the C-O bonds move toward the plane of the ring, over a pseudo-axial orientation on steric grounds.

4.1.2 Mutarotation

Monosaccharides do not occur exclusively as a single anomer or solely as a pyranose or furanose ring in solution. This is a consequence of the process of mutarotation[1,2] which occurs spontaneously in the presence of water and involves the breaking of the labile hemiacetal bond in the case of aldose and pentose sugars, or the hemiketal bond in the case of ketose sugars, as shown in Figure 4.6 for D-fructose. Each time this bond is broken the monosaccharide may adopt a different tautomeric form and this process continues until finally an equilibrium mixture of α- and β-anomers, pyranose and furanose rings

and also the open-chain form is reached. The composition of this thermodynamic equilibrium is determined by the balance of steric and electronic forces acting on the molecule, the most important of which is the anomeric effect.

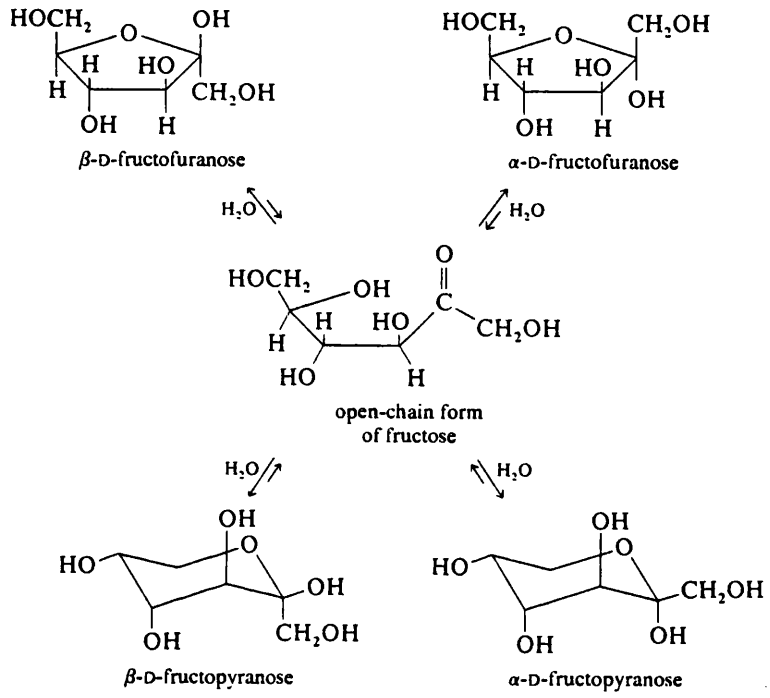

Figure 4.6 The mutarotation of D-fructose.

4.1.3 The Anomeric Effect

By comparing the situation in carbohydrates with that in cyclohexanol it might be expected that the hydroxyl group on the anomeric carbon would preferentially adopt an equatorial orientation on steric grounds. However, this is not the case on account of an electrostatic interaction known as the anomeric effect in which the presence of a ring oxygen provides an additional stabilisation to the axial orientation of the hydroxyl substituent at this position.[1-5] Although this effect was first identified in carbohydrate chemistry it is

now recognised as being of more general importance in all molecules having two heteroatoms linked to a tetrahedral centre.[3-5]

There are two widely accepted rationalisations for the anomeric effect. The first of these invokes the dipole-dipole interaction between the C-O-C bond on the ring and the C1-O bond. When the C1-O bond is in an equatorial orientation the angle between the dipoles is smaller than for an axial orientation, as depicted in Figure 4.7, and the molecule has a higher energy. However, this model does not account quantitatively for observed axial preferences and does not predict the bond length and angle changes that occur around the anomeric centre in carbohydrates.[6] A second mechanism that explains the observed lengthening of the exocyclic C1-O1 bond and the shortening of the endocyclic C1-O5 bond in the crystal structures of carbohydrates[6] involves delocalisation or back-donation of π-electrons from the lone-pair orbital on the ring oxygen to the anti-bonding orbital of the exocyclic C1-O1 bond. The axial orientation of the hydroxyl group is better suited to this delocalisation because the C1-O1 bond lies in the same plane as the lone-pair orbital of the ring oxygen. It is most likely in carbohydrate systems that both these mechanisms are contributing to some degree.

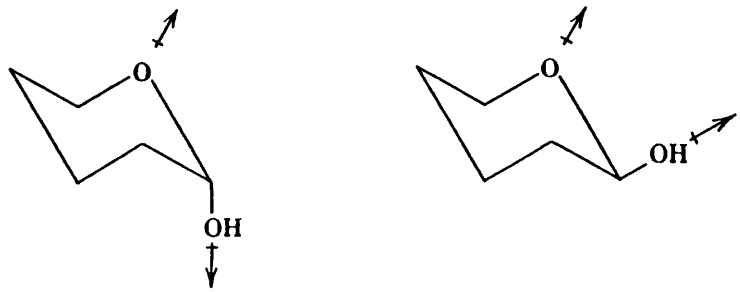

Figure 4.7 The dipole-dipole interaction mechanism for the explanation of the anomeric effect.

The magnitude of the anomeric effect is influenced by three main factors:[3-5] the nature of the anomeric substituent, the substituents at the other chiral centres and the solvent. It has been found that the polarity of the C1-X bond is fairly strongly correlated to the strength of the anomeric effect.[1] Thus, the halogens give the largest effect, hydroxyl groups are intermediate and species such as quaternary pyridinium cations in fact display a reverse anomeric effect where the axial orientation is destabilised relative to the equatorial orientation. The substituents on adjacent carbons can also have an important influence in what is known as the Δ2 effect. This involves an instability brought about by an axial substituent on the carbon adjacent to the anomeric centre on the equatorial orientation of the anomeric substituent. Solvents with large dielectric constants, such as water, have been found to exhibit small anomeric effects whilst those with small dielectric constants, such as chloroform, exhibit large anomeric effects.[1]

4.2 Disaccharides

Disaccharides are composed of two monosaccharide units joined together by a C-O-C bond known as the glycosidic link as illustrated in Figure 4.8 for D-maltose. This link always involves the anomeric carbon of one of these monosaccharide units which is known as the non-reducing residue as the linkage traps it in either the α- or β-anomeric form. The second unit is free to mutarotate and is known as the reducing residue. The terms reducing and non-reducing refer to the ability of the corresponding open-chain form, which will only be present in small quantities if the residue is mutarotating, to reduce Cu^{2+} ions.

To fully specify a disaccharide structure the following information is required: the type of monosaccharide residues, the order of residues, the linkage type and the linkage configuration. The linkage type refers to the carbon atoms that are involved in the linkage which will be the anomeric carbon of the non-reducing residue and any one of the carbon atoms of the reducing residue that carries an hydroxyl substituent. The linkage configuration can be specified as either α or β depending on the anomeric configuration in which the non-reducing residue is trapped.

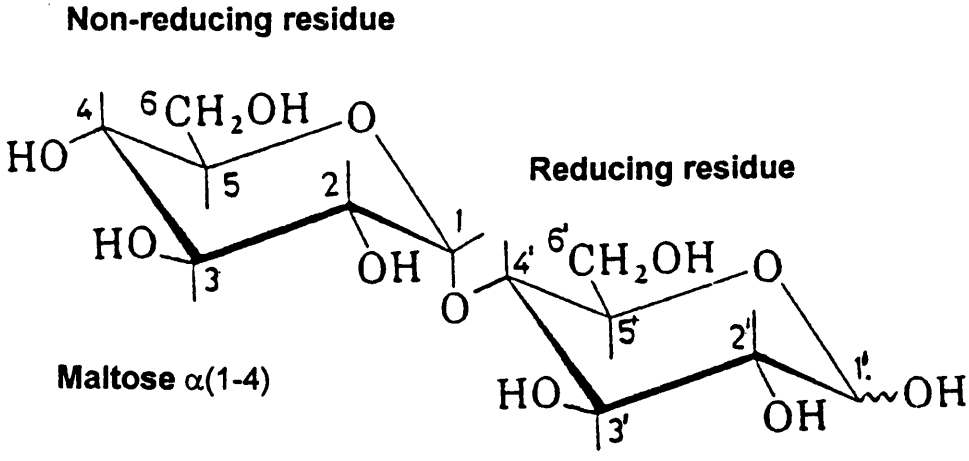

Figure 4.8 Structural formula and atomic numbering scheme of D-maltose.

The glycosidic link is the most important single feature in determining di-, oligo- and polysaccharide stereochemistry. Two torsion angles can be used to describe the linkage conformation. The torsion angles φ and ψ are defined as H1-C1-O1-C1' and C1-O1-Ci'-Hi', respectively, where a prime represents the reducing residue and i is the carbon atom of the reducing residue involved in the link (Figure 4.8). A special case is disaccharides linked through the hydroxymethyl group of the reducing residue. In this situation there are three bonds in the link and three torsion angles φ, ψ and ω that need to be defined. For these

(1-6) linked species φ, ψ and ω are defined as H1-C1-O1-C6', C1-O1-C6'-C5' and O1-C6'-C5'-O5', respectively.

4.3 Polysaccharides

Biological molecules such as proteins, nucleic acids and polysaccharides generally adopt higher order structures which define their molecular properties and biological activity.[1] The primary structure of a polysaccharide is determined by the identity of the constituent monosaccharide residues and by the type and configuration of the glycosidic linkages which connect them. Often the primary structure is characterised by a simple repeating unit consisting of between one and five residues.[2] The secondary structure is partially determined by the ring conformation of the individual residues but more importantly by the individual torsion angles, φ and ψ, about the glycosidic link which specify the relative orientations of adjacent monosaccharide rings.

Polysaccharides may under certain conditions adopt ordered secondary structures which are characterised by fixed values of the glycosidic torsion angles, rather than a statistical distribution as found in random coils.[1,2] Such ordered structures are promoted by favourable non-covalent interactions, which often involve co-operative processes, and in some cases may persist even in aqueous solution. The formation of ordered structures are inhibited by factors such as electrostatic repulsions, irregular primary structures, chain branching and loss of conformational entropy. Examples include cellulose which in the solid state adopts an extended ribbon-like conformation and V-amylose, agarose and laminarin which adopt single, double and triple helical structures, respectively.

Unlike certain other biopolymers such as proteins, polysaccharides are polydisperse.[1,7] This means that they have no distinct molecular weight and instead exhibit a range of values so that only a distribution about a mean value may be specified. This distribution is found to depend on the source, the method of molecular weight determination and the method of isolation of the polysaccharide.

There are a number of possible ways of characterising the structure of polysaccharides. They can be subdivided into linear and branched chains, the difference being that branched polysaccharides contain a number of residues that are glycosidically linked to three others, which form the branching points, whereas in linear polysaccharides each residue is attached to only two others, with the exception of the terminal residues. Also, if the constituent residues are all of the same type then the polysaccharide is known as a homoglycan; but if there are two or more types of residue present the polysaccharide is called a heteroglycan. The sequence of residues may also be classified into three general types: periodic, interrupted and aperiodic.[2] Polysaccharides with a periodic sequence have the residues arranged in a regular repeating unit, such as in amylose. Interrupted sequences also have regions of regular repeating units but they are separated by regions that have no regular structure, such as carrageenan for example. Finally, aperiodic sequences are characterised by irregular sequence of residues, linkage type and configuration, such as are found in the carbohydrate chains of glycoproteins.

Glycoproteins consist of carbohydrate chains covalently linked to polypeptide chains. The mode of linkage is usually either N-glycosidic, between the anomeric carbon of the reducing end of the glycan chain and the nitrogen atom of the amide group of an asparagine residue, or

O-glycosidic, between the anomeric carbon of the reducing residue of the glycan chain and the oxygen atom of the hydroxyl group of serine, threonine, hydroxylysine or hydroxyproline residues.[8] The glycan chains perform two major roles of which one is to impart particular physiochemical properties on the protein and the other is to act as signals for cell surface recognition events.

4.4 Physical Methods

4.4.1 X-Ray Crystallography

X-ray crystallography is capable of yielding complete structural information, to atomic resolution, on any carbohydrate that can be obtained in the crystalline form. Unfortunately, the crystal structure may deviate significantly from that found under physiological conditions. To make matters worse, carbohydrates are flexible molecules that usually exist as an equilibrium mixture of more than one conformation in solution[9] but only a single conformation will be present in the crystal. This flexibility also has the consequence of making carbohydrates difficult to crystallise. To date no single crystal of an oligosaccharide containing more than four residues has been obtained, with the notable exception of the cyclodextrins.[10] This last problem can be circumvented by co-crystallising an oligosaccharide complexed to a suitable protein receptor[11] but often this complexed form does not represent the lowest energy conformation of the free oligosaccharide.

Polysaccharides are not usually amenable to x-ray crystallography for the reasons discussed above. However, if they can be prepared as fibres in which the molecular axes are all aligned approximately parallel then fibre diffraction techniques can be applied.[12] A number of

polysaccharides have been studied in this manner and the results interpreted with the aid of potential energy calculations.[12,13]

In a small number of special cases the carbohydrate chains in glycoproteins can be resolved by x-ray crystallography as a result of the strong interactions between the polypeptide and carbohydrate chains, which serve to restrict the flexibility of the carbohydrate chain.[14,15]

4.4.2 Nuclear Magnetic Resonance

Nuclear magnetic resonance (NMR) is one of the most powerful methods for determining the solution stereochemistry of biopolymers. However, the power of NMR techniques is dependent on the number of resonances that can be assigned and even though fewer resonances appear in carbohydrate ^{1}H NMR spectra than in those of either proteins or nucleic acids almost all lie in an extremely narrow chemical shift region (3.5 to 4.0 ppm) with the consequent overlap problem.[16-18] One exception are the anomeric protons which resonate at lower field due to the electron-withdrawing properties of the ring oxygen. These well defined resonances are of some use in determining anomeric populations and ring conformations in monosaccharides.[19] However, in general two-dimensional techniques are not only desirable but a prerequisite for the elucidation of di-, oligo- and polysaccharide stereochemistry.[18] Indeed, it has even been proposed that three- and four-dimensional techniques be applied to the problems associated with resonance overlap in carbohydrates.[20,21]

As mentioned earlier the glycosidic link is probably the most important single feature in determining di-, oligo- and polysaccharide stereochemistry. NMR provides two main methods for studying the

conformation of the glycosidic link: the nuclear Overhauser enhancement (NOE) effect and spin-coupling constants.[16-18,22,23] The NOE effect is governed by a through space interaction between two nuclei the size of which depends on their separation. Thus, the distance between two protons across the glycosidic link can be determined and subsequently converted into a range of φ and ψ torsional angles provided assignments for suitable nuclei are available. The NOE effect is dependent on r^{-6}, where r is the inter-proton distance, which means that short separations will tend to be over-represented. Measurement of more than one NOE can introduce greater confidence in the results obtained but unfortunately due to the short range of the effect often only one NOE can be observed in carbohydrates. Another problem is the time-averaging experienced by the NOE signals as the rotation about the bonds of the glycosidic link is occurring fast on the NMR timescale. This results in a value for the NOE that represents an average or 'virtual' conformation of the molecule which may bear no relationship to the conformations that actually exist in solution.[23] Finally, as the NOE effect is dependent on the rate of tumbling, for medium sized oligosaccharides the effect can be very weak or even zero.

The data obtained from NOE measurements can be supplemented by measurement of coupling constants across the glycosidic link.[16-18,22,23] These measurements are somewhat restricted by the insensitivity of coupling constants to torsional angles and a poor understanding of their precise variation in carbohydrate systems. In addition, like NOE data, coupling constants will be time-averaged. Usually, NMR results are coupled to potential energy and molecular dynamics calculations which model the dynamics of the system. Such computations can then give meaning to the data collected from NOE and spin-coupling constants.

The overlap problem mentioned above for ^{1}H NMR can be alleviated by applying ^{13}C NMR which has a much larger chemical shift dispersion (0-200 ppm) but with approximately two orders of magnitude lower sensitivity. Although ^{13}C NMR is detectable in both solution and the solid state it is most readily observed in the cross polarization/magic angle spinning (CP-MAS) spectra of solids. It has been found that the chemical shifts of the glycosidic carbon atoms in the ^{13}C NMR spectra are dependent upon conformation and attempts have been made to correlate these chemical shifts with the glycosidic torsion angles of related carbohydrates obtained from crystallographic data.[24-28] Once correlations have been formulated it is then possible to use them to determine the conformation of polysaccharides in gels and samples of low crystallinity where no crystallographic data are available. One problem that arises in this technique is the fact that other factors such as hydrogen bonding, dipolar interactions and ring current interactions make it difficult to disentangle conformational effects.

4.4.3 Conventional Chiroptical Techniques

The two chiroptical techniques most commonly applied to carbohydrates are CD,[29] and optical rotation.[30-32] For unsubstituted carbohydrates the only chromophores present are the C-O and O-H groups which absorb below 190 nm in the vacuum UV region. Only the long wavelength tails of these bands, which provide little stereochemical information, are accessible to commercial instruments.[33] Specially designed CD instruments that combat the problem of oxygen absorption by operating in a vacuum can be employed for studying carbohydrates. However, such instruments are expensive and since so many different chromophores are present there is great difficulty in interpreting the CD spectra. Another possible solution is to substitute the hydroxyl

groups with chromophores that absorb above 190 nm, but this suffers from the problem problem that introducing new chromophores may alter the molecule away from the biologically active conformation.

Some naturally occurring carbohydrates do possess chromophores, such as sulphate, amide and carboxyl groups, that are accessible to commercial instruments and these have been the most extensively studied by CD spectroscopy.[29] The majority of data derived from CD studies on polysaccharides pertains to their secondary structure. In addition, because CD can be applied to solutions, gels and films and has a high degree of conformational sensitivity it is an accepted method for studying the transitions which polysaccharides will undergo between different states on altering environmental factors such as temperature, pH or salt concentration.

Because of the lack of general experimental data on the conformation of the glycosidic linkage even optical rotation of the Na_D line is regarded as useful. Based on empirical correlations a contribution to the optical rotation from the glycosidic link can be isolated. Calculations can then be performed to yield values for the optical rotation for all possible φ and ψ torsion angles and these are compared with the experimentally obtained values.[30-32] The crude approximations inherent in this technique mean that only conformational types rather than specific conformers can be identified. However, it does provide an additional source of data which can be used in conjunction with NMR and molecular mechanics calculations to refine the understanding of the linkage conformation.

4.4.4 Conventional Vibrational Spectroscopy

Infra-red and Raman spectroscopy are complementary techniques which measure absorption or scattering intensities of a particular vibrational transition which depend on changes in the dipole moment and polarizability with respect to the associated normal coordinate, respectively.[34] This means that polar groups such as O-H, N-H or C-O will yield intense IR and weak Raman bands but that for skeletal vibrations this situation is reversed. One consequence is that water has intense absorption bands in the IR spectrum that restricts the regions where aqueous solutions can be studied. There is no such problem in Raman spectroscopy as water is a poor scatterer and does not absorb the visible incident light.

The difficulties associated with spectral interpretation have rather curtailed the application of conventional vibrational spectroscopy to carbohydrate stereochemistry.[35] The normal modes in carbohydrates generally display a high degree of coupling, due to the similarity of a large proportion of the vibrational coordinates, which hinders the assignment of contributions from individual structural features. In addition, the large number of normal modes, 66 in glucose for example, and the small wavenumber separation between many of them results in a crowded vibrational spectrum with the consequent overlap problem. However, the structural sensitivity of vibrational techniques means they do find use as an analytical tool, especially, for substituted carbohydrates where the functional groups vibrate at some well defined group frequency and do not couple extensively with the other vibrational coordinates.

4.4.5 Vibrational Optical Activity

Carbohydrates are particularly favourable samples for vibrational optical activity studies. The complex, coupled normal modes that hinder assignment of the conventional vibrational spectra are in fact a prerequisite for strong vibrational optical activity. The cyclic structure of the individual monosaccharide residues confers a certain degree of conformational rigidity on these molecules leading to stronger vibrational optical activity. Another factor is that the crowded nature of the conventional vibrational spectrum is relieved to some degree as the ROA signals can have either a positive or negative sign. From a practical standpoint the high solubility in water and ready availability of carbohydrate samples make them attractive candidiates for study. In particular, the availability of a large number of diastereomers allows us to probe the influence that each chiral centre has on the vibrational optical activity. Finally, as other chiroptical techniques face severe restrictions when studying carbohydrates little utility has been made of the type of information that can be forthcoming from such techniques.

The application of VCD to carbohydrates has not been as widespread as for other biologically important molecules, such as peptides and proteins,[36] and to date only results on monosaccharides have been published.[37-42] The first VCD results on α- and β-methyl glucoside in D_2O in the C-H stretch region (2750 to 3050 cm^{-1}) were used to demonstrate the ability of VCD to focus on a single chiral centre even when a large number of chiral centres are present in the molecule.[37] A general survey of monosaccharide VCD in the C-H stretch region appeared a few years later together with some correlations.[38] Nafie *et al.* repeated a selection of these measurements and interpreted the results in terms of the ring current mechanism of VCD generation.[39,40]

Monosaccharides have also been studied in the mid-IR region (800 to 1650 cm^{-1}) using a FT-IR VCD instrument.[41,42] The main problems encountered in this wavenumber range are the strong IR absorption of water and the lack of sensitivity. The solvent used in these studies was DMSO which has absorption bands between 950 and 1100 cm^{-1} precluding VCD measurements in this wavenumber range. Measurements below 900 cm^{-1} are not possible without changing detector material and instrumental configuration.[36] However, this still leaves the region between ~ 1100 and 1500 cm^{-1} where some interesting results have been obtained. In particular, a VCD signal at ~ 1150 cm^{-1} has been correlated with the absolute configuration of all the chiral centres of the ring. The normal modes responsible for this signal involve coupled C-C and C-O stretching coordinates and by adding pairs of right and left helical contributions made by neighbouring chiral centres the sign of this VCD signal can be predicted.[41,42] The complementarity of the VCD and ROA mechanisms is clearly highlighted by comparison of the spectra of D-xylose and D-glucose between ~ 1200 and 1500 cm^{-1}. In this range the VCD spectra of D-xylose is stronger than that of D-glucose while the reverse is true for the ROA.

Only three papers devoted to the ROA spectra of carbohydrates had been published[43-45] prior to the commencement of the work presented in this thesis. The first of these was a preliminary study of some interesting mono- and disaccharides which reported on a number of prominent ROA signals that appeared in their spectra.[43] This was followed by a paper reporting the ROA spectra of α-, β- and γ-cyclodextrin which concentrated mainly on the enormous couplet found at ~ 920 cm^{-1} in their ROA spectra.[44] The ROA spectra presented in both these papers are of much lower quality than those discussed later in this thesis as at that time a low throughput

double-grating spectrometer was still employed and the CCD detector used was not back-thinned. The third paper in this series concentrated on fifteen monosaccharides and attempted to assign ROA signals to stereochemical features such as anomeric configuration, hydroxymethyl group conformation and ring hydroxyl group disposition.[45] The quality of the spectra presented in this paper are approximately the same as those discussed in the following chapters of this thesis but some problems with the interpretation of the data will be rectified here.

References

1. J. F. Stoddard in *Stereochemistry of Carbohydrates,* Wiley, New York, 1971.
2. D. A. Rees in *Polysaccharide Shapes,* Wiley, London, 1977.
3. I. Tvaroska and T. Bleha, *Adv. Carbohydr. Chem. Biochem.,* **49** (1989) 45.
4. E. Juaristi and G. Cuevas, *Tetrahedron,* **48** (1992) 5019-5087.
5. P. Deslongchamps in *Stereoelectronic Effects in Organic Chemistry,* Permagon, New York, 1983.
6. G. A. Jeffrey, J. A. Pople and L. Radom, *Carbohydr. Res.,* **25** (1972) 117-131.
7. I. Danishefsky, R. L. Whistler and F. A. Bettelheim in *The Carbohydrates Vol. IIa,* W. Pigman and D. Horton (Eds.), Academic Press, London, 1970, 375-412.
8. P. V. Wagh and O. P. Bahl, *Critical Reviews in Biochemistry,* (1981) 307-377.
9. K. G. Rice, P. Wu, L. Brand and Y. C. Lee, *Current Opinions in Structural Biology,* **3** (1993) 669-674.
10. K. Harata in *Inclusion Compounds, Vol. 2,* J. L. Atwood, J. E. D. Davies and D. D. MacNicol (Eds.), Academic Press, London, 1984.
11. Y. Bourne, P. Rouge and C. Cambillau, *J. Biol. Chem.,* **265** (1990) 18161-18165.
12. R. P. Millane, *ACS Symp. Ser. (Computer Modelling of Carbohydrate Molecules),* **430** (1990) 315-331.
13. Y. Deslandes, R. H. Marchessault and A. Sarko, *Macromolecules,* **13** (1980) 1466-1471.
14. J. Deisenhofer, *Biochemistry,* **20** (1981) 2361-2370.
15. A. J. Lapthorn, D. C. Harris, A. Littlejohn, J. W. Lustbader, R. E. Canfield, K. J. Machin, F. J. Morgan and N. W. Isaacs, *Nature,*

369 (1994) 455-461.

16. S. W. Homans, *Progress in NMR Spectrosc.*, **25** (1990) 55-81.
17. J. Vliegenthart, L. Dorland, H. van Halbeek, *Adv. Carbohydr. Chem. Biochem.*, **41** (1983) 209-373.
18. B. Meyer, *Topics in Current Chemistry*, **154** (1990) 141-208.
19. S. J. Angyal, *Angew. Chem. Int. Ed. Engl.*, **8** (1969) 157-166.
20. S. W. Homans, *Glycobiology*, **2** (1992) 153-159.
21. T. J. Rutherford and S. W. Homans, *Glycobiology*, **2** (1992) 293-298.
22. I. Tvaroska, T. Kozar and M. Hricovini, *ACS Symp. Ser. (Computer Modelling of Carbohydrate Molecules)*, **430** (1990) 162-176.
23. D. Cumming and J. Carver, *Biochemistry*, **26** (1987) 6664.
24. H. Saito, *Magn. Reson. Chem.*, **24** (1986) 835-852.
25. M. J. Gidley and S. M. Bociek, *J. Am. Chem. Soc.*, **110** (1988) 3820-3829.
26. F. Horii, H. Yanamoto, A. Hirai and R. Kitamaru, *Carbohydr. Res.*, **160** (1987) 29-40.
27. S. J. Heyes, N. J. Clayden and C. M. Dobson, *Carbohydr. Res.*, **233** (1992) 1-14.
28. M. C. Jarvis, *Carbohydr. Res.*, **259** (1994) 311-318.
29. W. C. Johnson, Jr., *Adv. Carbohydr. Chem. Biochem.*, **45** (1987) 73-124.
30. E. S. Stevens and B. K. Sathyanarayana, *Carbohydr. Res.*, **166** (1987) 181-193.
31. E. S. Stevens and B. K. Sathyanarayana, *J. Am Chem. Soc.*, **111** (1989) 4159-4154.
32. E. S. Stevens and B. K. Sathyanarayana, *Biopolymers*, **27** (1988) 415-421.
33. I. Listowsky and S. Englard, *Biochem. Biophys. Res. Commun.*, **30** (1968) 329-332.

34. M. Diem in *Introduction to Modern Vibrational Spectroscopy,* Wiley, Chichester, 1993.

35. M. Mathlouthi and J. L. Koenig, *Adv. Carbohydr. Chem. Biochem.,* **44** (1986) 7-89.

36. T. A. Keiderling and P. Pancoska in *Advances in Spectroscopy Vol 21, Biomolecular Spectroscopy Part B,* R. J. H. Clark and R. E. Hester (Eds.), Wiley, Chichester, 1993, 267-316.

37. C. Marcott, H. A. Havel, J. Overend and A. Moscowitz, *J. Am. Chem. Soc.,* **100** (1978) 7088-7089.

38. H. A. Havel, Ph.D thesis, University of Minnesota, Minneapolis, 1981.

39. M. G. Paterlini, T. B. Freedman and L. A. Nafie, *J. Am. Chem. Soc.,* **108** (1986) 1389-1397.

40. T. B. Freedman and L. A. Nafie, *Topics in Stereochemistry,* **17** (1987) 113.

41. D. M. Back and P. L. Polavarapu, *Carbohydr. Res.,* **133** (1984) 163-167.

42. C. M. Tummalapalli, D. M. Back and P. L. Polavarapu, *J. Chem. Soc. Faraday Trans I,* **84** (1988) 2565-2594.

43. L. D. Barron, A. R. Gargaro and Z. Q. Wen, *Carbohydr. Res.,* **210** (1990) 39-49.

44. L. D. Barron, A. R. Gargaro, Z. Q. Wen, D. D. MacNicol and C. Butters, *Tetrahedron: Asymmetry,* **1** (1990) 513-516.

45. Z. Q. Wen, L. D. Barron and L. Hecht, *J. Am. Chem. Soc.,* **115** (1993) 285-292.

Chapter 5

Vibrational Raman Optical Activity of Glucose

The Raman and ROA studies discussed in this chapter were prompted by a general study of fifteen representative monosaccharides initiated by Wen *et al.* which demonstrated that configurational changes at even a single chiral centre can have a comprehensive effect on the ROA.[1] Any attempt to assign ROA signals within a number of sugar molecules belonging to different homomorphic series can therefore be misleading. Instead, it is necessary to consider each homomorphic series separately in order to improve our understanding of the generation of ROA in monosaccharides.

The six monosaccharides discussed in this chapter belong to the *gluco-* homomorphic series which share the same absolute configuration at carbon atoms 2,3,4 and 5. This particular series was chosen as a number of deuterated analogues of D-glucose are commercially available and can be used to assist in the assignment of ROA signals to individual structural features. In addition, D-glucose has been extensively studied by normal coordinate analyses[2-6] relative to the other monosaccharides and is present as the sole constituent in the majority of the di- and polysaccharides discussed in the later chapters. D-glucosamine and 5-thio-D-glucose were also included in an attempt to determine the influence of substituents other than hydroxyl groups and the role of the ring oxygen, respectively, on the generation of ROA in D-glucose.

5.1 Experimental

All the carbohydrate samples used in this study were dissolved in distilled H_2O to a concentration of 4.5 M and were then allowed to equilibrate at room temperature for at least 24 h. The equilibrated samples were treated with charcoal to reduce fluorescence, filtered through 0.45 μm Millipore membrane filters into quartz microfluorescence cells, and then centrifuged for at least 15 min to remove any dust particles, which may cause spurious light scattering. Samples of D-glucose-1-d_1 and D-glucose-6,6-d_2 were supplied by Aldrich; 5-thio-D-glucose by Fluka; D-glucosamine hydrochloride by Sigma and D-glucose by BDH. A sample of D-glucose-O-d_5 was prepared by lyophilising D-glucose from D_2O solution twice. During spectral acquisition the laser power was ~ 700 mW at the sample and the slit width was set for 120 μm giving a spectral bandpass of 12 cm^{-1}. The spectra were recorded over 2 to 4 h, depending on the strength of the ROA signals, at constant ambient temperature.

5.2 Results and Discussion

The Raman and ROA spectra of D-glucose from ~ 350 to 1500 cm^{-1} and D-glucose-1-d_1, D-glucose-6,6-d_2, D-glucose-O-d_5, 5-thio-D-glucose and D-glucosamine hydrochloride in the range ~ 600 to 1500 cm^{-1} are displayed in Figures 5.1-5.6, respectively. Monosaccharide ROA spectra can be conveniently subdivided into three distinct regions: the *anomeric region* from ~ 600 to 950 cm^{-1}; the *fingerprint region* from ~ 950 to 1200 cm^{-1}; and the *CH_2 and COH deformations region* from ~ 1200 to 1500 cm^{-1}. At the time of recording the lower limit for backscattering ROA spectra was ~ 600 cm^{-1}. However, it is now possible to measure the backscattered ROA from ~ 250 cm^{-1} but only the spectrum of

D-glucose is shown in this extended wavenumber range as isotopic substitutions are unlikely to have any effect in this lower wavenumber region which is dominated by skeletal twisting and bending vibrations. Previous conventional vibrational spectroscopic studies on glucose isotopomers[5-8] relied on a mixture of solution Raman spectra for the O-deuterated samples and solid-state IR and Raman spectra for the C-deuterated samples, but no solution Raman studies of the C-deuterated samples have been previously reported.

An empirical approach is employed in the interpretation of the Raman and ROA spectra because, as has been mentioned in chapter 2, no *ab initio* ROA intensity calculations have yet been performed on any monosaccharides and the normal modes are too complex for the ROA intensities to be explained by simple models, such as the two group model or the bond polarizability model.[9]

5.2.1 Anomeric Region (~ 600-950 cm^{-1})

Unlike the other monosaccharides previously investigated in this laboratory,[1] the ROA spectrum of D-glucose (Figure 5.1) has few bands in this region, with only two weak positive signals appearing at ~ 913 cm^{-1} and ~ 633 cm^{-1}. In aqueous solution, D-glucose exists as an ~ 2:1 equilibrium mixture of β- and α-anomeric forms. From examination of the ROA spectra of α- and β-D-methyl glucopyranoside it is clear that the β-anomeric form of D-glucose yields almost no ROA signal in this region while the α-anomeric form gives rise to a number of signals.[1] It is therefore conceivable that the lack of signal in D-glucose is simply a result of the predominance of the β-anomeric form. Since the β-anomeric form of D-glucose has no axial hydroxyl ring substituents, we may conclude that the generation of ROA in this region somehow

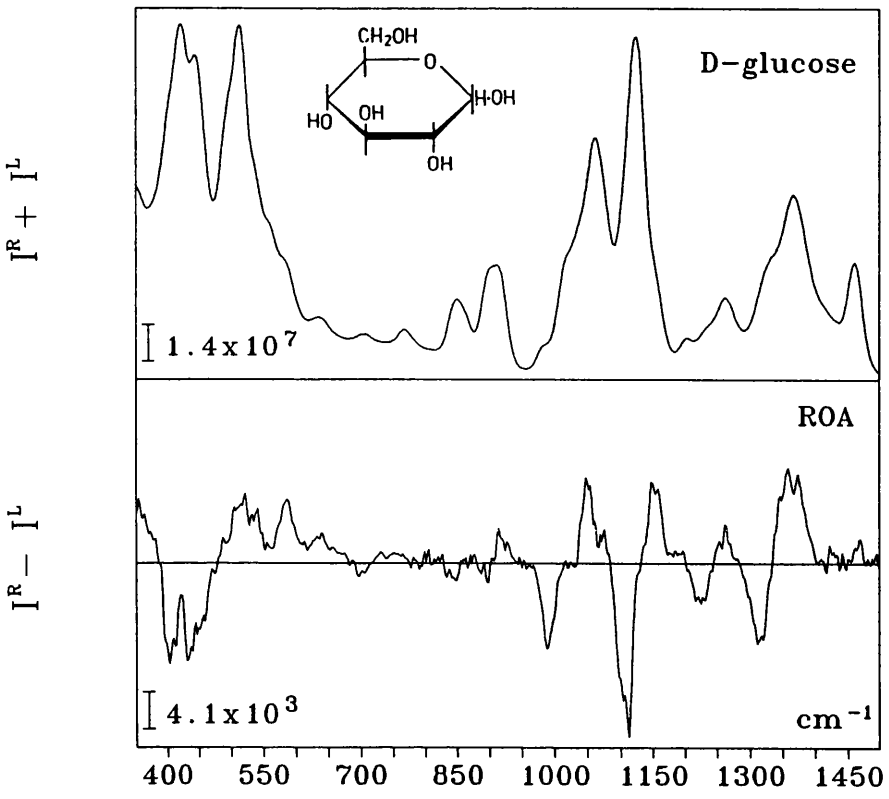

Figure 5.1 The backscattered Raman ($I^R + I^L$) and ROA ($I^R - I^L$) spectra of D-glucose in H_2O.

depends on the ability of hydroxyl groups in axial orientations to interact with the exocyclic hydroxymethyl group and the ring oxygen which are involved in the majority of normal modes found in this region:[2-6] indeed, other monosaccharides such as D-galactose and D-mannose, containing axial hydroxyl groups show large ROA signals here.[1] The relatively low density of bands simplifies the assignment of the conventional vibrational spectrum and patterns have been found that can identify anomeric configuration in monosaccharides and can distinguish between certain glycosidic linkage types.[9,10] Furthermore, the sensitivity of the ROA in this region to anomeric configuration also makes it important for studying the conformation of the glycosidic link in α-linked di- and polysaccharides of D-glucose as we shall see later.

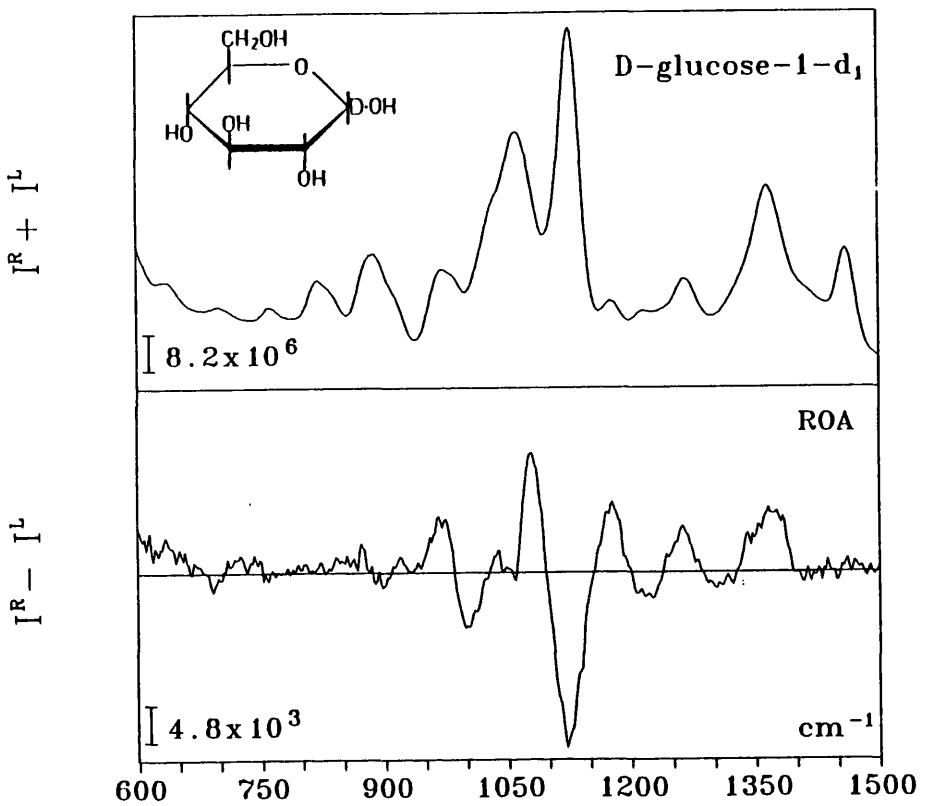

Figure 5.2 The backscattered Raman ($I^R + I^L$) and ROA ($I^R - I^L$) spectra of D-glucose-1-d_1 in H_2O.

The conventional Raman band of weak to medium intensity at ~ 910 cm^{-1} in D-glucose can in fact be resolved into two components with the higher wavenumber constituent giving rise to a positive ROA signal at ~ 913 cm^{-1}. This signal corresponds to the feature reported at ~ 920 cm^{-1} in the earlier work on monosaccharide ROA[1] (the disparity between the two quoted wavenumbers can be attributed to noise fluctuations on some signals which results in a greater uncertainty of the peak positions in the ROA signals than in the parent Raman bands). Comparison of the conventional Raman spectra of α- and β-D-methyl glucopyranoside[1] suggests that this band is characteristic of the α-anomeric form in accord with Barker *et al.*[10] who attributed this normal mode to a ring vibration of the α-anomer. This ROA signal

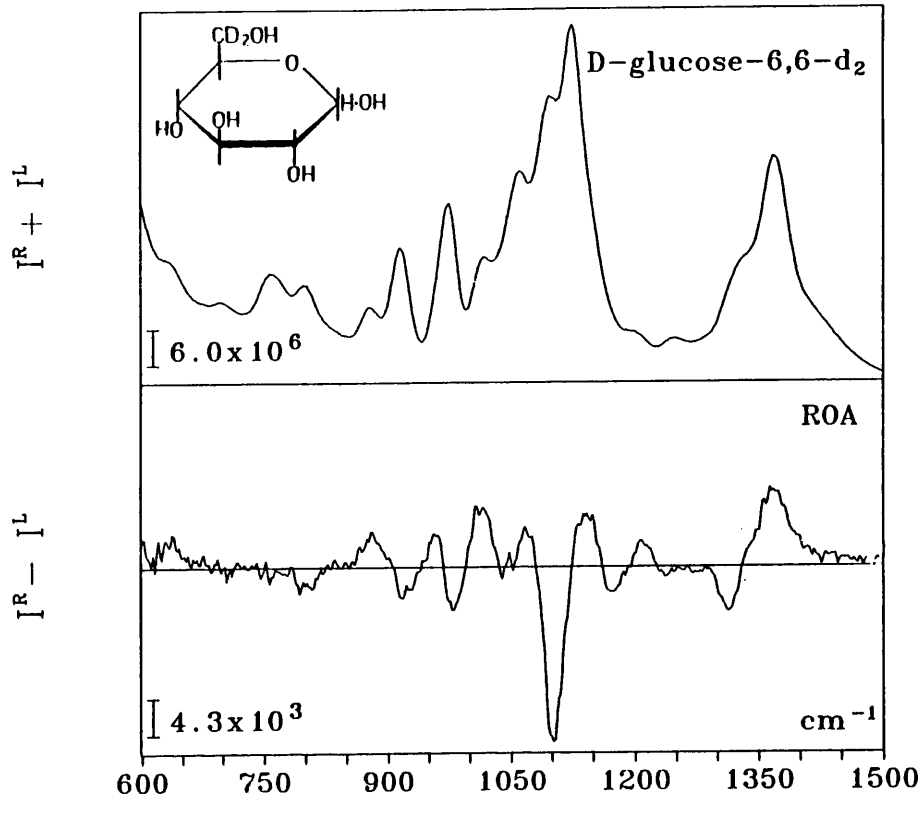

Figure 5.3 The backscattered Raman ($I^R + I^L$) and ROA ($I^R - I^L$) spectra of D-glucose-6,6-d_2 in H_2O.

vanishes upon deuteration of the C-1–H position (Figure 5.2) and gives rise to a weak negative feature when the C-6–H_2 positions are deuterated (Figure 5.3) thus exposing the role that motions of these groups play in the generation of the associated ROA. Finally, a C-O-H deformation contribution to the normal mode can be identified from the wavenumber shift of the conventional Raman band in D-glucose-O-d_5 (Figure 5.4); however, it is not clear whether the associated ROA band is also shifted as other ROA signals shifted into this region lead to a broad ROA signal at this wavenumber. Normal coordinate analyses[2-6] assign this mode to a highly coupled vibration involving the C-1–O stretching coordinate, endocyclic ring stretching coordinates and deformation coordinates around the anomeric carbon. Combining all

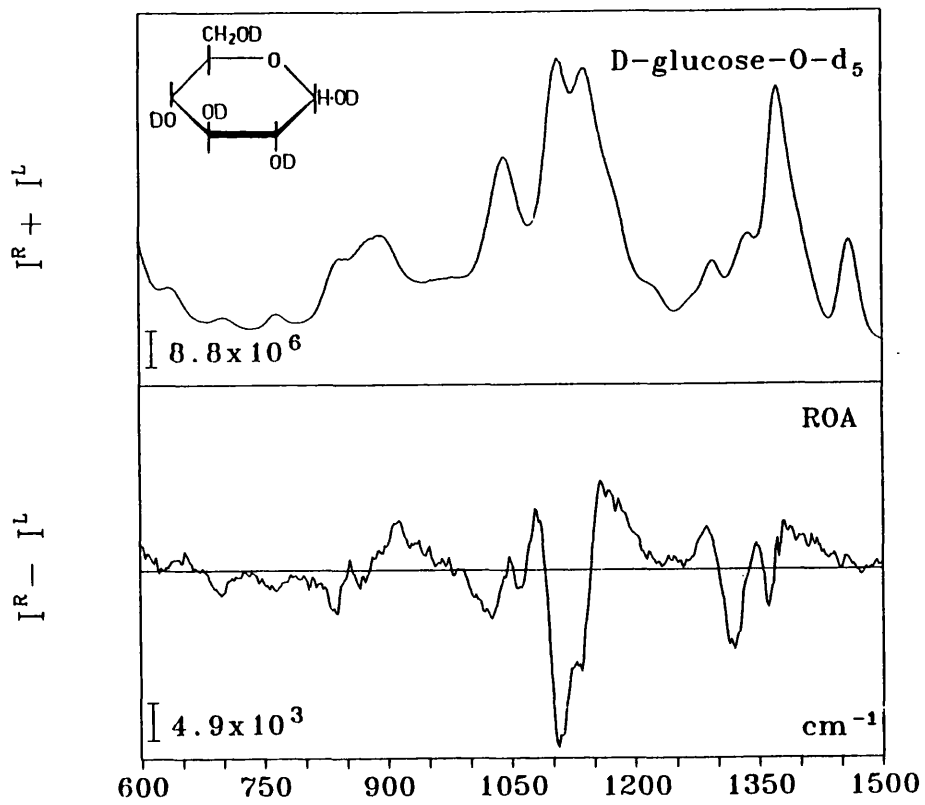

Figure 5.4 The backscattered Raman ($I^R + I^L$) and ROA ($I^R - I^L$) spectra of D-glucose-O-d_5 in D_2O.

these data it is possible to assign this vibrational mode to a ring vibration of the α-anomeric form coupled to C-O stretches around the ring with contributions from C-1–H and CH_2 motions.

Two conventional Raman bands which are considered indicative of the presence of the α- and β-anomers are found at ~ 840 cm^{-1} and ~ 890 cm^{-1}, respectively. Although neither gives any ROA signal in D-glucose both were highlighted in earlier work as being important signals in other monosaccharides and the band at ~ 840 cm^{-1} also gives rise to interesting ROA signals in α-linked disaccharides. Early conventional IR studies assigned these bands to vibrations involving C-1–H deformations of the α- and β-anomers.[10] However, only small changes are evident for these two bands in the Raman spectrum of D-glucose-1-d_1 and much

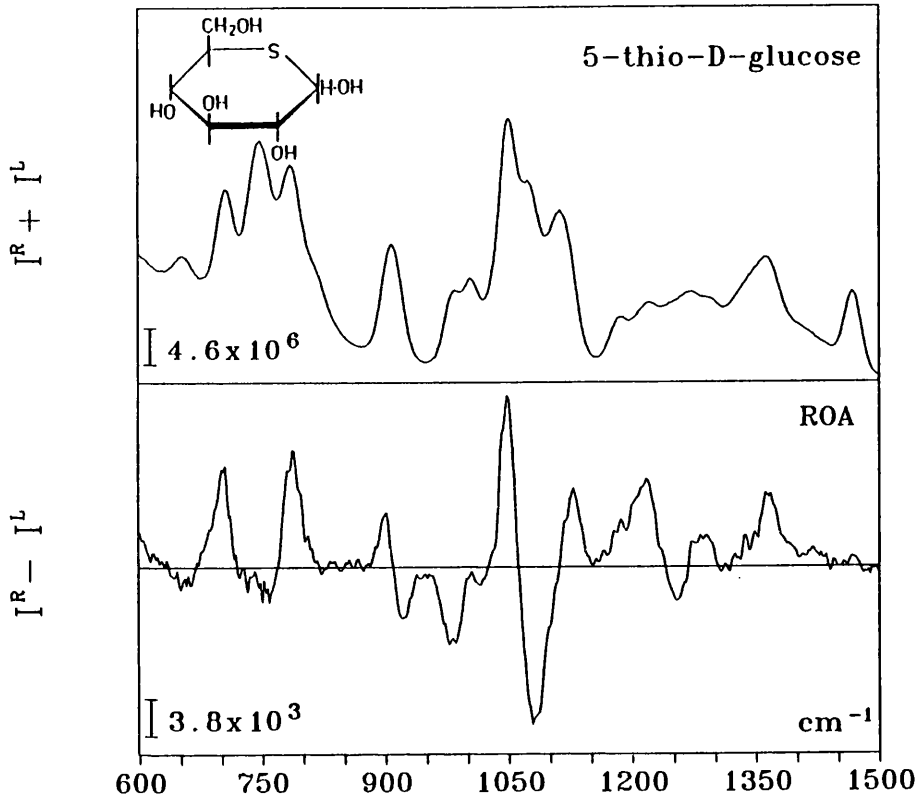

Figure 5.5 The backscattered Raman ($I^R + I^L$) and ROA ($I^R - I^L$) spectra of 5-thio-D-glucose in H_2O.

larger shifts are observed in the spectrum of D-glucose-6,6-d_2. For D-xylose,[1] which has the same configuration at all the chiral centres as D-glucose but lacks an exocyclic hydroxymethyl group, the band at 840 cm^{-1} disappears and in the spectrum of 5–thio–D-glucose (Figure 5.5), which has the ring oxygen replaced by a sulphur atom, the band is shifted to lower wavenumber. From these results it would appear that this vibration involves motions of the CH_2, C–O-5 and a small contribution from the C-1–H group which is almost identical to the normal mode predicted by Cael *et al.*[2] and concurs with the work of Korolevich *et al.*[4] who suggested that the C-1–H contribution was a minor one with the majority of the potential energy arising from motions of the O-1–C-1–O-5–C-5–C-6 chain.

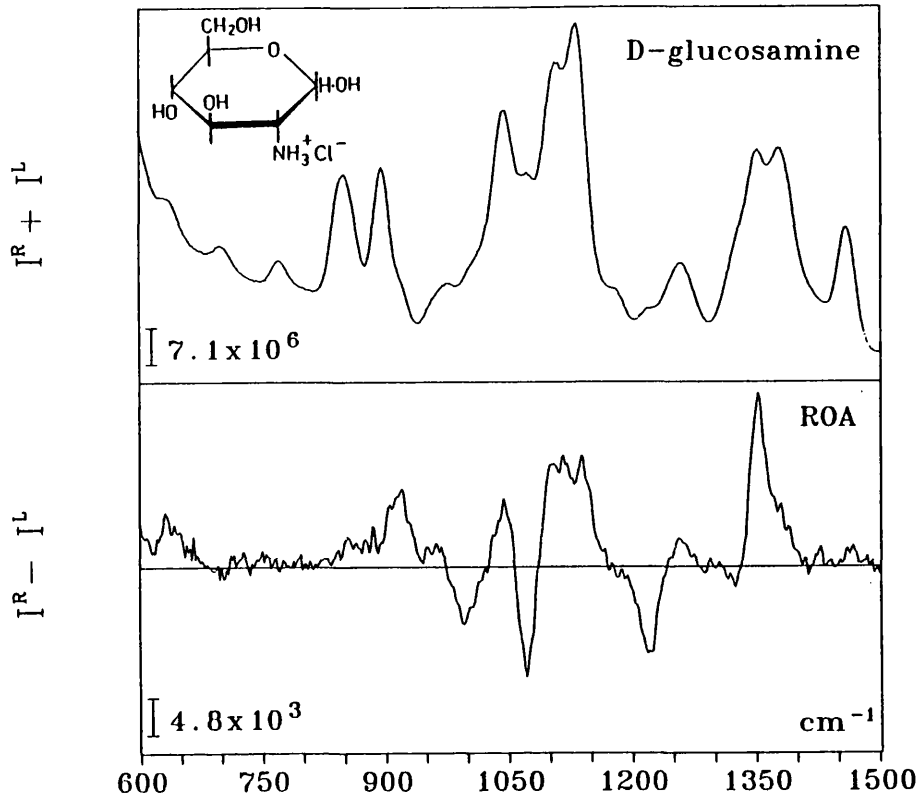

Figure 5.6 The backscattered Raman ($I^R + I^L$) and ROA ($I^R - I^L$) spectra of D-glucosamine hydrochloride in H_2O.

The replacement of oxygen by sulphur in 5-thio-D-glucose leads to a dramatic increase in the intensity of the Raman and ROA signals between ~ 700 and 800 cm^{-1}, leading to the conclusion that C-O-C bending motions about the ring oxygen are intimately involved in these normal modes in D-glucose, a view which is supported by normal coordinate analyses.[2-6] The ROA spectrum of D-glucosamine hydrochloride (Figure 5.6) is similar to that of D-glucose in this region with only the two positive bands appearing at ~ 913 cm^{-1} and ~ 633 cm^{-1}. It would appear then that the NH_3^+ substituent on carbon atom 2 has no direct effect on the ROA in this region.

5.2.2 Fingerprint Region (~ 950-1200 cm^{-1})

This region of the conventional Raman spectrum is dominated by exo- and endocyclic C-O and C-C stretches coupled with significant contributions from C-O-H deformations.[2-6] It was noted in a review of the vibrational spectra of carbohydrates[12] that this region is difficult to interpret on account of the widespread coupling of C-O and C-C stretches, the poor discrimination between exo- and endocyclic contributions and the small differences between the configurational positions of each C-O group. This is not the case for ROA where the extensive coupling is a prerequisite for strong ROA signals and configurational changes have a comprehensive and characteristic effect on the ROA pattern in this region.[1]

For D-glucose (Figure 5.1) the characteristic sign pattern is, starting from low wavenumber; negative at ~ 988 cm^{-1}, positive at ~ 1048 cm^{-1}, negative at ~ 1111 cm^{-1} and positive at ~ 1150 cm^{-1}. Previous ROA studies[1,13] compared D-glucose with D-xylose in this region and their sign patterns were found to be the same although small wavenumber shifts were evident. D-xylose differs from D-glucose only in that it has no exocyclic hydroxymethyl group; thus, it is clear that the ROA signals in this region are not dependent on motions of this group. The effect of endocyclic C-O stretches in this region can be gauged by examining the ROA spectrum of 5-thio-D-glucose (Figure 5.5) where it is noted that the signals at ~ 1150 cm^{-1} and ~ 1111 cm^{-1} in D-glucose are shifted to ~ 1128 cm^{-1} and ~ 1078 cm^{-1}, respectively, although they retain the same sign and intensity, and that the two other signals are unaffected. From these observations it can be deduced that the signals at ~ 1150 cm^{-1} and ~ 1111 cm^{-1} involve some endocyclic C-O stretch contribution, which is in accord with a normal coordinate analysis[4]

which placed a 41% potential energy contribution from the C-O-5 stretching coordinate to a normal mode at 1116 cm^{-1}.

The ROA spectrum of D-glucosamine hydrochloride (Figure 5.6), which has the hydroxyl group at carbon atom 2 replaced by an NH_3^+ group while retaining the same configuration, reveals profound changes in this region. The negative and positive signals at lower wavenumber are retained; however, at higher wavenumber the pattern changes quite dramatically. This is probably due to the C-2–N stretch coordinate which is expected[14] to contribute to normal modes between ~ 1020 and 1220 cm^{-1} and which will couple to the C-O and C-C stretching coordinates in a different way to the C-2-O stretch coordinate which is present in D-glucose.

Examining the ROA spectrum of D-glucose in D_2O (Figure 5.4) it is clear that it displays the same sign pattern in the fingerprint region as found for D-glucose in H_2O. The conventional Raman spectrum, however, does show changes, namely a new band at ~ 1108 cm^{-1} and a shift from ~ 1060 cm^{-1} to 1042 cm^{-1} of another. Furthermore, normal coordinate analyses attribute a significant contribution to C-O-H deformations in this region. From these data it may be concluded that, although C-O-H deformations make a significant contribution to the conventional Raman band frequencies and intensities in this region, they actually contribute very little to the associated ROA band intensities, which are generated mainly by the exo- and endocyclic C-O and C-C stretch coordinates within the normal modes.

The ROA of D-glucose-1-d_1 (Figure 5.2) shows only one minor change, namely a wavenumber shift of the positive signal at ~ 1150 cm^{-1} in D-glucose to ~ 1175 cm^{-1}, indicating that C-1–H deformations

are involved in this normal mode and that deuterating this position decouples the vibration. However, the ROA sign and intensity is unaffected which indicates that other motions must be largely responsible for generating the ROA. The origin of the changes evident in the D-glucose-6,6-d_2 Raman and ROA spectra (Figure 5.3) are difficult to determine because, in addition to shifts in the bands in the fingerprint region, many of the bands in the region above ~ 1200 cm^{-1} have also been shifted into this region. However, the new Raman band appearing at ~ 975 cm^{-1} has previously been assigned to a CD_2 motion[7] and the new Raman band at ~ 1098 cm^{-1} can probably be associated with CD_2 motions shifted from the ~ 1460 cm^{-1} mode in D-glucose which has been shown[2] to be an almost pure CH_2 vibration (this fits with the ratio of associated wavenumbers in D-glucose and D-glucose-6,6-d_2 which is close to the theoretical maximum of $\sqrt{2}$ for a corresponding isotopic wavenumber shift).[15]

5.2.3 CH_2 and COH Deformations Region (~ 1200-1500 cm^{-1})

The effects of deuteration in this region are far more pronounced than at lower wavenumber because there are no added complications of overlap from bands shifted from higher wavenumber. Previous assignments for C-deuterated glucoses were based on work carried out by conventional IR in the solid state[7] or FT-IR in D_2O,[8] but such results are not necessarily transferable to Raman in H_2O for two reasons: first IR and Raman are complementary techniques governed by different selection rules and giving different intensities, and second the solid state conformation will not necessarily be the same as the solution conformation. The major contributions to normal modes in this region come from CH_2, C-O-H and C-H deformations[1] so that samples with these groups deuterated, as discussed here, should be of particular

interest. Earlier ROA studies[1,13] concentrated on the influence of the exocyclic hydroxymethyl group in this region.

D-glucose (Figure 5.1) exhibits a ROA couplet, negative at low wavenumber and positive at high, centred at ~ 1240 cm^{-1} which is unaffected by C-1–H deuteration (Figure 5.2) but is shifted to lower wavenumber in D-glucose-6,6-d_2 (Figure 5.3) and is absent in D-glucose-O-d_5 (Figure 5.4). For D-glucose-6,6-d_2 the couplet remains intact and is centred at ~ 1190 cm^{-1}, which when combined with its sensitivity to O-deuteration implies that this couplet originates in a mode involving coupling between CH_2 and C-O-H vibrations. In fact, on the basis of O-deuteration of dextran, an α-(1-6) linked polysaccharide, which exhibits no change in the ~ 1260 cm^{-1} Raman band, Vasko *et al.*[7] assigned this band to a C-6–O-H bending mode. Support for this assignment was provided by a normal coordinate analysis[2] which described a mode at 1259 cm^{-1} involving motions of the CH_2, C-6–O-H and C-O-H groups all around the ring. Furthermore, recent conventional solid-state Raman work on glucose isotopomers assigned bands at 1267 cm^{-1} and 1206 cm^{-1} to CH_2 related modes.[6]

Although both α- and β-D-methyl glucopyranosides are known from NMR studies[16] to have similar distributions of *gauche-gauche* (GG) and *gauche-trans* (GT) rotamers of the exocyclic hydroxymethyl group (Figure 5.7) only the β-D-methyl glucopyranoside shows both the positive and negative constituents of the ~ 1240 cm^{-1} ROA couplet shown by D-glucose itself. The positive feature at 1260 cm^{-1} is absent from the ROA spectrum of α-D-methyl glucopyranoside,[1] and is also absent in the disaccharide trehalose (Figure 7.7) and in α-cyclodextrin (Figure 8.3), both of which exist solely in the α-anomeric form. On the other hand, these last three molecules all show the negative ROA

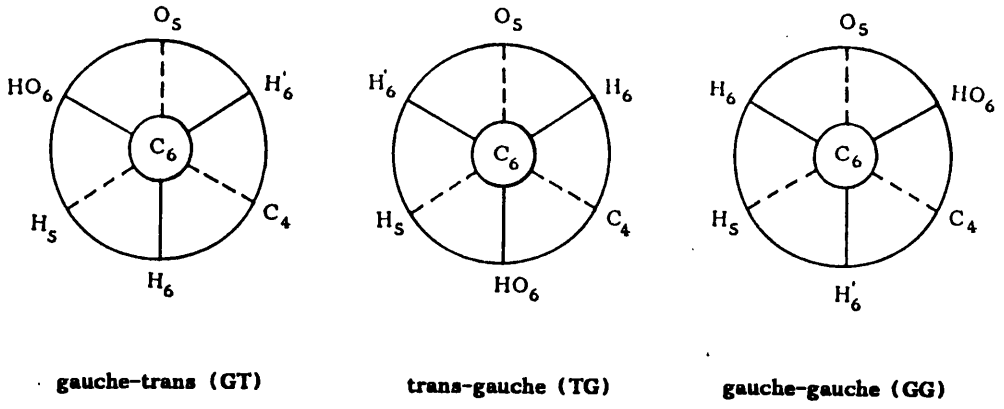

Figure 5.7 The three rotameric forms of the exocyclic hydroxymethyl group.

signal at ~ 1220 cm^{-1}. Thus, the couplet at ~ 1240 cm^{-1} in the ROA spectrum of D-glucosamine hydrochloride (Figure 5.6), which differs from D-glucose only at carbon atom 2, can be explained in terms of the anomeric ratio, which is ~ 2:1 in favour of the α-anomeric form.[17] These facts provide evidence that only the β-anomeric form contributes to the positive band at ~ 1260 cm^{-1} so we would expect it to be considerably weaker than the negative band at ~ 1220 cm^{-1} as is indeed the case for D-glucosamine hydrochloride.

Since our deuteration studies indicate that similar vibrational coordinates contribute to the ~ 1220 cm^{-1} and ~ 1260 cm^{-1} ROA signals, it is tempting to attribute these two signals to the corresponding normal vibrations of two distinct conformers; but these cannot be simply α- and β-anomers since, as mentioned above, β-D-methyl glucopyranoside shows both bands. One possibility is that the positive ~ 1260 cm^{-1} ROA signal arises from the GT rotamer of the β-anomer in the D-glucose homomorphic series, and that the negative ~ 1220 cm^{-1} ROA signal arises from the GG rotamer and is independent of the

anomeric configuration. Supporting evidence for this suggestion includes the observations on the D-galactose homomorphic series discussed below.

It was noted in the earlier monosaccharide work that D-galactose and both the methyl galactosides exhibit a strong positive ROA signal at ~ 1260 cm^{-1} which recent normal coordinate analysis results[18] have attributed to a normal mode involving C-4–O-H and C-6–O-H motions. In D-galactose the anomeric population is approximately the same as in D-glucose but the hydroxyl substituent on carbon atom 4 is in an axial orientation. This means that the hydroxymethyl group exists in either the *gauche-trans* (GT) or *trans-gauche* (TG) rotameric forms with the *gauche-gauche* (GG) form being strongly disfavoured as a result of the syn-diaxial relationship of the C-4–OH and C-6–OH groups[16] (Figure 5.7). The ROA signal at ~ 1260 cm^{-1} in D-galactose[1] is very intense and this may be due to the proximity of the C-6–O-H and C-4–O-H groups, especially in the TG rotameric form. This is an example of the local nature of many ROA signals and could explain why this signal is not sensitive to the configuration at carbon atom 1 in the galactose homomorphic series since the effect from carbon atom 4 overwhelms that from carbon atom 1. None of the spectra in the D-galactose series exhibits a negative ROA signal at ~ 1220 cm^{-1} which may provide further evidence for an assignment to the GG rotamer because, as mentioned above, the GG rotamer is strongly disfavoured in molecules with an axial C-4–O-H group so we would not expect any associated ROA signal in D-galactose.

The conventional Raman band at ~ 1332 cm^{-1} in D-glucose is found to have shifted to lower wavenumber in the spectra of D-glucose-1-d_1 and the associated ROA couplet, negative at low and positive at high

wavenumber disappears, but remains unchanged in the spectra of the other deuterated analogues. A conventional IR survey[19] of a variety of monosaccharides selectively deuterated at carbon atom 1 revealed that a C-1–H deformation mode appears between 1275 cm^{-1} and 1340 cm^{-1}. In particular, a band at 1312 cm^{-1} in the spectrum of β-D-glucose was found to shift to 972 cm^{-1} upon deuteration. Thus, the Raman band appearing at ~ 970 cm^{-1} along with the associated positive ROA signal in D-glucose-1-d_1 which is not present in D-glucose may be attributed to a C-1–D deformation that has been shifted from ~ 1332 cm^{-1}. It may be noted that the sign of the ROA band has changed and this probably reflects the different coupling opportunities of the C-1–D bending coordinate. The experimental data imply that the ~ 1332 cm^{-1} mode contains no C-O-H or CH_2 deformation contribution and consists of an almost pure C-1–H deformation motion instead. FT-IR studies[8] attributed this mode to a coupled motion of C-1–H and C-5–H bends and it is predicted by normal coordinate analysis to contain contributions from all the C-H deformations around the ring.[2-6] The deformations of the C-1–H bond would appear then to play an important role in the generation of the ROA couplet centred at ~ 1332 cm^{-1}.

The positive ROA band centred at ~ 1360 cm^{-1} in D-glucose displays distinct structure and would appear to consist of three components. The first component is the positive constituent of the ROA couplet centred at ~ 1332 cm^{-1}. Upon deuteration of the hydroxyl groups the central component is shifted from ~ 1364 cm^{-1} to ~ 1288 cm^{-1} and can thus be assigned to a C-O-H deformation. Assignment of the final component is more difficult as it is unaffected in the deuterated analogues but normal coordinate analyses seem to indicate that it is a C-H related mode.

5.3 Concluding Remarks

The ROA spectra reported and discussed in this chapter highlight a number of important features which pertain not only to carbohydrate examples but also to the fundamental nature of ROA generation. In particular, as we saw in the case of the ROA bands in the fingerprint region, not all of the internal stretching and bending coordinates which make up the normal mode and affect the intensity of the parent Raman band are necessarily involved in the generation of the associated ROA signals which often seem to be largely determined by the vibrational coordinates of the skeleton. Similar behaviour has been observed for the ROA associated with skeletal modes in other molecules, including tartaric acid and its O-deuterated analogue,[20] and illustrates how the sensitivity of ROA to chirality renders it a more effective probe of molecular conformation than conventional vibrational spectroscopy.

For carbohydrates, the three regions of the ROA spectrum have been found to give different types of stereochemical information which are summarised in Table 5.1. The anomeric region, although not very informative for the D-glucose monomer, has been shown to be sensitive to the anomeric configuration in many other monosaccharides[1] and also to contain signals related to the type and conformation of the glycosidic link in di- and oligosaccharides containing D-glucose residues.[13,21,22] The fingerprint region has proven to be sensitive to the configuration at the individual chiral centres and as such can provide a direct probe of the structural framework of carbohydrates. The stereochemistry of the pendant side groups is most important in the generation of the ROA signals occurring above ~ 1200 cm^{-1} and this region could, in the future, provide conformational data on features such as the rotameric populations of the exocyclic hydroxymethyl group.

The next step towards a complete understanding of the D-glucose ROA spectrum would obviously involve *ab initio* ROA intensity calculations, introduced in chapter 2, which would provide details of the vibrational coordinates contributing to each ROA signal and help elucidate stereochemical features such as CH_2OH rotameric populations. However, other future developments could include recording the ROA in the C-H stretch region where, despite the difficulties encountered, interesting stereochemical correlations may be found. Similarly, with the availability of improved filter technology more of the ROA spectrum towards lower wavenumber may become accessible. Another interesting possibility would be to study the kinetics of the anomeric equilibrium using ROA. Such a study would probably require shorter acquisition times than are presently possible but may prove to be a valuable source of information on the dependence of the ROA signals on the anomeric configuration.

Table 5.1 Assignment of ROA signals in the spectrum of D-glucose.

Wavenumber in cm^{-1} (sign)	*ROA assignments*	*Comments*
~ 913 (+)	C-C, C-O stretches C-O-H, C-1–H and CH_2 deformations	This ring vibration of the α-anomer is coupled to C-O stretches with C-1–H and CH_2 contributions
~ 950-1200 (-+-+)	C-C and C-O stretches	This sign pattern is characteristic for ring substitution. C-O-H deformations are not involved in the generation of the ROA
~ 1220 (-)	CH_2 and C-O-H deformations	This signal is characteristic for the GG rotamer in both α- and β-anomeric forms
~ 1260 (+)	CH_2 and C-O-H deformations	This signal is characteristic for the GT rotamer in the β-anomeric form
~ 1332 (-+)	C-1–H deformation	

References

1. Z. Q. Wen, L. D. Barron and L. Hecht, *J. Am. Chem. Soc.*, **115** (1993) 285-292.
2. J. J. Cael, J. L. Koenig and J. Blackwell, *Carbohydr. Res.*, **32** (1974) 79-91.
3. M. Dauchez, P.h.d. Thesis, University of Lille, 1990.
4. M. V. Korolevich, R. G. Zhbankov and V. V. Sivchik, *J. Molecular Structure*, **20** (1990) 301-313.
5. H. A. Wells and R. Atalla, *J. Mol. Struct.*, **224** (1990) 385-424.
6. M. Dauchez, P. Derreumaux, G. Vergoten, *J. Computational Chem.*, **14** (1993) 263-277.
7. P. D. Vasko, J. Blackwell and J. L. Koenig, *Carbohydr. Res.*, **19** (1971) 297-310.
8. D. M. Back and P. L. Polavarapu, *Carbohydr. Res.*, **165** (1987) 173-187.
9. L. D. Barron, *Molecular Light Scattering and Optical Activity*, Cambridge University Press, Cambridge, 1982.
10. S. A. Barker, E. J. Bourne, M. Stacey and D. H. Whiffen, *J. Chem. Soc.*, (1954) 171-176.
11. L. M. J. Verstraeten, *Anal. Chem.*, **36** (1964) 1040-1044.
12. M. Mathlouthi and J. L. Koenig, *Adv. Carbohydr. Chem. Biochem.*, **44** (1986) 7-89.
13. L. D. Barron, A. R. Gargaro and Z. Q. Wen, *Carbohydr. Res.*, **210** (1990) 39-49.
14. R. S. Tipson, *National Bureau of Standards Monograph*, **110** (1968).
15. S. Pinchas and I. Laulicht, *Infrared Spectra of Labelled Compounds*, Academic Press, London, 1971.
16. Y. Nishida, H. Ohrui and H. Meguro, *Tetrahedron Lett.*, **25** (1984) 1575-1578.

17. D. Horton, J. S. Jewell and K. D. Philips, *J. Org. Chem.*, **31** (1966) 4022-4025.

18. M. Sekkal, P. Legrand, G. Vergoten and M. Dauchez, *Spectrochim. Acta*, **48A** (1992) 959-973.

19. S. A. Barker, R. H. Moore, M. Stacey and D. H. Whiffen, *Nature*, **186** (1960) 307-309.

20. L. D. Barron, A. R. Gargaro, L. Hecht, P. L. Polavarapu and H. Sugeta, *Spectrochim. Acta.*, **48A** (1992) 1051-1066.

21. A. F. Bell, L. Hecht and L. D. Barron, *J. Am. Chem. Soc.*, **116** (1994) 5155-5161.

22. L. D. Barron, A. R. Gargaro, Z. Q. Wen, D. D. MacNicol and C. Butters, *Tetrahedron: Asymmetry*, **8** (1990) 513-516.

Chapter 6

Vibrational Raman Optical Activity of Ketoses

In this chapter the assignment of the ROA spectra of monosaccharides is extended by studying four ketohexoses, namely, D-fructose, L-sorbose, D-tagatose and D-psicose. The opportunity is also taken to complete and, where necessary, correct the ROA assignments proposed by Wen *et al.*[1] making use of the larger body of experimental data now available.

From a consideration of the stereochemistry of ketose sugars, which has already been discussed in chapter 4, it is clear that they provide an opportunity to study the influence of the exocyclic hydroxymethyl group on the ROA and provide additional examples of monosaccharides with which to extend our understanding of the generation of ROA. Furthermore, since D-fructose residues occur in many oligo- and polysaccharides, the results presented here will be useful in future classifications of the ROA spectra of these molecules.

The application of conventional vibrational spectroscopy to the study of ketose sugars has been even more limited than for the other monosaccharides. Mathlouthi *et al.* proposed on the basis of relative intensities that a number of Raman bands could be assigned to the pyranose and furanose forms.[2] It was later shown that the majority of the bands assigned to the furanose form were also present in the vibrational spectrum of crystalline β-D-fructose which is known to exist solely in the β-pyranose form.[3] For this reason it was concluded that conventional vibrational spectra were of limited potential for studying

the solution equilibrium between the five- and six-membered ring forms of sugars. However, of potential diagnostic value is a ketose marker band at 1175 cm^{-1} identified in the solid-state Raman spectra of D-fructose and L-sorbose.[4]

6.1 Experimental

Samples of D-fructose, D-tagatose and D-psicose were supplied by Sigma, and L-sorbose by Fluka. The ketose samples were dissolved in distilled H_2O to a concentration of 4.5 M then allowed to equilibrate at room temperature for at least 24 h. The equilibrated samples were treated with charcoal to reduce fluorescence, filtered into quartz microfluorescence cells through 0.45 μm Millipore membrane filters to remove any dust particles that may cause spurious light scattering, then centrifuged for at least 15 min. During spectral acquisition the laser power was ~ 700 mW at the sample and the slit width was set for 120 μm giving a spectral bandpass of ~ 12 cm^{-1} at 514.5 nm. The spectra were recorded over 2 to 4 h at constant ambient temperature. By employing the latest generation of holographic super notch plus filter[5] the backscattered ROA could be obtained from ~ 250 cm^{-1} for the first time.

6.2 Results and Discussion

The Raman and ROA spectra of D-fructose, L-sorbose, D-tagatose and D-psicose in aqueous solution for the range ~ 250 to 1500 cm^{-1} are presented in Figures 6.1-6.4, respectively. Table 6.1 compares the conformational equilibria in aqueous solution as determined by NMR[6-8] for the four ketose sugars presented in this chapter. All four heavily favour the anomeric configuration which places the bulky hydroxymethyl

Table 6.1 Conformational equilibria of ketose sugars in aqueous solution.

	D-Fructose	L-Sorbose	D-Tagatose	D-Psicose
α-pyranose	–	98%	79%	22%
β-pyranose	75%	–	16%	24%
α-furanose	4%	2%	1%	39%
β-furanose	21%	–	4%	15%
chair conformation	$^{2}C_{5}$	$^{2}C_{5}$	$^{5}C_{2}$	$^{5}C_{2}(\alpha)$, $^{2}C_{5}(\beta)$
reference	6-8	6	6	6,10

group in the less sterically hindered equatorial orientation for pyranose forms, and pseudo-equatorial orientation for furanose forms. (Note that the anomeric designators α- and β- correspond to the axial and equatorial orientations of the anomeric hydroxyl group for D-sugars in the $^{5}C_{2}$ chair conformation, respectively, and that changing either to a different chair conformation or to an enantiomeric L-sugar reverses the assignment of these anomeric designators). These differences in the conformational equilibria arise because each ketose sugar has a different orientation of the hydroxyl groups at carbon atoms 3,4 and 5, so that each has a unique set of steric and electronic interactions governing its structure.[9]

Comparison with the ROA of other monosaccharides is best accomplished by subdividing the sugars studied into groups having the same orientation of the hydroxyl groups (axial or equatorial) at carbon atoms 3,4 and 5 of the ketose sugars and carbon atoms 2,3 and 4 of the aldose and pentose sugars. Thus, the monosaccharides studied to date can be grouped into four distinct configurational types: the *xylo*- type, with all three hydroxyl groups in an equatorial orientation, the *lyxo*- type, with the hydroxyl group at carbon atom 2 in the aldose and pentose sugars but at carbon atom 3 in the ketose sugars in an axial orientation, the *ribo*- type, with the hydroxyl group at carbon atom 3 in the aldose and pentose sugars but at carbon atom 4 in the ketose sugars in an axial orientation, and, finally, the *arabino*- type, with the hydroxyl group at carbon atom 4 in the aldose and pentose sugars but at carbon atom 5 in the ketose sugars in an axial orientation. The differences between the ketose and the aldose and pentose sugars are due to the different numbering schemes that they have. (Note that monosaccharides of the same configurational type do not necessarily have the same anomeric populations or the same chair conformation).

The ROA spectra of monosaccharides of the same configurational type are known to be closely related,[1] as the orientation of groups around the ring determines the position and intensity of the ROA signals while the sign is dependent on the absolute configuration at each of the chiral centres embraced by the normal modes responsible. Therefore, it is possible to compare directly ketose sugars with aldose and pentose sugars with the same orientation of the ring hydroxyl substituents, to determine the similarities between monosaccharides of the same configurational type, and also to investigate the effect of the position and occurrence of the hydroxymethyl group and the orientation of the anomeric hydroxyl group on the ROA spectra. Furthermore, D-fructose,

L-sorbose and D-tagatose all exist predominantly in one anomeric form (Table 6.1) which would be expected to dominate the ROA and allow direct comparisons among the ketose sugars. Thus, the major anomers of D-fructose and L-sorbose both adopt a $^2C_5$ chair conformation and differ only in the orientation and absolute configuration of the hydroxyl group at carbon atom 5. On the other hand, D-tagatose adopts a $^5C_2$ chair conformation and the hydroxyl group substituted at carbon atom 3 is axial. Note that for D-psicose the predominant conformer is the α-furanose form and that the α- and β-anomeric forms of the pyranose ring adopt a $^5C_2$ and $^2C_5$ chair conformation, respectively, so both have the anomeric hydroxyl group in an axial orientation.[10]

6.2.1 Low Wavenumber Region (~ 250-600 cm^{-1})

In this region normal coordinate analyses of monosaccharides[11-15] assign the Raman bands to normal modes involving exo- and endocyclic bending deformations of the C-C-O, C-C-C, C-O-C and O-C-O groups coupled with associated exo- and endocyclic C-O torsions. It has also been suggested that the intense Raman bands in this region involving C-C-O deformations around the anomeric carbon atom are among the most sensitive to anomeric configuration in the entire monosaccharide spectrum.[16] Furthermore, the sensitivity of the skeletal bending and twisting vibrations located in this region to small structural changes results in large variations in the conventional vibrational spectra for monosaccharides.[17] This region has only recently become accessible to backscattering ROA measurements so the body of data is still limited.

The ROA spectra of the four ketose sugars presented here appear to be highly individual which is to be expected given the sensitive nature of the skeletal modes found in this region. One common feature is a

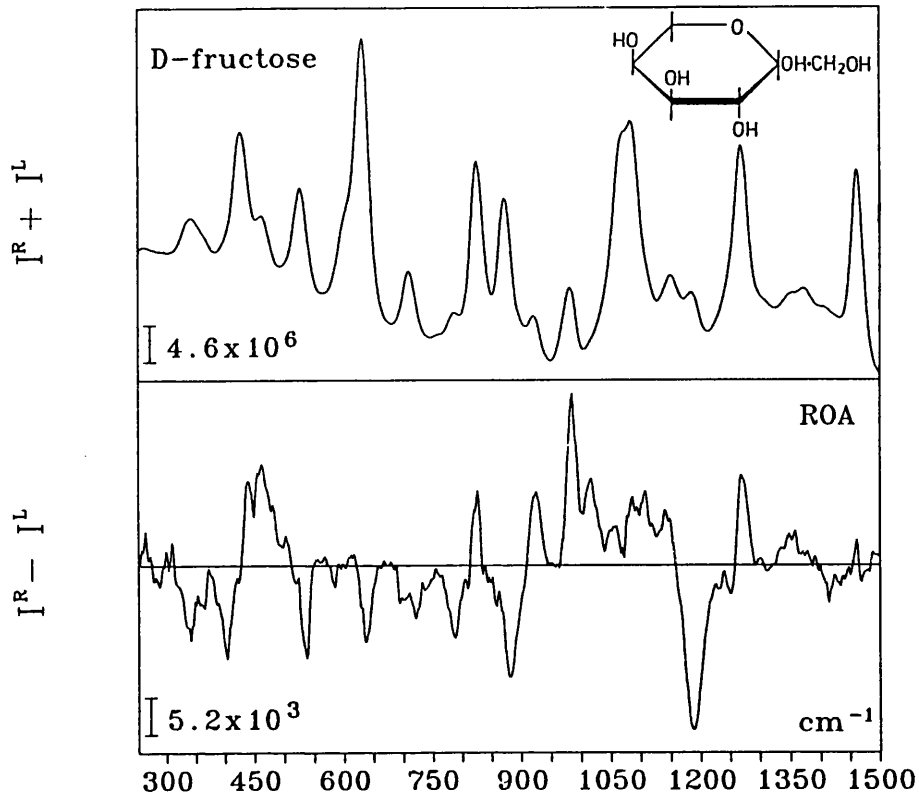

Figure 6.1 The backscattered Raman ($I^R + I^L$) and ROA ($I^R - I^L$) spectra of D-fructose in H_2O.

ROA couplet centred at ~ 426, 431, 406 and 428 cm^{-1} in D-fructose, L-sorbose, D-tagatose and D-psicose (Figures 6.1-6.4), respectively. This couplet is negative at low and positive at high wavenumber for D-fructose and L-sorbose; whereas its sign is reversed in D-tagatose and D-psicose. A ROA couplet in diglucosides at 430±10 cm^{-1} was believed to originate in vibrations of the glycosidic link due to its absence from the ROA spectrum of D-glucose and will be discussed in more detail in the following chapter. However, it would appear that this is not the case in other monosaccharides and instead this couplet may simply be associated with deformations around the anomeric centre. Thus, although all four ketose sugars have a preponderance of the axial orientation of the anomeric hydroxyl group, the absolute configuration at

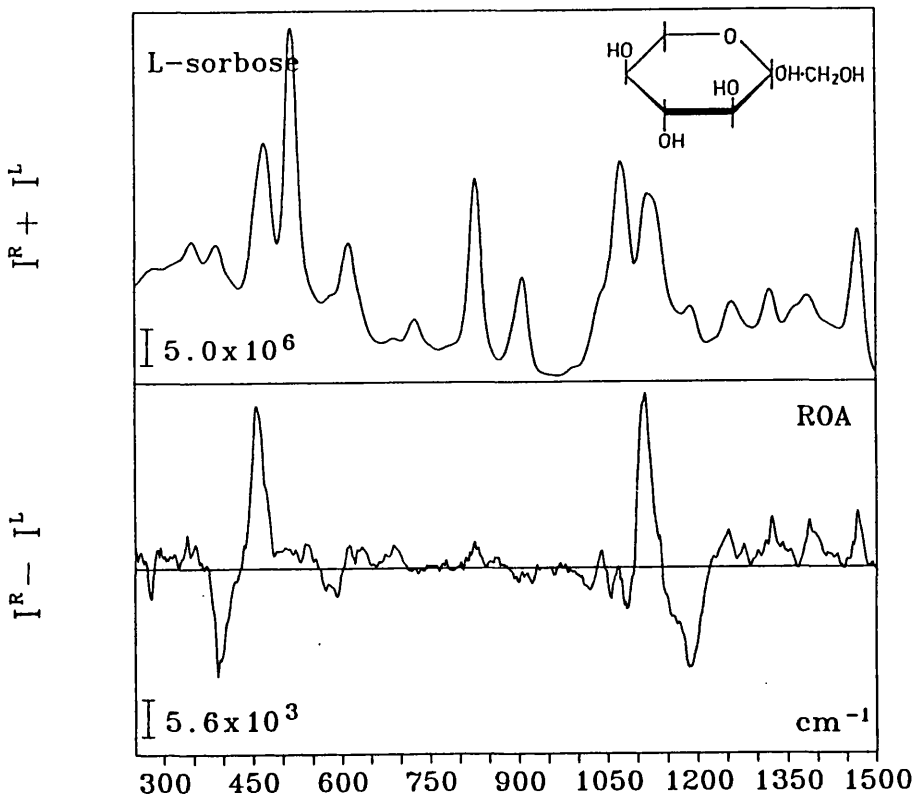

Figure 6.2 The backscattered Raman ($I^R + I^L$) and ROA ($I^R - I^L$) of L-sorbose in H_2O.

the anomeric centre is different for D-fructose and L-sorbose, which both adopt a $^2C_5$ chair conformation, as compared to D-tagatose, for which the α-pyranose form adopts a $^5C_2$ chair conformation, resulting in opposite signs for this couplet. D-psicose exhibits the same sign as D-tagatose because the α-pyranose and α-furanose forms, which account for 61% of the equilibrium mixture, have the same absolute configuration at the anomeric centre as α-D-tagatose. Furthermore, the sign of this couplet is the same in D-tagatose and D-psicose as in the α-linked disaccharides, which have the anomeric hydroxyl of the non-reducing residue trapped in an axial orientation by the linkage, and an absolute (S) configuration at the anomeric centre. Therefore, we can deduce that D-tagatose and D-psicose also exhibit an absolute (S) configuration at

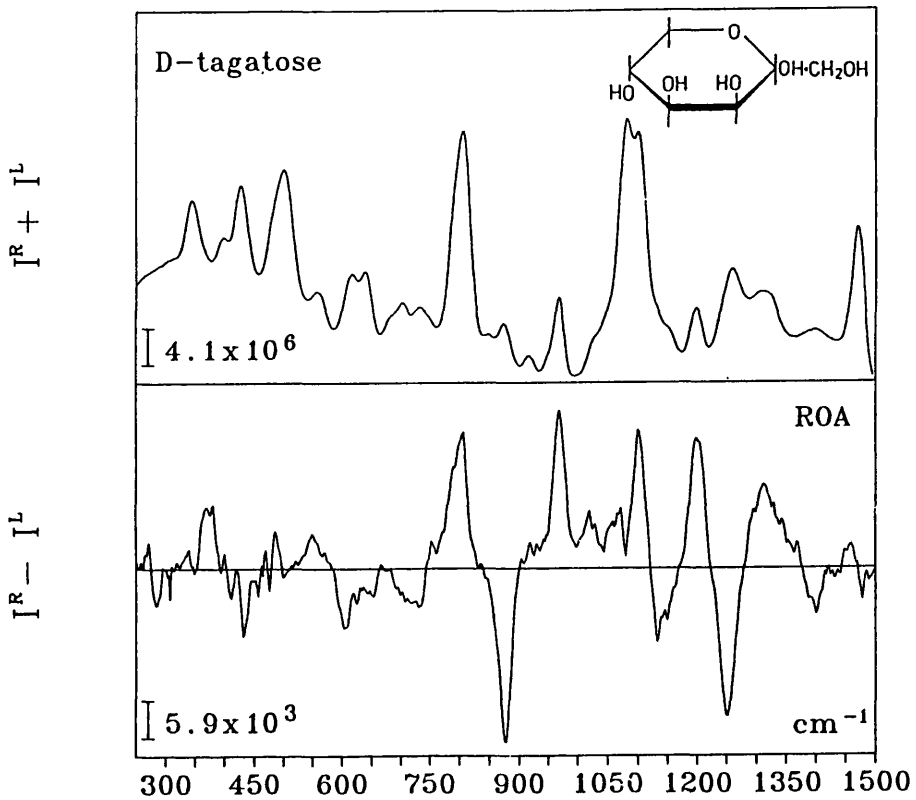

Figure 6.3 The backscattered Raman ($I^R + I^L$) and ROA ($I^R - I^L$) of D-tagatose in H_2O.

this particular chiral centre. Similarly, D-fructose and L-sorbose share the same sign as the β-linked disaccharides at this wavenumber and so it may be concluded that they have an absolute (R) configuration at the anomeric centre. Thus, the sign of this couplet does not depend upon the orientation of the hydroxyl group but rather on the absolute configuration of the anomeric centre.

6.2.2 Anomeric Region (~ 600-950 cm^{-1})

In this region of the conventional vibrational spectrum three sets of bands designated type Ia and Ib at ~ 917±13 and 920±5 cm^{-1}, type IIa and IIb at ~ 844±8 and 891±7 cm^{-1} and type IIIa and IIIb at ~ 766±10

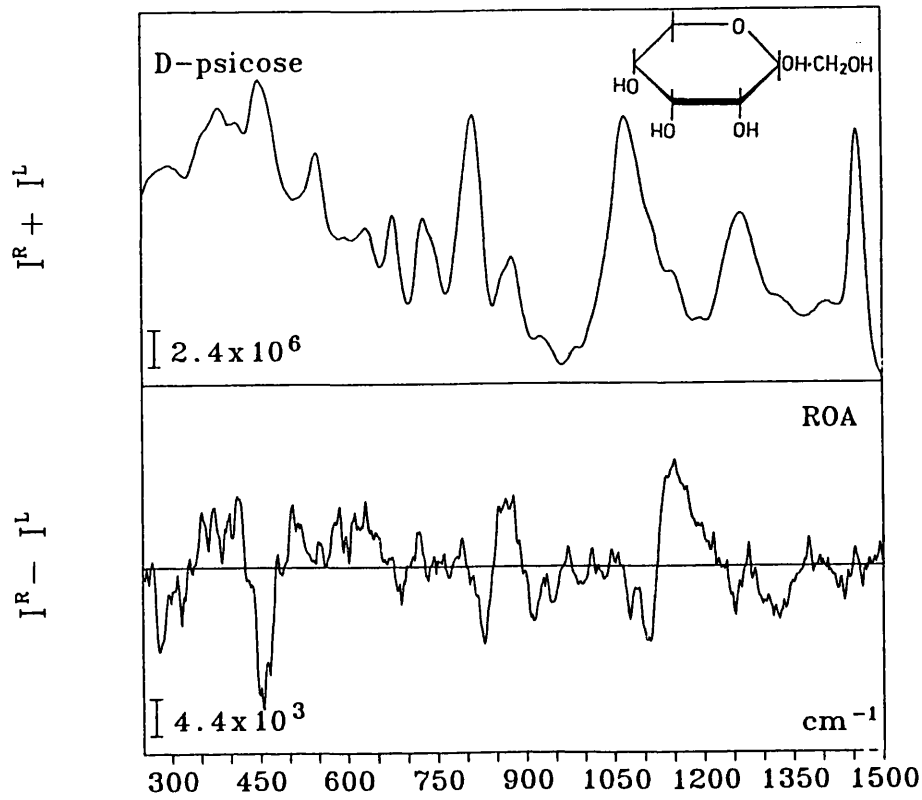

Figure 6.4 The backscattered Raman ($I^R + I^L$) and ROA ($I^R - I^L$) of D-psicose in H_2O.

and 774±9 cm^{-1}, have been found to be sensitive to the anomeric configuration.[18] The three distinct type a and b bands are connected with the axial and equatorial orientation of the anomeric hydroxyl groups, respectively. Furthermore, type IIc bands at 876±9 cm^{-1} and 871±7 cm^{-1} were found to be characteristic of monosaccharides of the *lyxo-* and *arabino-*, respectively.[18]

An earlier ROA study[1] attempted to interpret the monosaccharide spectra in terms of the absolute configuration at the anomeric carbon atom and the signs of the ROA signals of the type IIa and IIb bands at ~ 844 and 891 cm^{-1}. However, in order to fit the ROA data with the absolute configuration at the anomeric centre, type Ia, Ib and type IIc

bands were invoked in some cases but not others and the fact that the vibrational origins of these bands may differ for monosaccharides of different configurational types was not taken into account. This leads to some confusion concerning the generation of ROA in the range between ~ 800 and 950 cm^{-1} which we will attempt to clarify below.

The key to interpretation of the ROA spectra in this range is to separate the monosaccharides into configurational types and to then deal with the axial and equatorial orientations of the anomeric hydroxyl groups separately. The ROA data in this range are listed in Table 6.2 and have been grouped according to the four monosaccharide types: *xylo-*, *arabino-*, *lyxo-* and *ribo-*, respectively. This table also includes relevant information concerning the predominant anomer, its absolute configuration at the anomeric centre, its chair conformation and the orientation of the anomeric hydroxyl group. Normal coordinate analyses of the anomers of D-glucose and D-galactose assigned bands in this range to highly complex, coupled modes involving C-C, C-O, and C-O-C stretching together with CH_2 rocking coordinates.[11-15] These calculations also seem to indicate that, although deformations around the anomeric centre are involved, they may provide only a small percentage of the overall potential energy distribution of the normal modes and that the majority of normal modes are rather delocalised over the ring framework. This would certainly appear to be the case from the ROA spectra for, although the ketose sugars have different substituents on the anomeric carbon as compared to the pentoses and aldoses, indeed they lack any anomeric C-H bond, they still display the same sign pattern as the corresponding pentose or aldose sugars although with some slight wavenumber shifts.

Table 6.2 ROA data in the range ~ 800 to 950 cm^{-1} for monosaccharides.

mono-saccharide	type Ia	type IIb	type IIc	type IIa	major anomer and configuration	chair form
xylo- type						
D-glucose	913(+)			845(0)	64%β eq. (R)	$^4C_1$
D-xylose		895(+)			64%β eq. (R)	$^4C_1$
β-D-methyl-glucoside		896(0)			100%β eq. (R)	$^4C_1$
α-D-methyl-glucoside	904(sp)			860(sp)	100%α ax. (S)	$^4C_1$
L-sorbose	907(sp)			828(sp)	98%α ax. (R)	^2C_S
arabino- type						
D-galactose	906(-)	891(+)	870(-)	821(-)	64%β eq. (R)	$^4C_1$
D-arabinose	924(+)		881(-)	826(+)	60%α ax. (R)	$^4C_1$, $^1C_4$
α-D-methyl-galactoside	917(-)		867(+)	824(-)	100%α ax. (S)	$^4C_1$
β-D-methyl-galactoside		896 (+)	872(-)		100%β eq. (R)	$^4C_1$
D-fructose	924(+)		881(-)	826(+)	75%β ax. (R)	^2C_S
lyxo- type						
D-mannose	914(+)		885(-)	825(+)	67%α ax. (S)	$^4C_1$
D-lyxose	903(+)		883(-)	838(+)	72%α ax. (S)	$^4C_1$, $^1C_4$
α-D-methyl-mannoside	913(+)		877(-)	831(+)	100%α ax. (S)	$^4C_1$
D-tagatose	920(+)		879(-)	805(+)	79%α ax. (S)	$^5C_2$
ribo- type						
D-allose			878(+)		70%β eq. (R)	$^4C_1$
D-ribose	911(-)		883(+)	850(-)	56%β eq. (R)	$^4C_1$
D-psicose	913(-)		879(+)	828(-)	*	$^5C_2$, ^2C_S

sp- strongly polarized, * significant quantities of both anomers

In the preceding chapter the ROA spectra of D-glucose and a number of its deuterated analogues, which come into the category of *xylo*- type monosaccharides, were discussed in detail. It was found that the β-anomeric form generates no ROA between ~ 700 and 880 cm^{-1}. For the α-anomeric form two bands in the conventional Raman spectrum at ~ 904 and 860 cm^{-1} were identified as being strongly polarized and so the corresponding weak ROA signals were treated as unreliable. Nonetheless, the α-anomeric form does exhibit three weak ROA signals in the range ~ 700 to 800 cm^{-1}. The lack of signals for the β-anomeric form can be used to distinguish between the two anomers in mono-, oligo-, and polysaccharides of D-glucose. However, of greater importance is the fact that, for disaccharides of D-glucose, characteristic signatures for many linkage types have been identified in this region which will be discussed in the next chapter. L-sorbose (Figure 6.2) exists almost exclusively in the α-anomeric form in solution and like the α-anomeric form of D-glucose exhibits two strongly polarized Raman bands at ~ 907 and 828 cm^{-1}, the latter being characteristic of the α-anomeric form, but does not exhibit any ROA signals between ~ 700 and 800 cm^{-1}.

It is clear from the Raman and ROA spectra of the *arabino*- type monosaccharides that they generate a larger number of signals than those of the *xylo*- type. This can probably be ascribed to the fact that one of the ring hydroxyls, other than the anomeric one, is in an axial orientation leading to a different normal mode composition. This type of monosaccharide can be subdivided into two groups: those with the anomeric hydroxyl group predominantly in the axial orientation and those with this group predominantly equatorial. Further classification according to the absolute configuration at the anomeric centre is also possible and this information is displayed in Table 6.2. From

consideration of the relative orientation and absolute configuration of the anomeric group it is possible to rationalise the sign pattern displayed by each of the monosaccharides of this particular type.

The position and occurrence of ROA signals in this range are a function of the orientation of the anomeric hydroxyl group, while the sign of the individual ROA signals depend on the absolute stereochemistry of the part of the molecule embraced by the particular normal modes. Thus, the anomers may be distinguished from one another by the position of the ROA signals. Also an empirical correlation exists between the absolute configuration of the anomeric centre and the sign of the ROA signals within individual groups of related monosaccharides. In particular, monosaccharides with the anomeric hydroxyl group equatorial do not exhibit the type IIa Raman band or any associated ROA signal at ~ 840 cm^{-1}. A correlation also exists between the ROA signals at ~ 920 cm^{-1} and 890 cm^{-1} and the axial and equatorial orientations of the anomeric hydroxyl group, respectively. The other ROA signal listed in Table 6.2, observed in the wavenumber range between ~ 870 and 880 cm^{-1}, is characteristic of a monosaccharide ring structure with one of the hydroxyl groups, other than the anomeric, in an axial orientation. This ROA signal is associated with the type IIc band in the Raman spectrum and undergoes only a small wavenumber shift on going from the axial to the equatorial orientation of the anomeric hydroxyl group.

For the *arabino*- type reducing sugars D-galactose and D-arabinose,[1] for which significant quantities of both the anomers are present, the resultant ROA spectra are a superposition of the spectra of the two anomeric species. For example, D-galactose exhibits a negative ROA signal at ~ 906 cm^{-1} and a positive ROA signal at ~ 891 cm^{-1}

corresponding to the α- and β- anomeric forms, respectively. Note that the fact that these two ROA signals for the α- and β-anomeric forms have opposite signs and are at closely separated wavenumbers does not necessarily mean that they have the same vibrational origins as is evidenced by the normal coordinate analysis of D-galactose.[12] Also, the signal at ~ 870 cm^{-1} is weak and negative as both anomers are contributing signals of opposite sign at this wavenumber which cancel out to some degree. The appearance of a ROA signal at ~ 821 cm^{-1} is indicative of the presence of the axial orientation of the anomeric hydroxyl group.

The ROA spectrum of D-fructose (Figure 6.1) is almost identical to that of D-sucrose (not shown here) in this range indicating that signals from the furanose form of D-fructose (as found exclusively in D-sucrose) are indistinguishable from those of the pyranose form in this region. Comparison with the ROA spectra of α-methyl-D-galactoside,[1] which has the same orientation of all the ring hydroxyl groups, reveals that in D-fructose the sign pattern is reversed reflecting the fact that, although both have the same orientation of hydroxyl groups around the ring, the absolute configuration at each of the chiral centres is different.

The four *lyxo*- type monosaccharides listed in Table 6.2 all have the same absolute configuration at the four chiral centres and therefore exhibit the same sign pattern in this range. Note that the sign pattern and wavenumbers are the same as identified for the *arabino*- type monosacccharides with an axial orientation and an absolute (R) configuration at the anomeric centre even though the *lyxo*- type monosaccharides considered here all have an axial orientation but an absolute (S) configuration at the anomeric centre. It might be

misleading to assign bands to the same modes for different configurational types but the similarities in the ROA in this range for the *arabino-*, *lyxo-* and *ribo-* type sugars suggests that the signals do have a similar origin. It is probably important to consider all the chiral centres of the ring and not just the absolute configuration at the anomeric centre in order to tie up the assignments in this region.

Only three monosaccharides of the *ribo-* type have been studied to date and these are listed in Table 6.2. D-psicose (Figure 6.4) exists in aqueous solution as a complex mixture of anomers and ring types (Table 6.1). D-ribose in aqueous solution exists as 20% α-pyranose in the $^{1}C_{4}$ chair conformation, 56% β-pyranose in the $^{4}C_{1}$ chair conformation, 6% α-furanose and 22% β-furanose.[19] Both the pyranose forms of D-ribose have an equatorial orientation of the anomeric hydroxyl group while both the pyranose forms of D-psicose have an axial orientation of this group. However, in the range discussed here the ROA spectra of the two are remarkably similar. As the ROA signals at ~ 911 cm^{-1} and 850 cm^{-1} would be assigned to the axial orientation of the anomeric hydroxyl group in the other monosaccharides, which is almost completely absent in D-ribose, it seems likely that these signals originate from another source. A conventional Raman study of D-ribose[20] proposed that bands at 913 and 834 cm^{-1} be assigned to vibrations of the furanose ring and this would explain the presence of ROA signals at these wavenumbers. In addition, it is possible that the positive ROA signals at ~ 883 and 879 cm^{-1} in D-ribose and D-psicose, respectively, have different vibrational origins for monosaccharides of the *ribo-* type having axial and equatorial orientations of the anomeric hydroxyl group. It is worth noting here that the sign pattern in D-psicose, which has an axial orientation of the anomeric hydroxyl

group with an absolute (S) configuration, is the same as monosaccharides of the *arabino-* and *lyxo-* types with an axial orientation of the anomeric hydroxyl group and an absolute (S) and (R) configuration, respectively.

The other monosaccharide of this series, D-allose, has no detectable furanose component, exists only in the $^4C_1$ chair conformation and favours the β-anomeric form by a ratio of 2:1.[6] The ROA spectrum of D-allose is indistinct in this region and indeed resembles more closely that of a member of the *xylo-* type than of the *ribo-* type. However, the presence of a conventional Raman band at ~ 874 cm^{-1} along with an associated positive ROA signal is indicative of a monosaccharide with a hydroxyl group, other than the anomeric, in an axial orientation.

As we have seen above, considering the individual configurational types and anomeric orientations separately is fairly successful in explaining the ROA spectra in this range. However, as we shall see later, this correlation may be purely fortuitous and may obscure the underlying mechanism for the generation of ROA in this range as the sign of the ROA signals in the fingerprint region, where the anomeric centre is of no particular significance for the vibrations, display the same sign dependence as the ROA signals between ~ 800 and 950 cm^{-1}. Nonetheless, the normal modes in this range are certainly sensitive to anomeric configuration and this wavenumber range will probably be of most value in assessing the orientation of the anomeric hydroxyl group from the wavenumber at which signals appear and also in providing estimates of anomeric equilibria. Furthermore, the similarity with the fingerprint region implies that there is some information overlap between the two regions: this can be useful because in some substituted analogues of monosaccharides, such as D-glucosamine,[1]

vibrations originating in the substituent may interfere with the characteristic sign pattern in the fingerprint region.

6.2.3 Fingerprint Region (~ 950-1200 cm^{-1})

This region of the vibrational spectrum is dominated by exo- and endocyclic C-O and C-C stretches with significant contributions from C-O-H deformations.[11-15] The interpretation of the conventional vibrational spectra in this region is difficult on account of the widespread coupling of C-O and C-C stretches, the poor discrimination between exo- and endocyclic contributions and the small differences between the configurational positions of each C-O group.[17] It has been demonstrated in the preceding chapter that, although C-O-H deformations contribute to the Raman intensity and position of bands in this region, they make no significant contribution to the associated ROA intensity and that configurational changes have a comprehensive and characteristic effect on the ROA sign pattern.[1] This latter discovery implies that detailed assignment of the individual Raman bands is unnecessary as the ROA spectrum provides a "fingerprint" characteristic of the backbone structure.

From a comparison of the ROA spectra in this region of the ketose, aldose and pentose sugars of the same configurational type it is clear that, although the sign patterns within a series are generally retained, some minor changes including small wavenumber shifts and the disappearance of certain signals are evident. One possible explanation is that the exocyclic C-C bond linking the hydroxymethyl group to the ring, which is substituted at a different position for the ketose and aldose sugars and is not present at all for the pentose sugars, is involved in the normal modes. The decoupling of this stretching

coordinate from the normal modes or changing its local environment may be responsible for some of the changes observed.

In this region of the ROA spectra, D-glucose and D-xylose generate a characteristic negative, positive, negative and positive sign pattern.[1] In the previous chapter it was determined that the endocyclic C-O stretching coordinates involving the ring oxygen contribute to the normal modes but do not influence the ROA intensity and that motions of the exocyclic hydroxymethyl group and the C-O-H deformations do not affect the sign pattern. Introduction of a ring substituent other than a hydroxyl group was found to disrupt this sign pattern. The *ribo*-type monosaccharides have many features in common with those of the *xylo*- type in this region. Thus D-glucose, D-allose, D-ribose and D-xylose all exhibit the same characteristic sign pattern.[1] Furthermore, the two ketose sugars, L-sorbose and D-psicose (Figures 6.2 and 6.4) exhibit only the two ROA signals at higher wavenumber. Note that the sign of these two signals is reversed in L-sorbose relative to the others because, although they all have the same orientation of the hydroxyl groups at carbon atoms 3,4 and 5 the absolute configuration at these chiral centres is different for the L-sugar. Despite the similarities in this region the two configurational types are readily distinguishable by considering the anomeric region where, as discussed above, monosaccharides of the *ribo*- type are different from those of the *xylo*- type. In addition, the two configurational types differ dramatically in the fingerprint region from monosaccharides of the *lyxo*- and *arabino*- types which further assists the identification.

The ROA spectra in this region are closely related to those in the anomeric region in the sense that monosaccharides of the *arabino*- type which exist in the $^{2}C_{5}$ or $^{1}C_{4}$ chair conformation, such as D-fructose

(Figure 6.1), and monosaccharides of the *lyxo*- type which exist in the $^5C_2$ or $^4C_1$ chair conformations, such as D-tagatose (Figure 6.3), show a remarkably similar sign pattern. Unfortunately, without prior knowledge of either the chair conformation or the configurational type it is difficult to distinguish between the two using only the ROA sign pattern in this region. However, in some cases inspection of the CH_2 and COH deformations region can be productive in this respect.

Monosaccharides of the same configurational type but in different chair conformations have the opposite absolute configuration at the ring carbons so the ROA sign pattern is reversed. For example, D-fructose and D-galactose exhibit nearly mirror image ROA spectra in this region and in the range from ~ 800-950 cm^{-1} as they have the same orientation of the ring hydroxyl groups, both being *arabino*- type monosaccharides, but different absolute configurations at all the chiral centres except the anomeric one. The fact that the ROA signals in the anomeric region show the same dependence on orientation and absolute configuration implies that the vibrations responsible for the ROA in the anomeric region have a similar origin to those in the fingerprint region, i.e. delocalised ring modes rather than deformations about the anomeric centre. Thus, although the ROA signals in the anomeric region are certainly more sensitive to the anomeric configuration they do not appear to be solely dependent on motions of this group. This means that the correlation made between sign and absolute configuration at the anomeric centre is probably fortuitous which explains why the rules break down for different configurational types. The precise origin of the observed ROA signals and the mechanism by which they are generated will probably have to await detailed *ab initio* ROA intensity calculations on monosaccharides.

One feature in this region which does not appear to be delocalised over the ring is a ROA signal unique to the ketose sugars appearing at ~ 1190, 1186 and 1200 cm^{-1} in D-fructose, L-sorbose and D-tagatose, respectively, and as a shoulder at ~ 1195 cm^{-1} in D-psicose. The parent Raman band was attributed to C-O stretching and H-C-O bending modes of the hydroxymethyl group attached to the anomeric carbon and is only found at this wavenumber in the ketose sugars.[4] Therefore, not only does this band act as an excellent ketose marker, as both aldose and pentose sugars do not show any signal in this wavenumber range, but the ROA signal also depends on the absolute configuration at the anomeric centre. Thus, D-fructose and L-sorbose have a negative sign implying an absolute (R) configuration; whereas D-tagatose and D-psicose have a positive sign implying an absolute (S) configuration.

6.2.4 CH_2 and COH Deformations Region (~ 1200-1500 cm^{-1})

The preliminary ROA study of the aldose and pentose monosaccharides highlighted influences of the orientation of the anomeric hydroxyl and also the adjacent hydroxyl group on the conformation of the exocyclic hydroxymethyl group and the consequences for the ROA spectra in this region.[1] This was followed by the study of D-glucose and several of its deuterated analogues presented in the previous chapter which produced a number of interesting results. The normal modes responsible for the negative and positive ROA signals at ~ 1220 cm^{-1} and 1260 cm^{-1} in D-glucose were shown to involve coupled CH_2 and C-O-H deformations and it was proposed that these two signals were associated with the *gauche-gauche* (GG) and *gauche-trans* (GT) rotamers of the exocyclic hydroxymethyl group, respectively. In addition, it was demonstrated that only the β-anomeric form would generate a ROA signal at ~ 1260 cm^{-1}. Other

ROA signals in this region were attributed to C-1–H, C-H and C-O-H deformations.

The ROA of the ketose, aldose and pentose sugars differ more dramatically in this region than in any other part of the spectrum. This is presumably due to the changes in the substitution position of the hydroxymethyl group in ketose and aldose sugars and the absence of this group from the pyranose form of pentose sugars. The lack of a hydroxymethyl group from the structure of the pyranose form of pentose sugars has previously been the explanation for the weak intensity of the ROA signals found in these sugars in this region. In addition, although not all the ROA signals in this region are sensitive to deuteration of the hydroxymethyl group, the absence of signals from the ROA spectra of the pentose sugars point to the key role this group has in generating the ROA. The exception to the above is D-ribose which has a ROA spectrum closely resembling that of D-galactose in this region.[1] A possible explanation is that, although D-ribose has no exocyclic hydroxymethyl group in the pyranose form, in aqueous solution there is a fairly large furanose component which does and which may be responsible for the ROA. Furthermore, the hydroxyl group adjacent to the hydroxymethyl group in the furanose form has an axial orientation and the same situation in the pyranose form of D-galactose is thought to be responsible for generating the associated ROA sign pattern.[1]

One feature common to both the ketose and aldose sugars is a band in their conventional Raman spectra at ~ 1260 cm^{-1} which has been assigned to coupled CH_2 and C-O-H deformations.[11-15] The associated ROA signals are positive in D-fructose and L-sorbose and negative in D-tagatose and D-psicose so it would appear that, like the signals at

~ 430 cm^{-1} and 1180 cm^{-1}, the sign is dependent on the absolute configuration at the anomeric centre to which the hydroxymethyl group is linked in the ketose sugars. In all the aldose sugars studied so far this ROA signal has a positive sign presumably because the configuration at the chiral centre to which the hydroxymethyl group is joined has an absolute (R) configuration for all the D-sugars. Likewise D-fructose and L-sorbose, which also exhibit a positive ROA sign at this wavenumber, have the hydroxymethyl group attached to a chiral centre with an absolute (R) configuration. This would imply also that the normal mode responsible is localised somewhat around the exocyclic hydroxymethyl group and the part of the ring to which it is directly attached.

6.3 Concluding Remarks

With this study of four ketose sugars the assignment of monosaccharide ROA has been successfully extended. It is important to note that in the anomeric and fingerprint regions of the ROA spectra the sign patterns for the ketose sugars are remarkably similar to those of the corresponding aldose and pentose sugars of the same configurational type. This reinforces the opinion that the normal modes in these two regions are delocalised over the chiral centres of the ring and sample the chirality of the ring framework rather than the pendant side-groups.[12,14,15] In contrast, the key role of the exocyclic hydroxymethyl group is again in evidence in the CH_2 and COH deformations region with striking differences apparent between the ROA spectra of aldose, pentose and ketose sugars. In addition, three ROA signals appearing at ~ 430, 1180 and 1260 cm^{-1} depend only upon the absolute configuration at the anomeric centre. Definite conclusions about the low wavenumber region will probably have to await the detailed

investigation of the aldose and pentose monosaccharides which have only been studied down to ~ 600 cm^{-1} to date.

Future studies on monosaccharides may involve substituted monosaccharides and exploitation of the low wavenumber and C-H stretch regions for existing monosaccharides. For the refinement of assignments *ab initio* ROA intensity calculations[21] would appear to be essential although as demonstrated in the previous chapter studying closely related analogues and deuterated samples can provide considerable insight into the generation of the ROA. However, the work to date does provide valuable background material that is required for interpreting the ROA of di-, oligo- and polysaccharides presented in the following two chapters.

References

1. Z. Q. Wen, L. D. Barron, and L. Hecht, *J. Am. Chem. Soc.*, **115** (1993) 285-292.
2. M. Mathlouthi and D. V. Luu, *Carbohydr. Res.*, **78** (1980) 225-233.
3. D. Steele, J. Lall, and J. Pamnani, *Carbohydr. Res.*, **133** (1984) 313-318.
4. W. A. Szarek, S. L. Korppi-Tommola, H. F. Shurvell, V. H. Smith Jr., and O. R. Martin, *Can. J. Chem.*, **62** (1984) 1512-1518.
5. C. L. Schoen, S. K. Sharma, C. E. Helsley and H. Owen, *Appl. Spectrosc.*, **47** (1993) 305-308.
6. S. J. Angyal and G. S. Bethell, *Aust. J. Chem.*, **29** (1976) 1249-1265.
7. M. Jaseja, A. S. Perlin and P. Dais, *Magnetic Resonance in Chemistry*, **28** (1990) 283-289.
8. F. Lichtenthaler and S. Ronninger, *J. Chem. Soc. Perkins Trans. II*, (1990) 1489-1497.
9. J. F. Stoddard in *Stereochemistry of Carbohydrates*, Wiley, New York, 1971.
10. A. F. French and M. K. Dowd, *J. Comput. Chem.*, **15** (1994) 561-570.
11. M. Dauchez, P. Derreumaux and G. Vergoten, *J. Compu. Chem.*, **14** (1992) 263-277.
12. M. Sekkal, P. Legrand, G. Vergoten and M. Dauchez, *Spectrochim. Acta. Part A*, **48** (1992) 959-973.
13. P. D. Vasko, J. Blackwell and J. L. Koenig, *Carbohydr. Res.*, **23** (1972) 407-416.
14. M. V. Korolevich, R. G. Zhbankov and V. V. Sivchik, *J. Mol. Struct.*, **20** (1990) 301-313.
15. H. A. Wells and R. Atalla, *J. Mol. Struct.*, **224** (1990) 385-424.

16. M. Mathlouthi and D. V. Luu, *Carbohydr. Res.*, **81** (1980) 203-213.

17. M. Mathlouthi and J. L. Koenig, *Adv. Carbohydr. Chem. Biochem.*, **44** (1986) 7-89.

18. R. S. Tipson, *Natl. Bur. Stand. Monogr.*, **110** (1968).

19. S. J. Angyal and V. A. Pickles, *Aust. J. Chem.*, **25** (1972) 1695.

20. P. Carmona and M. Molina, *J. Raman Spectrosc.*, **21** (1990) 395-400.

21. P. L. Polavarapu, *J. Chem. Phys.*, **94** (1990) 8106-8112.

Chapter 7

Vibrational Raman Optical Activity of Disaccharides

In this chapter the ROA spectra of D-maltose, D-maltose-O-d_8, D-cellobiose, D-isomaltose, D-gentiobiose, D-laminaribiose, D-trehalose and D-lactose are presented. All the spectra with the exception of D-lactose, which consists of a D-galactose residue linked to a D-glucose residue, are of disaccharides consisting of two D-glucose residues joined by an O-glycosidic linkage. This particular choice of samples made it possible to build upon the work on the D-glucose monomer presented in chapter 5 and to investigate the influence of the glycosidic link on the ROA spectra. D-lactose was included in this study to ascertain whether useful information could still be extracted from the ROA spectrum despite the additional complexity arising from the presence of two different residues.

7.1 Experimental

Samples of D-cellobiose, D-gentiobiose, D-isomaltose and D-laminaribiose were supplied by Sigma; D-trehalose and D-lactose by Fluka and D-maltose by Aldrich. A sample of D-maltose-O-d_8 was prepared by lyophilising D-maltose from D_2O solution twice before dissolving in D_2O to a concentration of 3 M. All the other carbohydrate samples were dissolved in distilled H_2O to a concentration of 3 M, except for D-cellobiose and D-laminaribiose (1.2 M) and D-lactose 2 M), and allowed to equilibrate at room temperature for at least 24 h. The equilibrated samples were treated with charcoal to reduce fluorescence, filtered into quartz microfluorescence cells through 0.45

μm Millipore membrane filters to remove any dust particles that may cause spurious light scattering, then centrifuged for at least 15 min. During spectral acquisition the laser power was ~ 700 mW at the sample and the slit width was set for 120 μm giving a spectral bandpass of ~ 12 cm^{-1} using 514.5 nm laser excitation. The spectra were recorded over 2 to 4 h.

7.2 Results and Discussion

The Raman and ROA spectra of D-maltose, D-maltose-O-d_8, D-cellobiose, D-isomaltose, D-gentiobiose, D-laminaribiose, D-trehalose, and D-lactose in the range ~ 350-1500 cm^{-1} are shown in Figures 7.1-7.8, respectively.

7.2.1 Low Wavenumber Region (~ 350-600 cm^{-1})

In this region normal coordinate analyses of monosaccharides[1,2] assign the Raman bands to vibrations involving exo- and endocyclic bending deformations of the C-C-O, C-C-C, C-O-C and O-C-O groups coupled with associated exo- and endocyclic torsions about C-O bonds. It has also been suggested[3] that the intense Raman bands involving C-C-O deformations around the anomeric carbon which are found in this region are among the most sensitive to anomeric configuration in the entire monosaccharide spectrum. It has been calculated that the normal mode composition is similar in disaccharides[4,5] but that there is also the possibility of additional contributions arising from motions of the C-O-C group which forms the glycosidic link.

The complexity of the normal modes and the lack of specific conventional Raman assignments in this region hinder the assignment of

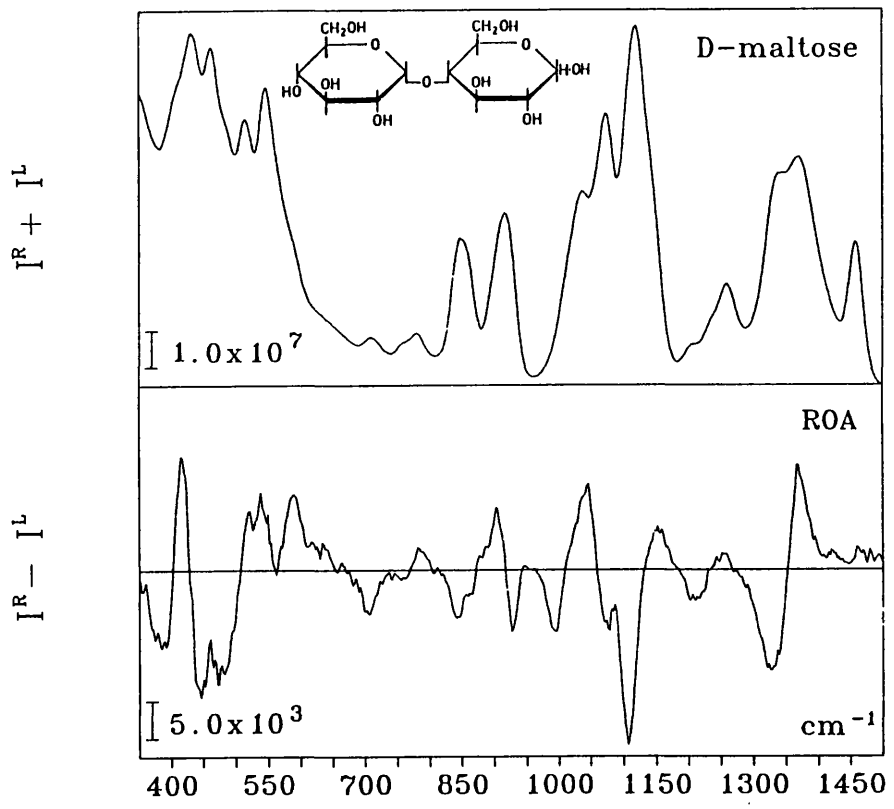

Figure 7.1 The backscattered Raman ($I^R + I^L$) and ROA ($I^R - I^L$) spectra of D-maltose in H_2O.

ROA signals to particular vibrations. These difficulties are compounded by the fact that until recently backscattering ROA studies[6-9] did not investigate below ~ 600 cm^{-1}. However, it is clear from comparison of the spectra of D-maltose (Figure 7.1) and D-maltose-O-d_8 (Figure 7.2) that C-O-H vibrations do not contribute significantly to either the Raman or ROA intensities in this region. Thus, it would appear that in common with the fingerprint region[6-9] the ROA signals in this region probe the backbone structure of carbohydrates and may prove even more sensitive to conformation.

One important correlation that can be made in this region is between the configuration of the glycosidic link and the sign of a ROA

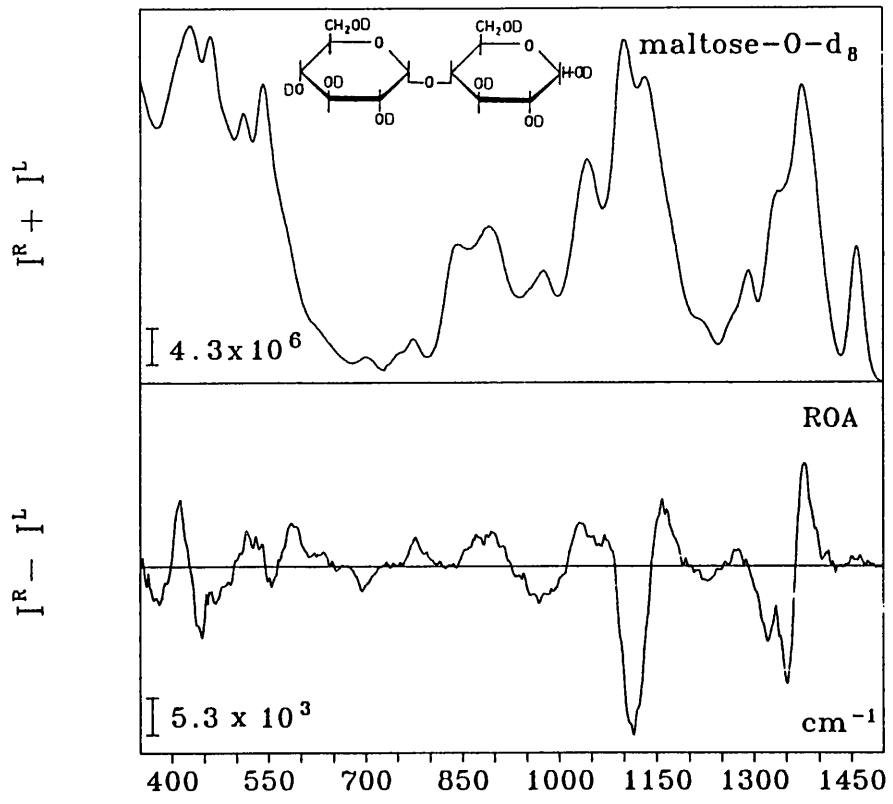

Figure 7.2 The backscattered Raman ($I^R + I^L$) and ROA ($I^R - I^L$) spectra of D-maltose-O-d_8 in D_2O.

couplet centred at ~ 430±10 cm^{-1} found in all the disaccharides containing only D-glucose residues studied so far. This couplet is positive at low and negative at high wavenumber for α-linked species and negative at low and positive at high wavenumber for β-linked species. At present it is not clear whether the normal modes responsible for generating the ROA couplet are closely related, such as the in-phase and out-of-phase combinations of the same local vibrational coordinates, or are composed of quite different vibrational coordinates embracing different regions of the molecule. The fact that this couplet is centred within an ~ 20 cm^{-1} range for all the disaccharides studied and that α- and β-linked species exhibit ROA signals of opposite signs strongly suggests that it has a similar origin

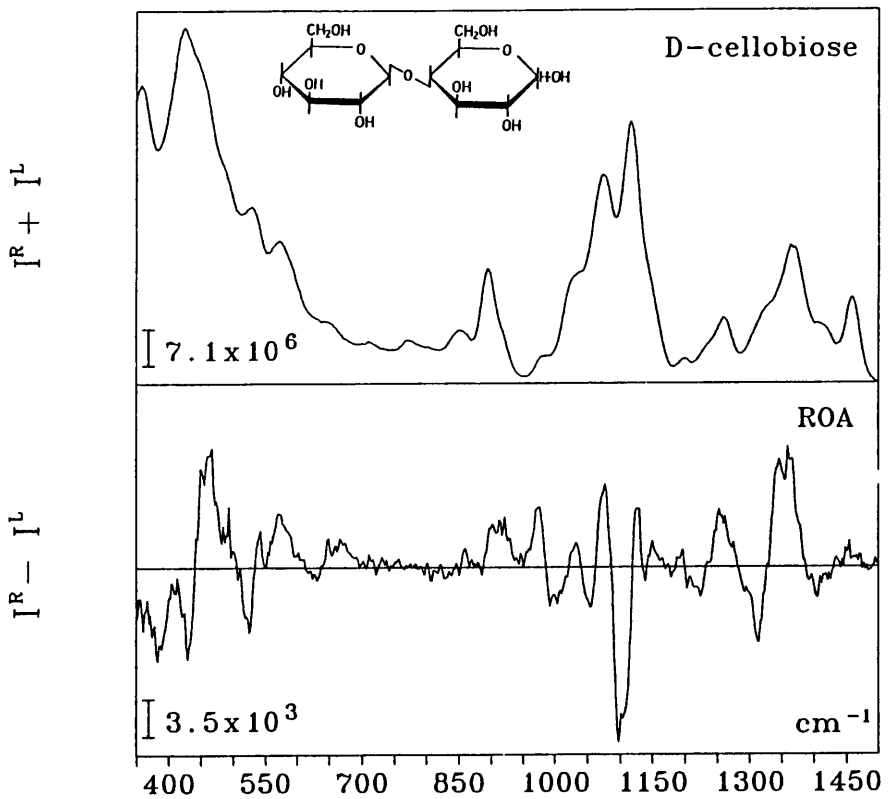

Figure 7.3 The backscattered Raman ($I^R + I^L$) and ROA ($I^R - I^L$) spectra of D-cellobiose in H_2O.

in all the disaccharides and that deformations around the anomeric carbon of the non-reducing residue play a crucial role in generating the ROA signals. The work presented in the previous chapter on the ketose monosaccharides identified a ROA couplet in the same wavenumber range showing the same sign dependence on absolute configuration at the anomeric centre as found in the disaccharides. However, since no such couplet is evident in the ROA spectra of D-glucose (Figure 5.1) or the methyl glucosides[8] it is likely that motions of the glycosidic link also make some important contributions here.

Table 7.1 Position and width (cm^{-1}) of low wavenumber glycosidic couplet.

disaccharide	linkage type and configuration	position and sign of ROA couplet	deconvoluted couplet width
D-maltose	α(1-4) ax.-eq.	431 (+,-)	31
D-maltose-O-d_8	α(1-4) ax.-eq.	428 (+,-)	34
D-cellobiose	β(1-4) eq.-eq.	440 (-,+)	34
D-isomaltose	α(1-6) ax.-eq.	424 (+,-)	39
D-gentiobiose	β(1-6) eq.-eq.	420 (-,+)	41
D-laminaribiose	β(1-3) eq.-eq.	423 (-,+)	33
D-trehalose	α(1-1) ax.-ax.	431 (+,-)	19

From inspection of Table 7.1, which lists the wavenumber at which this ROA couplet is centred along with its sign and width measured from the band maxima to the band minima of the ROA spectra for a selection of disaccharides, it is clear that the width of this couplet displays a dependence on the linkage type. It was found by deconvolution of the Raman spectra presented here that this dependency is a function of the differences in the separation of the parent Raman bands along with the appearance of additional Raman bands contributing ROA signals of opposite sign for the different anomeric forms.

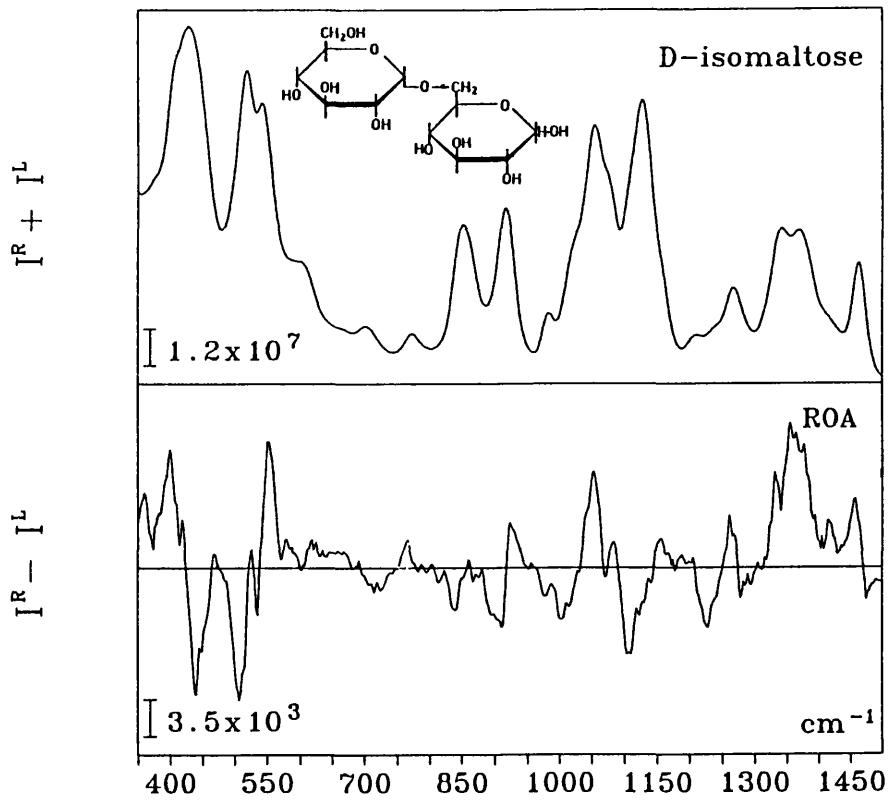

Figure 7.4 The backscattered Raman ($I^R + I^L$) and ROA ($I^R - I^L$) spectra of D-isomaltose in H_2O.

For the 1-4 linked species D-maltose, D-maltose-O-d_8 and D-cellobiose (Figures 7.1-7.3), the ROA signals of opposite sign for α- and β-linkages associated with three distinct Raman bands were found by deconvolution to have an overall separation of 31, 34 and 34 cm^{-1}, respectively. D-laminaribiose (Figure 7.6), the only example of a 1-3 linked species, is found to have an almost identical couplet to D-cellobiose with the same Raman band structure and a deconvoluted separation of 33 cm^{-1}. This similarity between the D-cellobiose and D-laminaribiose is evident throughout the ROA spectra indicating that the two exhibit very similar conformational behaviour as predicted by molecular modelling calculations.[10] A similar band structure was also found for the α(1-1) linked species D-trehalose (Figure 7.7) but with an

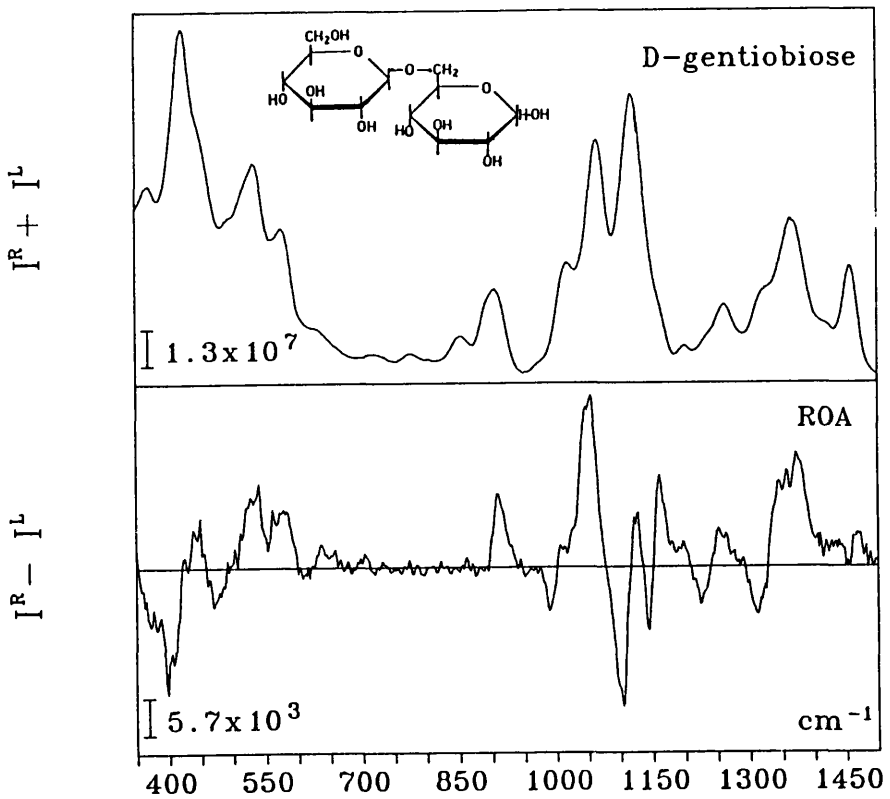

Figure 7.5 The backscattered Raman ($I^R + I^L$) and ROA ($I^R - I^L$) spectra of D-gentiobiose in H_2O.

overall separation of only 19 cm^{-1}. This results in a narrow ROA couplet which may reflect the rigidity of this particular linkage type[11] or possibly the fact that both the anomeric centres are fixed in the α-anomeric form by the linkage in D-trehalose. The corresponding ROA signals in the 1-6 linked species, D-isomaltose and D-gentiobiose (Figures 7.4 and 7.5), associated with at least four and possibly five Raman bands were found by deconvolution to have an overall separation of 39 and 41 cm^{-1}, respectively, thereby showing a dependence on the linkage type. The presence of additional bands, also dependent on the configuration of the linkage, serves to broaden this couplet relative to the other disaccharides studied here. This may reflect the fact that the 1-6 linked species have the CH_2 group of the reducing residue

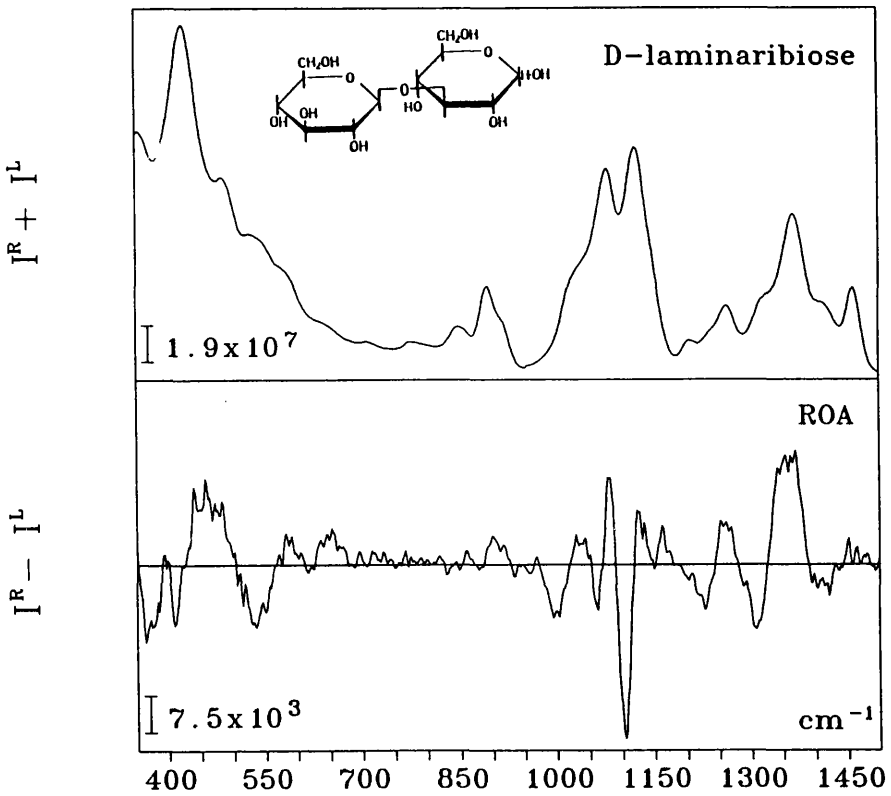

Figure 7.6 The backscattered Raman ($I^R + I^L$) and ROA ($I^R - I^L$) spectra of D-laminaribiose in H_2O.

incorporated into the linkage which results in an increase in the conformational freedom[12,13] and may also alter the composition of the normal modes in this wavenumber range.

It would appear then that not only can this couplet differentiate between different linkage configurations but also between distinct linkage types in molecules containing D-glucose residues using the width of the ROA couplet. Furthermore, detailed analysis of the Δ-values of these ROA signals may provide valuable information on the conformation of these linkages.

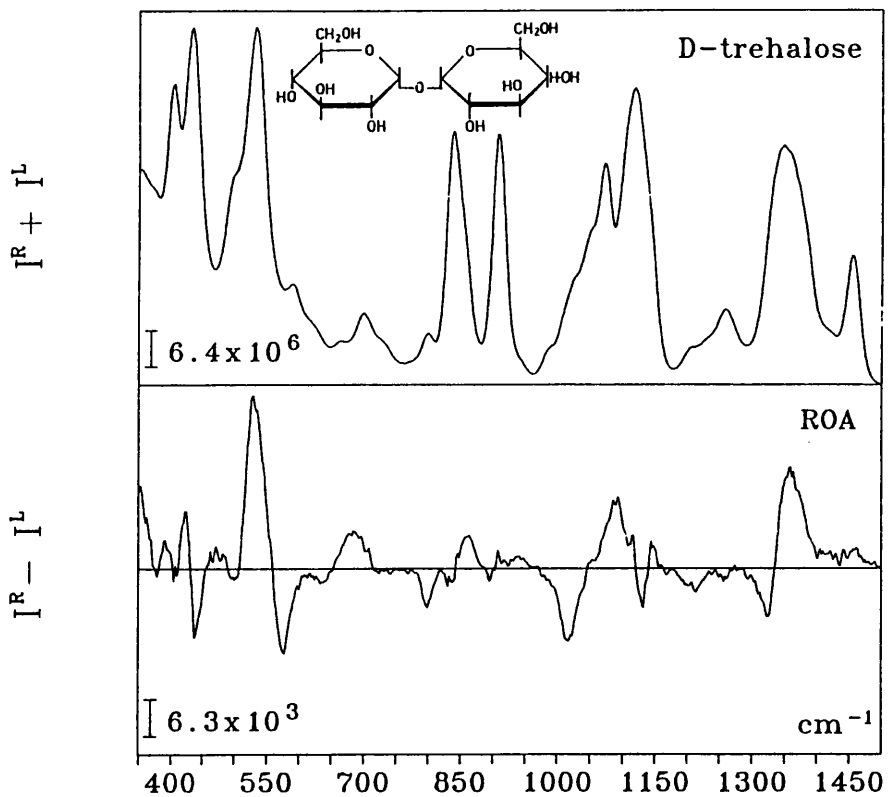

Figure 7.7 The backscattered Raman ($I^R + I^L$) and ROA ($I^R - I^L$) spectra of D-trehalose in H_2O.

7.2.2 Anomeric Region (~ 600-950 cm^{-1})

It is clear from examination of the ROA spectra of the three β-linked disaccharides, D-cellobiose (Figure 7.3), D-gentiobiose and D-laminaribiose (Figure 7.6), that they lack any ROA signals in the range from ~ 700 to 880 cm^{-1}. A similar result was also found for the β-anomeric form of the D-glucose monomer.[9] In contrast, the α-linked disaccharides, D-maltose (Figure 7.1) and D-isomaltose (Figure 7.4) exhibit three ROA signals in this range as does the α-anomeric form of the D-glucose monomer. It is well established that the Raman band at ~ 845 cm^{-1} is characteristic of the α-anomer,[14] and normal coordinate analyses[4,5] assign the bands in the range ~ 700 to 800 cm^{-1} to

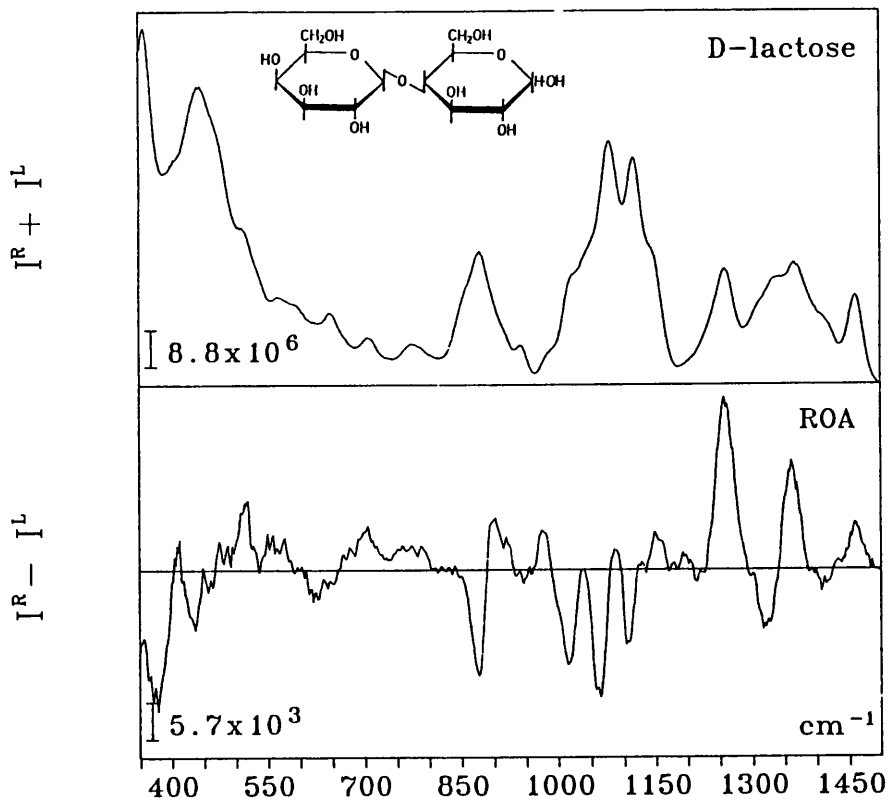

Figure 7.8 The backscattered Raman ($I^R + I^L$) and ROA ($I^R - I^L$) spectra of D-lactose in H_2O.

bending coordinates of the heavy atoms involved in the glycosidic link or possibily of the hemi-acetal fragment. Thus, the presence of ROA signals in the spectra of the α-linked species may reflect some chirality inherent in the linkage or the hemi-acetal fragment when the C-1–O-1 group is in an axial position. This simple observation holds for all the di-, oligo- and polysaccharides of D-glucose studied so far and provides an easy method of distinguishing between homogeneously α- and β-linked species of D-glucose.

One of the most intriguing and potentially useful features in this region is a ROA couplet in the spectrum of D-maltose centred at ~ 917 cm^{-1} which is positive at low and negative at high wavenumber.

Previous ROA studies[6,7] assigned this couplet to a vibration of the α(1-4) glycosidic link since it was neither present in the spectra of the monomer, D-glucose, nor in the spectra of the β-linked disaccharides and was found to have approximately twice the intensity in the trimer, D-maltotriose (Figure 8.2), which contains two such links per molecule. On the basis of the assignment of a band at 901 cm^{-1} in the conventional IR spectrum of α-D-glucose to a C-1-H deformation mode[15] this ROA couplet was attributed to interactions between the anomeric C-1-H deformation and the glycosidic C-O-C stretch.[6,7] However, we have already shown in chapter 5 that C-1–H deformations play only a minor role in this normal mode and furthermore this assignment neglects the fact that a D-glucose Raman band at 913 cm^{-1} was demonstrated to be sensitive to O-deuteration and hence to contain a significant contribution from C-O-H deformations.[15] It is clear from a comparison of D-maltose with its O-deuterated analogue (Figure 7.2) that the ROA couplet collapses and broadens and the associated Raman band is weakened and shifted to lower wavenumber upon deuteration. In a normal coordinate analysis of amylose,[16] for which D-maltose is the repeating unit, a conformation-sensitive mode at 946 cm^{-1} was described as a skeletal vibration of the α(1-4) linkage and contributions were predicted not only from the linkage atoms but also from the ring atoms and deformations of the C-2-O-H and C-3-O-H groups. In addition, a second Raman band at 923 cm^{-1} was shown to be sensitive to O-deuteration and was assigned to a C-O-H deformation mode. This leads us to the conclusion that it is probably more accurate to describe this couplet as originating in the C-O-C stretch coordinates of the glycosidic link interacting with ring stretching coordinates and C-O-H deformations, and to suggest that the O-2-H···O-3' intramolecular hydrogen bond found in the crystal structure of D-maltose[17] and thought to persist to some degree in aqueous solution[18] may also be

important in generating this ROA signal. This theme is developed more fully in the next chapter in the discussion of cyclodextrins.

A similar couplet is present in the ROA spectrum of D-isomaltose centred at ~ 918 cm^{-1} but with the signs reversed relative to that found in D-maltose. Deconvolution of the parent Raman bands demonstrate that both these couplets are associated with two closely separated Raman bands yielding ROA signals of opposite sign. As these two molecules have the same configuration at all the chiral centres, the sign reversal of this glycosidic couplet must originate in the different linkage type in D-isomaltose with its characteristic conformations and distinct associated normal modes. Thus, this couplet not only provides a signature characteristic of certain types of α-linked species but also carries conformational data.

The two bands at ~ 839 cm^{-1} and 909 cm^{-1} in the Raman spectrum of D-trehalose (Figure 7.7) are strongly polarized, and as such bands are known to be particularly susceptible to polarization artifacts[19] the weak associated ROA signals must be treated as unreliable. The ROA spectrum in this region does, however, contain two unique features: a broad positive signal at ~ 687 cm^{-1} and a negative signal at ~ 798 cm^{-1}. Normal coordinate analysis[4] assigns a mode at 697 cm^{-1} to the C-O-C deformation of the glycosidic link coupled to C-C-O deformations and torsions about C-O bonds and a mode at ~ 784 cm^{-1} to C-O-C, C-C-O and O-C-O deformations around the anomeric centres in D-trehalose. These two ROA signals could therefore be characteristic of the α(1-1) linkage type although the importance of this observation is limited, except as a model, as it does not form molecules larger than the disaccharide.

The ROA spectrum of D-lactose (Figure 7.8) in the anomeric region is almost identical to that of β-D-methyl galactoside published by Wen *et al.*[8] This may be understood by considering D-lactose as a non-reducing D-galactose residue trapped in the β-anomeric form by the glycosidic link plus a reducing D-glucose residue. As noted in chapter 5 D-glucose yields only two weak ROA signals in this region; whereas the non-reducing D-galactose residue, as typified by β-D-methyl galactoside, gives rise to a number of strong ROA signals. In effect the signals from the β-D-galactose residue are swamping those from the D-glucose residue, the glycosidic link or from inter-residue interactions. A similar result is found for D-melibiose (not shown here) where the D-galactose residue is trapped in the α-anomeric form by a (1-6) link and the resulting spectrum closely resembles that of α-D-methyl galactoside.

7.2.3 Fingerprint Region (~ 950-1200 cm^{-1})

The α-linked disaccharides, D-maltose (Figure 7.1) and D-isomaltose (Figure 7.4), exhibit the same characteristic negative, positive, negative and positive sign pattern as D-glucose in this region[8,9] but with an additional weak ROA signal, negative in D-maltose and positive in D-isomaltose, appearing at ~ 1077 cm^{-1} and 1083 cm^{-1}, respectively. A normal coordinate analysis of D-maltose described a normal mode appearing at 1063 cm^{-1} involving C-O stretching motions with a major contribution from the C-1-O-1 and C-4'-O-1 stretching coordinates of the glycosidic link.[4] Combining this with the fact that this signal is not present in D-glucose leads to the conclusion that this ROA signal is generated by motions of the glycosidic link. Furthermore, the sign change for D-maltose relative to D-isomaltose also reveals a conformational sensitivity. The other α-linked species, D-trehalose (Figure 7.7), deviates significantly from the D-glucose signature

presumably due to its unique diaxial link.

In general, the β-linked species, D-cellobiose (Figure 7.3) D-gentiobiose (Figure 7.5) and D-laminaribiose (Figure 7.6), exhibit more changes relative to the characteristic D-glucose signature than the α-linked species. In particular, D-cellobiose shows an additional positive ROA signal at ~ 976 cm^{-1}, a negative ROA signal at ~ 1054 cm^{-1} and a ROA couplet negative at low and positive at high wavenumber centred at ~ 1120 cm^{-1} which is overlapping the negative ROA signal at lower wavenumber. As mentioned above D-laminaribiose is very similar to D-cellobiose in this region except it does not exhibit the positive ROA signal at ~ 976 cm^{-1}. By comparison, D-gentiobiose differs only in the presence of a couplet centred at ~ 1133 cm^{-1} with the opposite sense to that observed in D-cellobiose. In addition, both exhibit changes in the relative intensities of the signals relative to D-glucose and the α-linked disaccharides. Normal coordinate analysis[4] again seems to indicate that the glycosidic stretching coordinates contribute significantly to the normal modes responsible for the ROA couplets in the range ~ 1120 to 1140 cm^{-1} for disaccharides with a β-linkage. Thus, it appears likely that the observed changes may be attributed to the glycosidic link and also that these signals have a sign dependence on conformation.

The complex nature of vibrations in this region make it difficult to assign accurately the vibrations involved in generating the ROA. However, it does mean that this region provides a "fingerprint" characteristic of the individual disaccharide units and not just a sum of the two constituent sugar residues so that it actually provides information complementary to that available from the CH_2 and C-O-H deformations region as will be discussed below. Furthermore, the

isolation of ROA signals originating in the link yields an additional perspective on their conformation to those already identified in the low wavenumber and anomeric regions. Finally, it appears that the glycosidic link of the β-linked species has more influence in this region than the α-linked species which is in contrast to the anomeric region where the opposite is true.

7.2.4 CH_2 and COH Deformations Region (~ 1200-1500 cm^{-1})

The study of the ROA spectra of D-glucose and several deuterated analogues presented in chapter 5 produced a number of interesting results in this region. The normal modes responsible for the negative and positive ROA signals at ~ 1220 cm^{-1} and 1260 cm^{-1} in D-glucose were shown to involve coupled CH_2 and C-O-H deformations and it was proposed that these two bands were associated with the *gauche-gauche* and *gauche-trans* rotamers of the exocyclic hydroxymethyl group, respectively. In addition, it was demonstrated that only the β-anomeric form of D-glucose would generate a ROA signal at ~ 1260 cm^{-1}. The results obtained from monosaccharides are expected to have a strong bearing on the interpretation of the disaccharide spectra presented here as a normal coordinate analysis of the dimer repeating unit of cellulose predicted that the majority of normal modes above 1200 cm^{-1} are localised within the individual residues and are almost identical to those calculated for the monomer, β-D-glucose.[22]

The positive ROA signal at ~ 1260 cm^{-1}, mentioned above, was assigned to the β-anomeric form because the ROA spectra of α-D-methyl glucoside,[8] D-trehalose (Figure 7.7) and α-D-cyclodextrin (Figure 8.3), all of which exist solely in the α-anomeric form, exhibit no ROA signal at this wavenumber; whereas that of β-D-methyl

glucoside,[8] which exists solely in the β-anomeric form, registers an increase in intensity relative to D-glucose. If we assume that the rotameric distribution of the exocyclic hydroxymethyl group in the molecules studied here is similar to that of D-glucose (or is not the decisive factor in determining the ROA intensity of this band) then it may be used to estimate the anomeric proportions of D-glucose residues.

Table 7.2 lists the experimental Δ-values for the ~ 1260 cm^{-1} signal for a number of mono- and disaccharides which were calculated by dividing the intensity of the ROA signal by the intensity of the deconvoluted parent Raman band. The Δ-value of 4.7×10^{-4} for β-D-methyl glucoside was taken as a standard representing a molecule which has a population of 100% β-anomer and the populations of the others were calculated relative to this standard. For the disaccharides there are two anomeric centres contributing to the total value: one in the non-reducing residue and one in the reducing residue. For α-linked species the non-reducing residue is trapped in the α-anomeric form by the linkage so it makes no contribution to the ROA intensity of the ~ 1260 cm^{-1} signal. Thus, the total β-anomeric percentage is equal to half the β-anomeric percentage of the reducing residue. However, for β-linked species the anomeric centre of the non-reducing residue is trapped by the linkage in the β-anomeric form. Therefore, to find the population of the anomeric centre of the reducing residue it is necessary to remove the contribution from the non-reducing residue. This is achieved by considering the two residues separately. The non-reducing residue is 100% in the β-anomeric form so it makes a contribution of 50% to the total as there are two residues contributing. The reducing residue makes up the remainder so by subtracting 50% from the total percentage and multiplying by two we can find the anomeric population of the reducing residue.

Table 7.2 Δ-values for the 1260 cm^{-1} ROA signal and calculated anomeric percentages.

saccharide	Δ-value ($\times 10^{+4}$)	total % of β-anomer	% of β-anomer in the reducing residue
β-D-methyl glucoside[a]	+4.7	100	–
D-glucose[b]	+3.0	64	64
D-glucosamine[b]	+1.4	30	30
D-maltose[c]	+1.8	38	76
D-isomaltose[c]	+1.8	38	76
D-cellobiose[c]	+3.7	78	56
D-gentiobiose[c]	+3.7	78	56
D-laminaribiose[c]	+3.8	81	62

[a] data from ref. 8, [b] data from ref. 9, [c] this work.

The percentage of β-anomer present for the two monosaccharides D-glucose and D-glucosamine[6] listed in Table 7.2 have been well characterised by NMR spectroscopy.[23,24] For D-glucose the value of 64% obtained is in agreement with the accepted value of 64% obtained from NMR experiments[23] and our value of 30% for D-glucosamine hydrochloride is not too far removed from the recognised value[24] of

37%. These figures demonstrate that although our technique does not at present offer the precision of other methods (due to the weak intensity of this ROA signal, the uncertainty as to where exactly the baseline should lie and the difficulty of deconvoluting the parent Raman band accurately) it can still provide a reasonable guide to the anomeric populations.

It is clear from inspection of Table 7.2 that the two α-linked species, D-maltose and D-isomaltose, have identical Δ-values for the positive ROA signal at ~ 1260 cm^{-1} as have the three β-linked species, D-cellobiose, D-laminaribiose and D-gentiobiose. Furthermore, comparison of the ROA spectra of D-maltose (Figure 7.2) with D-cellobiose (Figure 7.4) reveals that the β-linked species exhibits a much stronger ROA signal at ~ 1260 cm^{-1}. This difference is reflected in the Δ-values presented in Table 7.2 and can be ascribed to the fact that the anomeric centre of the non-reducing residue of D-maltose is trapped in the α-anomeric form by the linkage. When the contribution from the non-reducing residue is removed the α- and β-(1-4) and (1-6) linked disaccharides are found to have 76% and 56% β-anomer present in the reducing residue, respectively and the β(1-3) linked species 62%. NMR studies on maltose and cellobiose[25] and on gentiobiose[26] came to the conclusion that the reducing residue of these molecules had approximately the same proportions as the D-glucose monomer, i.e. 64% β-anomer. Our results seem to indicate that there is a strong correlation between the intensity of the ~ 1260 cm^{-1} ROA signal and the β-anomeric population; however, due to the problems mentioned above it is difficult at this stage to decide whether the differences found between α- and β-linked species are genuine or simply reflect the inaccuracies currently inherent in our method.

Between ~ 1300 cm^{-1} and ~ 1400 cm^{-1} the three β-linked disaccharides, D-cellobiose, D-laminaribiose and D-gentiobiose have almost identical Raman and ROA spectra to D-glucose which can be attributed to the preponderance of the β-anomeric form in these molecules. It would appear then that the ROA signals in the β-linked species are localised in the individual residues and may be assigned to the same normal modes as in D-glucose. The situation is somewhat different for the α-linked species as the Raman band at 1332 cm^{-1} increases in intensity in these spectra relative to that in D-glucose with concomitant changes in the ROA spectra. This intensity increase was ascribed to the presence of an additional band in the conventional Raman spectrum of the α-anomeric form of D-glucose which was assigned by deuteration studies[15] to a normal mode involving C-O-H deformations and CH_2 twisting motions. Normal coordinate analyses of α-D-glucose[21] and amylose,[16] for which D-maltose is the dimer repeating unit, revealed that this mode was a complex mixture of C-C-H and O-C-H deformations of the ring hydrogens with contributions from CH_2 twisting motions and significant involvement of C-O-H deformations. It is clear from inspection of the Raman and ROA spectra of D-maltose-O-d_8 (Figure 7.2) that this band is indeed sensitive to O-deuteration as there is a drop in intensity in both the Raman and ROA bands.

Further evidence for the ROA being localised in the individual residues in this region comes from the ROA spectra of D-lactose (Figure 7.8), which displays a remarkable similarity to that of the sum of the two constituent monomers, β-D-galactose and D-glucose. The only major difference is the appearance of a small negative ROA signal at ~ 1407 cm^{-1} in the spectrum of D-lactose which is also present in the ROA spectrum of D-cellobiose and D-laminaribiose. Dauchez *et al.*

assigned disaccharide Raman bands in the range ~ 1400-1500 cm^{-1} to angle bending vibrations around the carbons involved in the glycosidic link.[4,5] Thus, it is possible that this ROA signal is associated with the β(1-4) link found in both D-lactose and D-cellobiose.

7.3 Concluding Remarks

The ROA spectra of disaccharides based on D-glucose contain a number of new signals sensitive to the glycosidic link in addition to many signals similar to those found in D-glucose itself. These signals can have quite different intensities, or even opposite signs, for different linkage conformations and can appear at different frequencies for different linkage types. This suggests that ROA could be particularly useful for studying oligo- and polysaccharides where the solution conformations can be difficult to assign using existing physical methods on account of the flexibility of the glycosidic links which results in multiple conformations co-existing in solution.[27]

It is apparent that there are four distinct regions in our disaccharide ROA spectra that each provide complementary information. The anomeric region contains information on the glycosidic link. The fingerprint region provides a sign pattern characteristic of the entire disaccharide unit and in the CH_2 and COH deformations region the ROA signals are localised in the individual residues. These three regions could provide estimates of the residue content and linkage types present in oligosaccharides provided a sufficiently large database of model mono- and disaccharides could be built up. Future development of the assignments in a fourth region at low wavenumber could provide further information of this nature.

In this chapter the number of parameters used to extract information from the ROA spectrum has been extended. Previous ROA studies have concentrated mainly on the frequency and sign, and in general terms the intensity, of the ROA signals. For the ROA couplet at ~ 430±10 cm^{-1} we have used the shape of this signal to extract information on the linkage type, and for the positive ROA signal at ~ 1260 cm^{-1} we have accurately calculated the Δ-value and used it to determine the anomeric population of reducing residues in disaccharides. This shows that a consideration of shape and intensity of the ROA signals can significantly increase the information extracted from ROA spectra.

Future development of the work presented in this chapter could involve studying the remaining linkage types for diglucosides and extending the work to higher order homologues, such as trimers and tetramers, to help clarify which ROA signals are attributable to the glycosidic link. In addition, disaccharides consisting of residues other than D-glucose need to be studied separately although certain correlations may be found for molecules with the same linkage type but different residues content, such as the ~ 1407 cm^{-1} ROA signal in D-cellobiose and D-lactose.

References

1. M. Dauchez, P. Derreumaux and G. Vergoten, *J. Compu. Chem.*, **14** (1992) 263-277.
2. M. Sekkal, P. Legrand, G. Vergoten and M. Dauchez, *Spectrochim. Acta*, **48A** (1992) 959-973.
3. M. Mathlouthi and D. V. Luu, *Carbohydr. Res.*, **81** (1980) 203-13.
4. M. Dauchez, P. Derreumaux, M. Sekkal, P. Legant, P. Legrand and G. Vergoten, *Spectrochim. Acta.*, **50A** (1994) 87-105.
5. M. Dauchez, P. Lagant, M. Sekkal, B. Sombret, P. Derreumaux and G. Vergoten *Spectrochim. Acta.*, **50A** (1994) 105-119.
6. L. D. Barron, A. R. Gargaro and Z. Q. Wen, *Carbohydr. Res.*, **210** (1990) 39-49.
7. L. D. Barron, A. R. Gargaro, Z. Q. Wen, D. D. MacNicol and C. Butters, *Tetrahedron: Asymmetry*, **8** (1990) 513-516.
8. Z. Q. Wen, L. D. Barron and L. Hecht, *J. Am. Chem. Soc.*, **115** (1993) 285-292.
9. A. F. Bell, L. D. Barron and L. Hecht, *Carbohydr. Res*, **257** (1994) 11-24.
10. M. K. Dowd, A. D. French and P. J. Reilly, *Carbohydr. Res.*, **233** (1992) 15-34.
11. M. Dowd, P. Reilly and A. French, *J. Compu. Chem.*, **13** (1992) 102-114.
12. S. Melberg and K. Rasmussen, *Carbohydr. Res.*, **78** (1980) 215-224.
13. I. Tvaroska, A. Imberty and S. Perez, *Biopolymers*, **30** (1990) 369-379.
14. M. Mathlouthi and J. L. Koenig, *Adv. Carbohydr. Chem. Biochem.*, **44** (1986) 7-89.

15. P. D. Vasko, J. Blackwell and J. L. Koenig, *Carbohydr. Res.*, **19** (1971) 297-310.

16. J. J. Cael, J. L. Koenig and J. Blackwell, *Biopolymers*, **14** (1975) 1885-1903.

17. G. J. Quigley, A. Sarko and R. H. Marchessault, *J. Am. Chem. Soc.*, **92** (1970) 5834-5439.

18. I. Tvaroska, *Biopolymers*, **21** (1982) 1887-1897.

19. W. Hug, *Appl. Spectroscopy*, **1981**, 35, 115-124.

20. M. V. Korolevich, R. G. Zhbankov and V. V. Sivchik, *J. Mol. Structure*, **20** (1990) 301-313.

21. J. J. Cael, J. L. Koenig and J. Blackwell, *Carbohydr. Res.*, **32** (1974) 79-91.

22. J. J. Cael, K. H. Gardner, J. L. Koenig and J. Blackwell, *J. Chem. Phys.*, **62** (1975) 1145-1153.

23. S. J. Angyal, *Angew. Chem. Int. Ed. Engl.*, **8** (1969) 15-68.

24. D. Horton, J. S. Jewell and K. D. Philips, *J. Org. Chem.*, **31** (1966) 4022-4025.

25. A. Heyraud, M. Rinaudo, M. Vignon and M. Vincedon, *Biopolymers*, **18** (1979) 167-185.

26. D. Bassieux, D. Gagnaire and M. Vignon, *Carbohydr. Res.*, **56** (1977) 19-33.

27. K. G. Rice, P. Wu, L. Brand and Y. C. Lee, *Current Opinion in Structural Biology*, **3** (1993) 669-674.

Chapter 8

Vibrational Raman Optical Activity of Cyclodextrins, Polysaccharides and Glycoproteins

In this chapter the Raman and ROA spectra of a number of cyclodextrins and polysaccharides and of a single glycoprotein are presented. The interpretation of these spectra emphasise the influence of the secondary structure through ROA signals that were identified in the preceding chapter as originating in the coordinates of the glycosidic link. The particular examples chosen are the ring structure of CDs, the random coil type conformation exhibited by dextran, glycogen and pullulan and the helical conformations adopted by laminarin, each of which will be discussed separately. Also included is an example of a glycoprotein to demonstrate the potential of ROA for studying this class of biopolymers.

8.1 Cyclodextrins

Cyclodextrins (CDs) are cyclic, non-reducing oligosaccharides composed of six, seven or eight D-glucose residues bonded through α(1-4) glycosidic linkages and classified α-, β- and γ-CD, respectively.[1-4] Although larger analogues are possible it has been shown that CDs with fewer than six residues cannot form on steric grounds.[5] The D-glucose residues all exhibit the $^4C_1$ chair conformation with the result that CDs adopt the shape of a truncated cone, with all the secondary hydroxyl groups projecting from one side of the ring and all the primary hydroxyl groups from the other, as depicted schematically in Figure 8.1. The size of the cavity formed by CDs

depends on the number of D-glucose residues, and as all the C-H groups face inwards the molecule has a hydrophobic centre and a relatively hydrophilic outer suface which confers water solubility to these molecules.

A remarkable property of CDs is their ability to form inclusion complexes in aqueous solution and the solid state.[1-4] In general, inclusion complexes comprise two or more molecules in which a host molecule traps a guest molecule without the formation of covalent bonds. CDs are capable of forming inclusion complexes with a wide variety of molecules providing the guest's size is compatible with the dimensions of the cavity. Indeed, the entire guest molecule need not fit as it is also possible for complexes to be formed with the guest molecule only partially submerged in the CD cavity. However, the extent of complexation depends not only on the steric fit but also on the polarity of the molecule, with non-polar molecules being favoured. These inclusion complexes are of great interest to scientists in a number of fields as they provide models for enzyme catalysis and polymeric starch, they find application in the food industry and in the solubilisation of drugs, and in chromatography for separating closely related species or even enantiomers.[4,6]

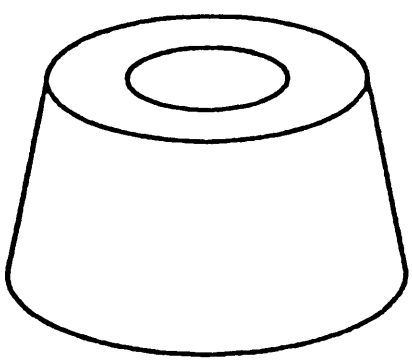

Figure 8.1 Schematic representation of the truncated cone shape adopted by CDs

8.1.1 Experimental

All the samples discussed in this section were supplied by Sigma. A sample of α-CD-O_{18} was prepared by lyophilising α—CD twice from D_2O solution before dissolving in D_2O to a concentration of 0.4 M. All the other samples were dissolved in H_2O to a concentration of 0.2 M, except for D-maltotriose which was made up as a 3 M solution, and allowed to equilibrate for 24 h. The equilibrated samples were treated with charcoal to reduce fluorescence, before being filtered into a quartz microfluorescence cell through 0.45 μm Millipore filters and centrifuged for at least 15 min. During spectral acquisition the laser power was ~ 700 mW at the sample and the slit width set to 120 μm giving a spectral bandpass of ~ 12 cm^{-1} at 514.5 nm. The spectra were recorded over 3 h for α-CD, dimethyl β-CD and trimethyl β-CD and over 2 h for D-maltotriose and γ-CD.

8.1.2 Results and Discussion

The Raman and ROA spectra of D-maltotriose, α-D-cyclodextrin, α-D-cyclodextrin-O-d_{18}, γ-D-cyclodextrin, heptakis(2,6 di-O-methyl)-β-cyclodextrin (dimethyl β-CD) and heptakis(2,3,6 tri-O-methyl)-β-cyclodextrin (trimethyl β-CD) are presented in the range ~ 650 to 1500 cm^{-1} in Figures 8.2-8.7, respectively. Both α- and γ-CD are moderately soluble in aqueous solution but β-CD did not have a high enough solubility to allow the ROA spectrum to be recorded reliably. However, the two methylated derivatives of β-CD, namely, dimethyl β-CD and trimethyl β-CD, which have the hydroxyl groups at carbon atoms 2 and 6 and at 2,3 and 6 methylated, respectively, were sufficiently soluble. The ROA spectra discussed in earlier chapters were subdivided into four distinct regions, but for the CDs we shall instead

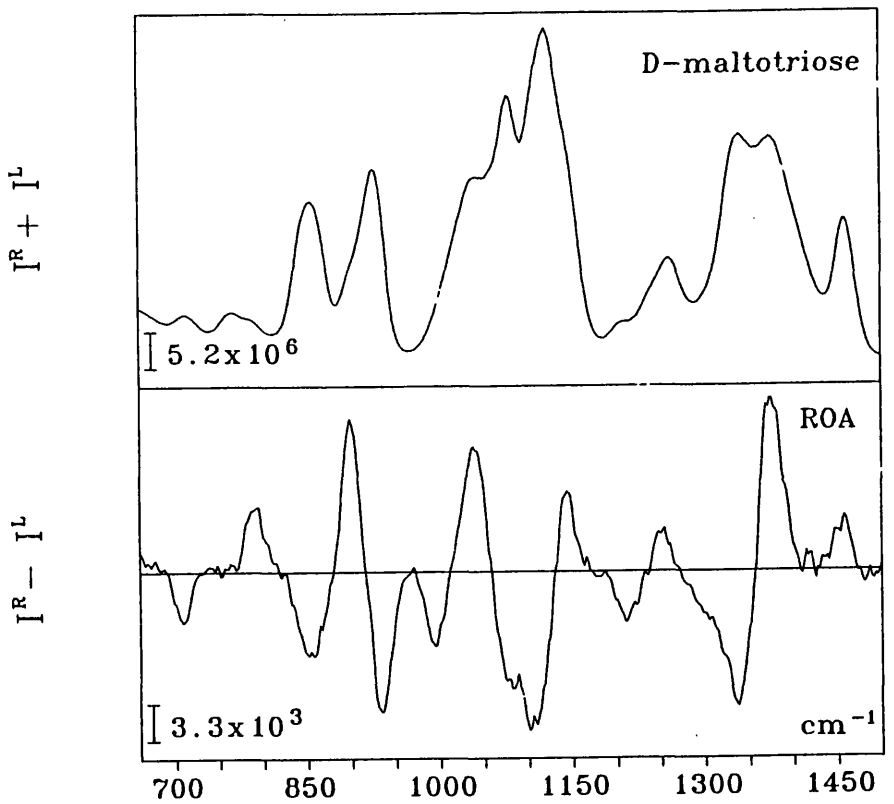

Figure 8.2 The backscattered Raman ($I^R + I^L$) and ROA ($I^R - I^L$) spectra of D-maltotriose in H_2O.

concentrate solely on the glycosidic couplet that is centred at ~ 917 cm^{-1} in D-maltose, thereby extending its discussion from chapter 7.

8.1.3 The Glycosidic Couplet

The most pronounced signal in the ROA spectrum of α-CD (Figure 8.3) is the glycosidic couplet, positive at low and negative at high wavenumber, centred at ~ 922 cm^{-1}. The Δ-value and the centre wavenumber for this couplet in a number of CDs and D-maltose oligomers are listed in Table 8.1 together with the ratio of this value to that found in D-maltose. These values were calculated without deconvolution of the parent Raman band with the background simply

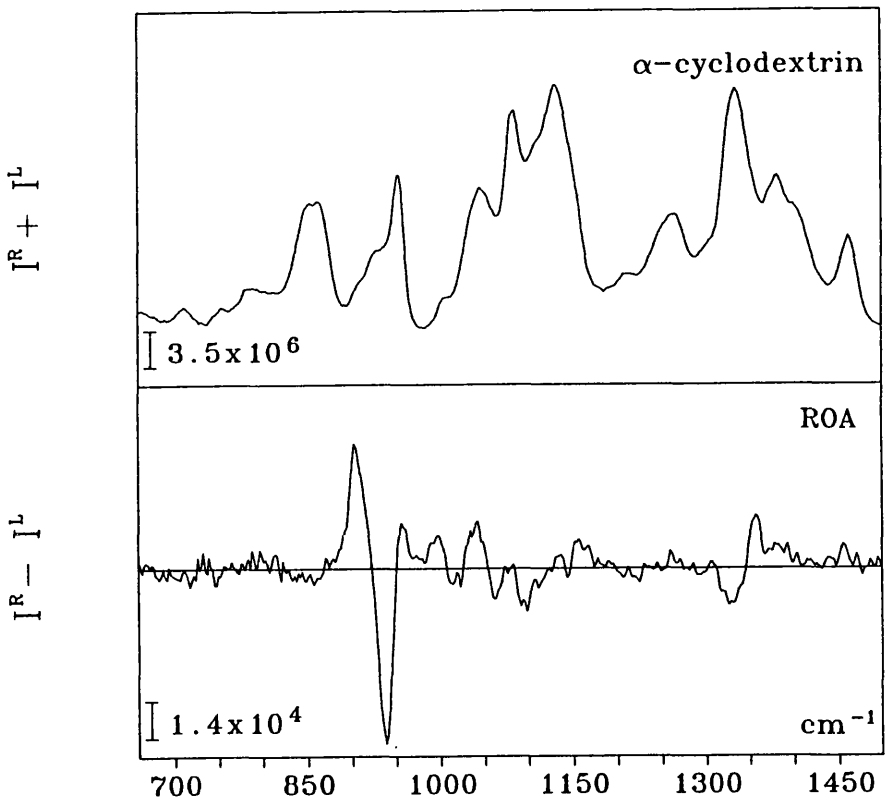

Figure 8.3 The backscattered Raman ($I^R + I^L$) and ROA ($I^R - I^L$) spectra of α-cyclodextrin in H_2O.

taken as a slope from the minima of the Raman spectrum at higher wavenumber to the minima at lower wavenumber. The Δ-values were calculated for the negative component of the couplet as the associated Raman band is more distinct.

The most interesting result from Table 8.1 is that the Δ-value for cyclic α-CD is approximately six times larger than five times the Δ-value of the dimer, D-maltose, which approximately represents the Δ-value of the corresponding linear hexamer. An initial survey of the ROA of CDs proposed that this dramatic increase in the intensity was attributable to the delocalisation of the normal modes responsible for the couplet over the CD ring.[7] We now extend this work by suggesting

Table 8.1 The Δ-value for the negative component of the glycosidic couplet in a selection of maltose oligomers and cyclodextrins.

oligosaccharide	Δ-value ($\times 10^4$)	ratio to D-maltose	centre wavenumber
D-maltose	2.3	1	917
D-maltotriose	5.4	2.3	917
D-maltotetraose	8.5	3.7	917
α-CD	70	30	922
α-CD-O-d_{18}	9.7	4.2	894
dimethyl β-CD	82	36	925
trimethyl β-CD	14.5	6.3	926
γ-CD	37	16	926

that the mechanism by which the additional ROA intensity is generated involves C-O-H deformations and possibly intramolecular hydrogen bonding. The existence of such hydrogen bonds is well known from the crystal structures of CDs[8-11] and is likely to persist to some degree even in aqueous solution, with water molecules competing for the hydrogen bonds, because of the cyclic structure of CDs.

CDs are notable amongst oligosaccharides for their ability to form single crystals which makes them readily amenable to determination of their solid state conformation by x-ray crystallography.[8-11] For α-CD, the crystal structure of the hexahydrate is distorted from a regular hexagonal symmetry thereby reducing the angle strain on the glycosidic oxygen caused by cyclisation. This is achieved by rotating one of the D-glucose residues into a position more nearly normal to the axis of the CD torus and has the consequence of breaking two of the six intramolecular hydrogen bonds that can form between hydroxyl groups

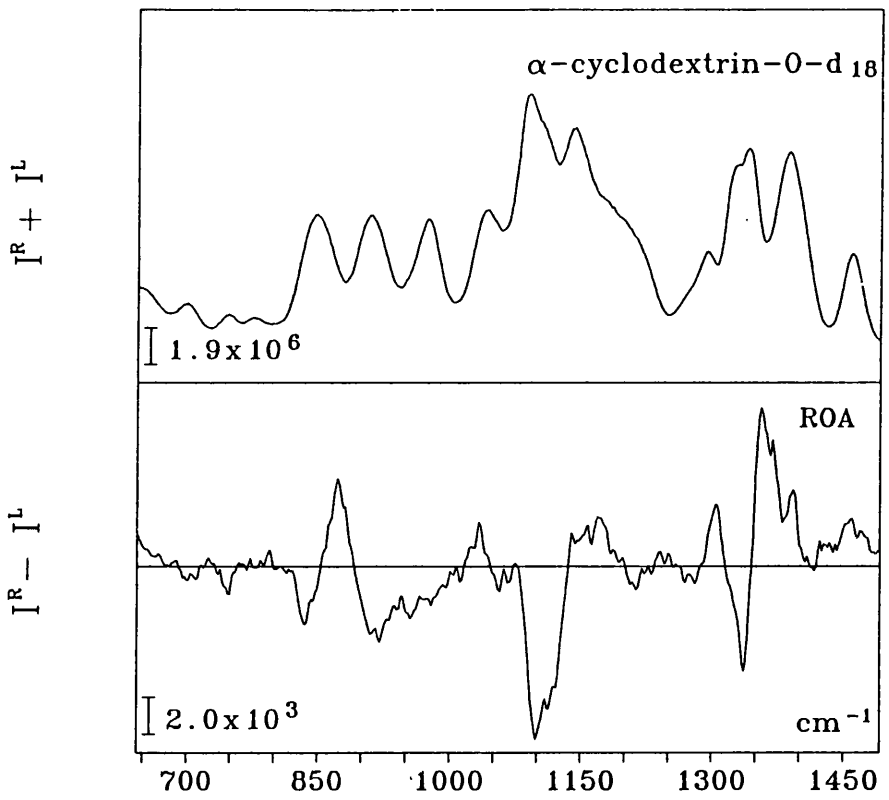

Figure 8.4 The backscattered Raman ($I^R + I^L$) and ROA ($I^R - I^L$) spectra α-cyclodextrin-O-d_{18} in D_2O.

on carbon atoms 2 and 3 of adjacent residues.[8] Upon complexation, α-CD is found to adopt a much more symmetrical conformation in the solid state.[11] The strain on the glycosidic oxygen angle is lower in β-CD and γ-CD and this is reflected in their more symmetrical crystal structures and correspondingly stronger intramolecular hydrogen bonds.[9,10] In all three CDs it was found that the glycosidic oxygen atoms approximately define a plane.

In aqueous solution, NMR is unable to distinguish between any of the D-glucose residues in CDs which implies that they all adopt structures with C_n symmetry, where n is the number of D-glucose residues, at least on the NMR timescale.[12] However, there is

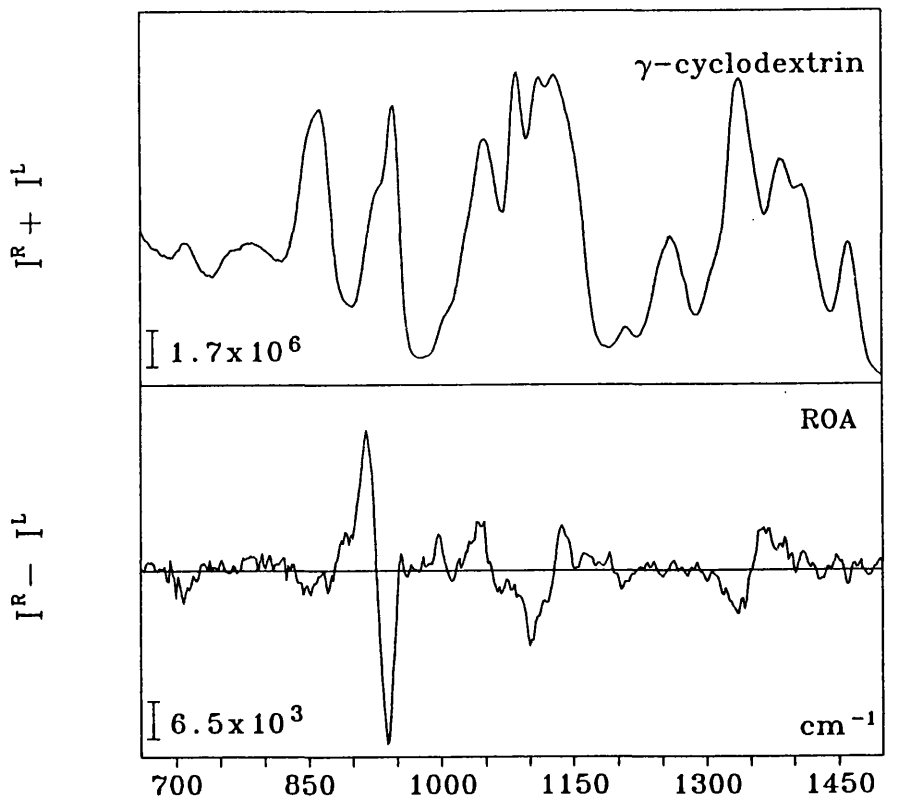

Figure 8.5 The backscattered Raman ($I^R + I^L$) and ROA ($I^R - I^L$) spectra of γ-cyclodextrin in H_2O.

considerable evidence from molecular dynamics (MD) simulations[13-15] that CDs are in fact rather flexible molecules with variations of up to ±40° on the mean glycosidic torsion angles found in one simulation of α-CD in aqueous solution.[13] This same study also revealed that, while α-CD can adopt a regular structure with all six intramolecular hydrogen bonds rather weakly formed, this is slightly unfavourable and usually either one or two of these hydrogen bonds will be broken with the others formed at their expense. Another MD study, this time of α-, β- and γ-CD, demonstrated that structures of lower symmetry actually had a lower energy than the highly symmetric C_n structures.[14] It was also noted that the hydroxyl groups at carbon atoms 2 and 3 had a propensity for forming small clusters (dimers, trimers or tetramers) of

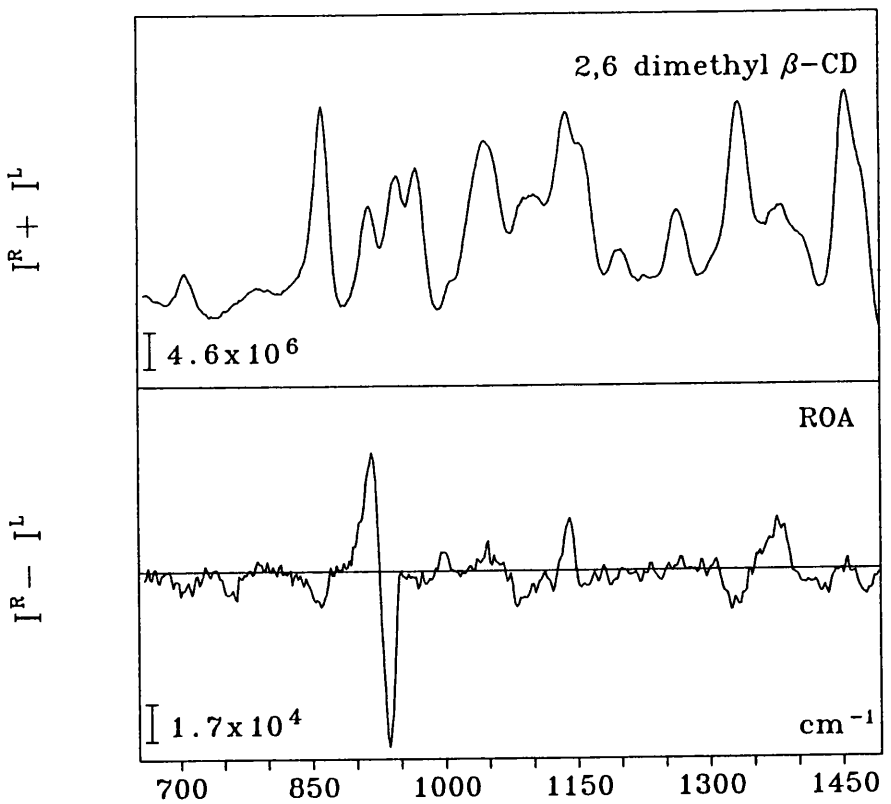

Figure 8.6 The backscattered Raman ($I^R + I^L$) and ROA ($I^R - I^L$) spectra of dimethyl β-CD in H_2O.

intramolecular hydrogen bonds. These results imply that the NMR structure simply represents a time-averaged view of the CD conformation.

The evidence for the involvement of C-O-H deformations and possibly intramolecular hydrogen bonds in the generation of the glycosidic couplet originates from three main sources. From the ROA spectrum of α-CD-O-d_{18} (Figure 8.4), where all the exchangeable hydroxyl hydrogen atoms have been replaced by deuterium atoms, it is clear that the glycosidic couplet has collapsed dramatically in intensity, has shifted by 28 cm^{-1} to lower wavenumber and has considerably broadened. This clearly indicates that C-O-H deformations are involved

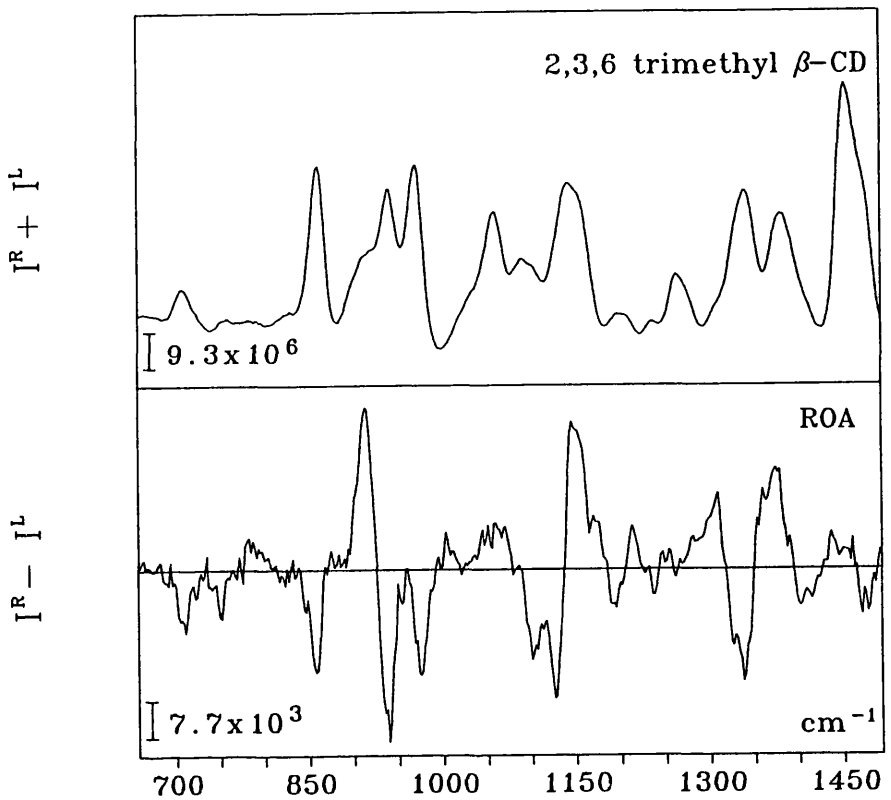

Figure 8.7 The backscattered Raman ($I^R + I^L$) and ROA ($I^R - I^L$) spectra of trimethyl β-CD in H_2O.

in the normal modes responsible for the glycosidic couplet and from the size of the decrease in intensity it seems reasonable to suggest that contributions of this type are responsible for the boost in intensity observed in the ROA spectra of CDs. Further evidence is forthcoming from the ROA spectra of di- and trimethyl β-CD (Figures 8.6 and 8.7). In dimethyl β-CD the Δ-value for the glycosidic couplet is slightly larger than in α-CD implying that methylating the hydroxyl groups at carbon atoms 2 and 6 has no effect on the generation of this couplet. This concurs with the crystal structure of dimethyl β-CD which is basically the same as that of β-CD except that the host cavity is extended by the methyl groups.[16] However, for trimethyl β-CD neither of the oxygen atoms substituted at carbon atoms 2 and 3 has a

hydrogen atom with which to form an intramolecular hydrogen bond and in fact the methyl groups substituted on the oxygen atoms cause steric hindrance which tends to increase the O2···O3' distance. This is reflected in the ROA spectrum of trimethyl β-CD where the glycosidic couplet is reduced to approximately the same intensity as the other large signals in the ROA spectrum. More specifically the Δ-value is found to be 1.45×10^{-3}, roughly the expected figure for a linear heptamer. The crystal structure of complexed trimethyl β-CD is considerably distorted relative to that of β-CD with the seven glycosidic oxygen atoms no longer defining a plane and five of the residues being tilted in the same direction as the lone residue in α-CD, with the hydroxymethyl group inclined towards the cavity, as a result of the lack of any intramolecular hydrogen bonds.[17] The final piece of evidence is a normal coordinate analysis[18] of V-amylose, for which D-maltose is the dimer repeating unit, which predicts that C-2-OH and C-3—OH deformations are involved in a normal mode at 946 cm^{-1} that also has contributions from the glycosidic link as discussed in chapter 7.

From comparison of the change in the glycosidic couplet in D-maltose (Figure 7.1) and α-CD (Figure 8.3) upon deuteration it is evident that C-O-H deformations, and thus the intramolecular hydrogen bond, has a much weaker influence in D-maltose. In aqueous solution, D-maltose is thought to exhibit two main conformational types; those with an intramolecular hydrogen bond present and those that adopt a hydrophobically folded structure with no intramolecular hydrogen bonding. The consensus from both experimental and theoretical studies is that the hydrophobically folded conformation is the major component in aqueous solution.[19–24] The fact that the Δ-values for D-maltotriose and D-maltotetraose are slightly more than two and three times greater than in D-maltose may reflect an increasing propensity toward

intramolecular hydrogen bond formation with increasing chain length, although further work on higher analogues is probably required to confirm this conclusion. It is also worth noting from Table 8.1 that γ-CD (Figure 8.5) has approximately half the Δ-value of α-CD. In the previous study of CD ROA it was noted that the spectrum of γ-CD was less distinct and more closely related to the trimer than that of α-CD and this was attributed to the greater flexibility afforded to the eight membered ring over a six membered ring.[7] A similar explanation could also be invoked to cover the decrease in the intensity of the glycosidic couplet. Whether or not the intramolecular hydrogen bond is a part of the mechanism is still uncertain; however, it would appear that this conformation, which brings the O2 and O3 groups on adjacent residues into closest contact, is the most important in generating the ROA which would explain the sharp rise in the CDs.

8.2 Dextran, Glycogen and Pullulan

Dextran is essentially an α(1-6) linked polysaccharide of D-glucose, but containing ~ 5% α(1-3) links that form branching points.[25] The majority of linkages in glycogen are α(1-4) but the molecule is highly branched with an α(1-6) link appearing, on average, every 10 to 14 residues.[26] In contrast, pullulan is an entirely linear glucan consisting of D-maltotriose units joined together by α(1-6) linkages.[27] All three polysaccharides are thought to adopt disordered, random coil type conformations in aqueous solution on account of the flexible α(1-6) links in the main chains in the case of dextran and pullulan and the frequent branching in the case of glycogen.

8.2.1 Experimental

Samples of dextran from *Leuconostoc mesenteroides* and glycogen from rabbit liver with number average degrees of polymerisation ($\overline{DP}_n$) of ~ 300 and 10^5, respectively, were supplied by Fluka and a sample of pullulan from *Aureobasidium pullulans* with a $\overline{DP}_n$ of ~ 250 from Sigma. All three were dissolved in Tris(hydroxymethyl)aminomethane (Tris) buffer (pH=7.5, 50mM) to a concentration of 200 mg/ml, 50 mg/ml and 200mg/ml for dextran, glycogen and pullulan, respectively. The three solutions were treated with charcoal to remove trace fluorescence impurities, and filtered through 0.45 μm Millipore filters into quartz microfluorescence cells. Each was then left to equilibrate for 24 h before being centrifuged for at least 15 min. It was found in the case of dextran and pullulan that the fluorescence background was burnt away by the laser within approximately 1 h, but that in the case of glycogen the sample had to be left in the laser beam overnight before ROA acquisition could begin. The higher concentration of the dextran and pullulan solutions allowed recording of the ROA in the low wavenumber region but this was not possible for glycogen because of its high Raman background, due to its relatively low concentration, and its immense light scattering, which is related to its high molecular weight. The Tris buffer gives rise to Raman bands at 1475, 1056, 782, 593, 498 and 474 cm^{-1} but these are weak and hardly interfere with the Raman spectrum of the polysaccharides. In any case as the buffer is achiral, it should not generate any associated ROA signals. The laser power was ~ 700 mW at the sample and the slit width was set to 120 μm corresponding to a spectral band pass of ~ 12 cm^{-1} at 514.5 nm. The acquisition times were 8, 8 and 13 h for dextran, glycogen and pullulan, respectively.

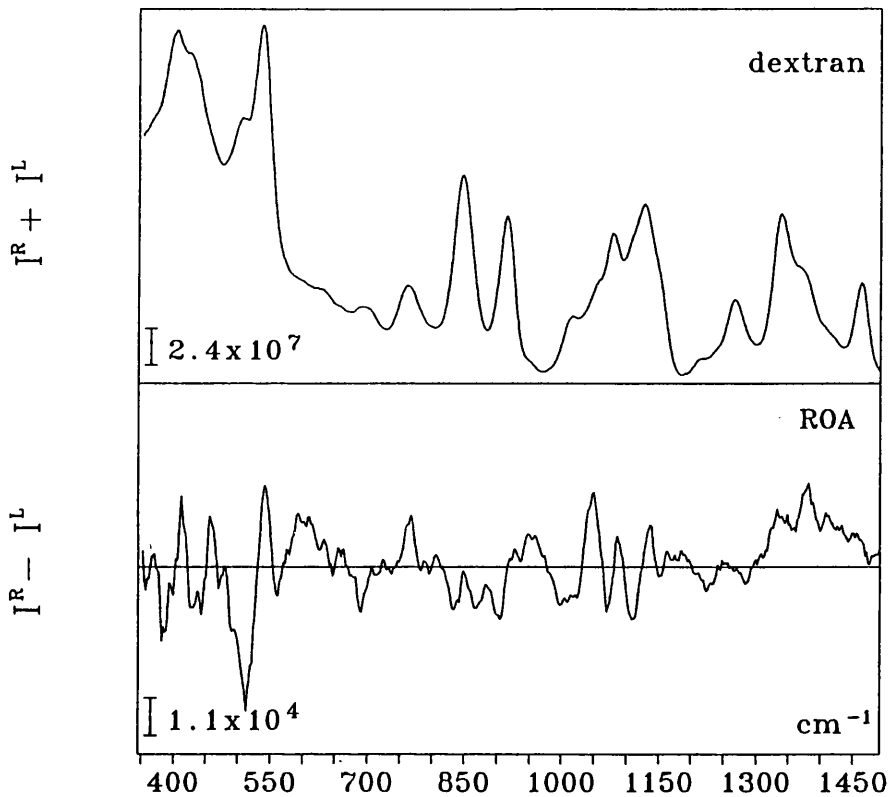

Figure 8.8 The backscattered Raman ($I^R + I^L$) and ROA ($I^R - I^L$) spectra of dextran in tris buffer (pH=7.5, 50 mM).

8.2.2 Results and Discussion

The Raman and ROA spectra of dextran and pullulan in Tris buffer in the range ~ 350 to 1500 cm^{-1} and glycogen in the range ~ 700 to 1500 cm^{-1} are presented in Figures 8.8-8.10, respectively. In the following discussion the spectra are not subdivided into distinct regions, as they were in earlier chapters, but instead treated as a whole. The Raman and ROA spectra of dextran, pullulan and glycogen (Figures 8.8-8.10) are compared with their repeating units D-isomaltose (Figure 7.4), D-maltotriose (Figure 8.2) and D-maltose (Figure 7.1), respectively.

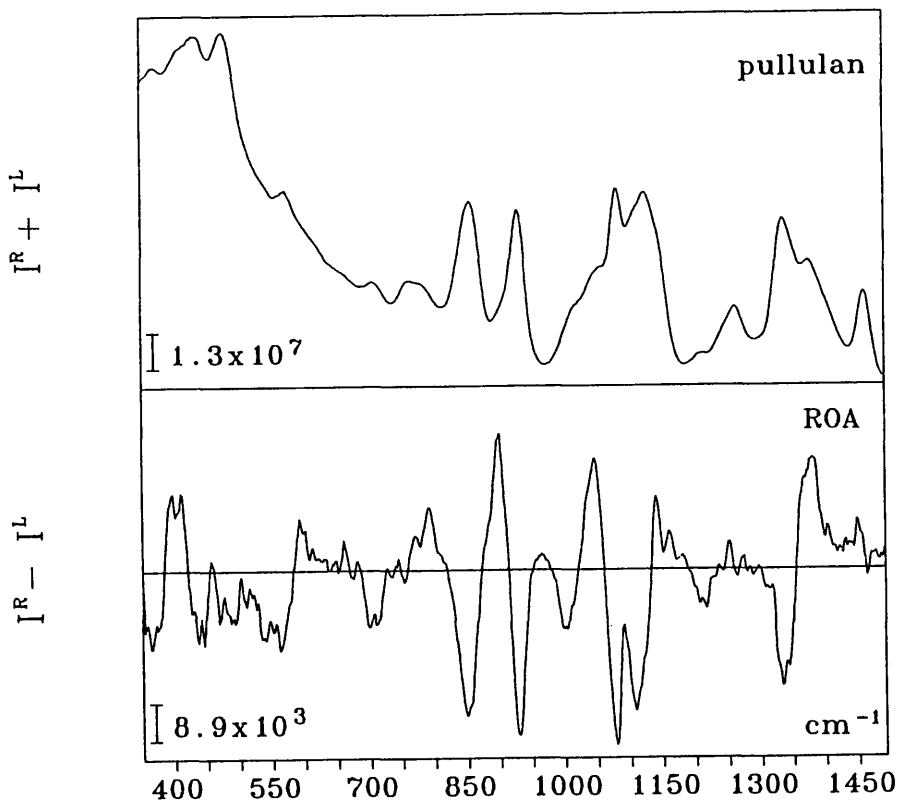

Figure 8.9 The backscattered Raman ($I^R + I^L$) and ROA ($I^R - I^L$) spectra of pullulan in tris buffer (pH=7.5, 50 mM).

Inspection of the Raman and ROA spectra of dextran and D-isomaltose and also of glycogen and D-maltose reveals that within each pair there is a close resemblance but that there are some notable differences. These include the absence of the positive ROA signal at ~ 1260 cm^{-1} from the ROA spectra of dextran and glycogen and also changes in the relative intensities of a number of Raman bands, in particular, those occurring at 1338, 1080, 848, 763 and 693 cm^{-1}. In addition, two new ROA signals at ~ 955 and 867 cm^{-1} appear only in the spectrum of dextran.

The positive ROA signal at ~ 1260 cm^{-1} was assigned in the earlier chapters to the β-anomeric form of D-glucose. It is not surprising that

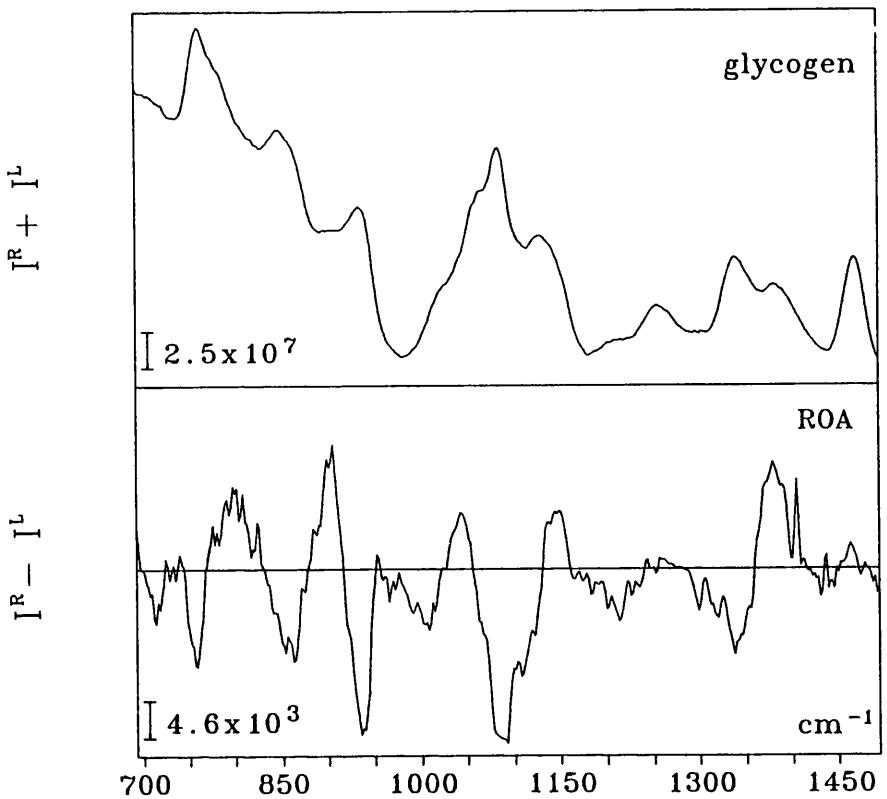

Figure 8.10 The backscattered Raman ($I^R + I^L$) and ROA ($I^R - I^L$) spectra of glycogen in tris buffer (pH=7.5, 50 mM).

this signal does not appear in the ROA spectra of dextran and glycogen as only a negligible amount of the β-anomeric form, from the terminal reducing residues, will be present in these molecules. Similarly, for other bands sensitive to anomeric configuration differences in the relative intensities may be due to the increased ratio of the α-anomeric form to the β-anomeric form in the polysaccharides. Another possibility is that because in the dimers there is only a single glycosidic link for every two residues, whereas in the polymers there is approximately one such link per residue, signals originating in the linkage become more prominent. Thus, the higher homologues of D-isomaltose and D-maltose should more closely resemble the polymers and, indeed, this appears to be true in the case of D-maltotriose.

The most intriguing features of the ROA spectrum of dextran are the two new signals positive at ~ 955 cm^{-1} and negative at ~ 867 cm^{-1}. The appearance of these signals, which are absent from the ROA spectrum of the dimer, may represent glycosidic linkage conformations adopted by the polymer in aqueous solution that are not available to the dimer. Alternatively, these signals could arise in the α(1-3) linked branching points that account for about 5% of the residues. Until either an unbranched dextran sample or the α(1-3) disaccharide have been studied it is unclear if either of these two explanations is correct.

Comparison of the ROA spectra of pullulan and D-maltotriose reveals that the two are very similar even though every third linkage is of the α(1-6) type in pullulan. The majority of the ROA signals of α(1-4) and α(1-6) linked species have the same sign so they would be expected to reinforce one another. However, one exception is the glycosidic couplet at ~ 917 cm^{-1} which has opposite signs for α(1-4) and α(1-6) linked species. In the ROA spectrum of pullulan there is no evidence that this couplet is reduced in intensity relative to the trimer; in fact, the Δ-value of 8.9×10^{-4} is approximately the same as the value for the tetramer (Table 8.1). These results are consistent with the possibility that the maltotriose units in pullulan are more rigid than in the free trimer and that the α(1-6) linkages are rather flexible.

8.3 Laminarin

Laminarin from the *Laminaria digitata* species is essentially a β(1-3) linked glucan which is found in algae where it acts as the main carbohydrate food reserve.[29-31] It occurs in two main forms which have different fine structure and are distinguished by their cold water solubility. The $\overline{DP}_n$ of the cold water soluble form is between 26 and

31 with an average chain length of between 7 and 10 units corresponding to an average of two or three branches per chain. The branching points have been identified as β(1-6) linkages and there is evidence to suggest in some species that the branch chain is only a single residue long.[32] It has also been found that ~ 40% of the laminarin chains terminate with a D-mannitol group.[29-31]

8.3.1 Experimental

A sample of laminarin from *Laminaria digitata* was supplied by Sigma. A sample of O-deuterated laminarin was prepared by lyophilising laminarin from D_2O twice then dissolving in deuterated Tris buffer (pD=7.3, 50 mM) to a concentration of 200 mg/ml. Undeuterated laminarin was dissolved in Tris buffer (pH=7.5, 50 mM) to the same concentration. Neither sample was treated with charcoal as this was found to be difficult to remove from laminarin solutions. After 24 h equilibration the samples were placed in quartz microfluorescence cells and centrifuged for at least 15 min. Both samples were found to be highly scattering and to have very large fluorescence backgrounds so they were required to be left in the laser beam overnight before ROA acquisition could begin. The laser power was ~ 700 mW at the sample and the spectral band pass was ~ 12 cm^{-1} at 514.5 nm. The acquisition time for both laminarin and O-deuterated laminarin was 8 h.

8.3.2 Results and Discussion

The Raman and ROA spectra of the cold water soluble form of laminarin and O-deuterated laminarin in the range ~ 350 to 1500 cm^{-1} are presented in Figures 8.11 and 8.12, respectively. The conformation of β(1-3) linked glucans with a variety of $\overline{DP}_n$ and degrees of branching

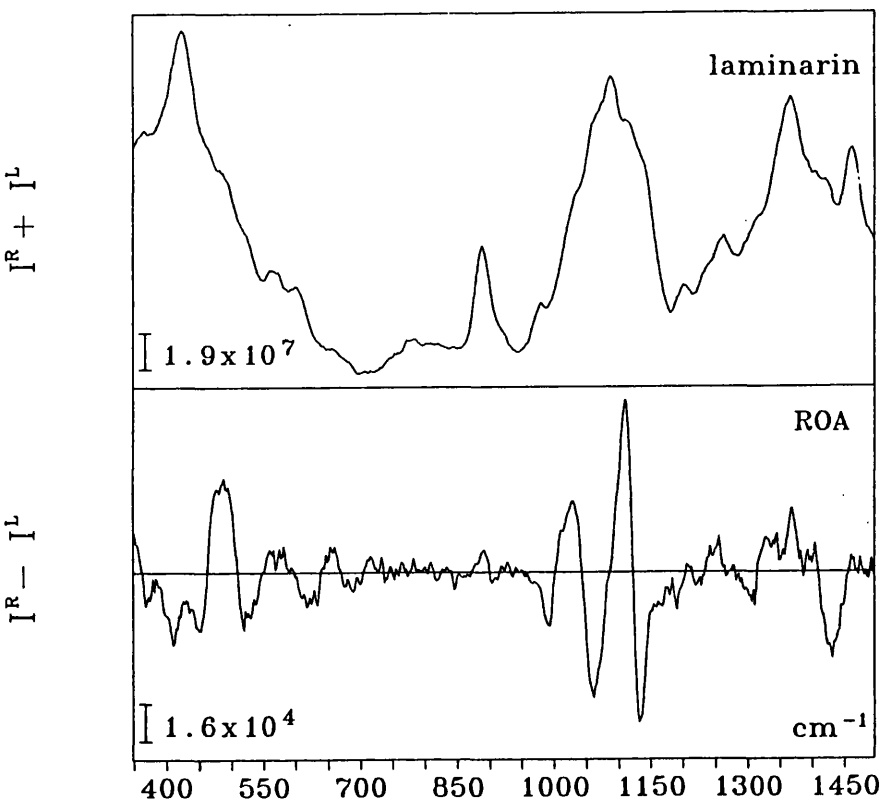

Figure 8.11 The backscattered Raman ($I^R + I^L$) and ROA ($I^R - I^L$) spectra of laminarin in tris buffer (pH=7.5, 50 mM).

have been studied by a combination of x-ray fibre diffraction and ^{13}C NMR.[32-40] The NMR studies are based on the x-ray data[32-37] but are extended to include glucans that form gels in solution or do not possess sufficient crystallinity to show fibre diffraction patterns.[38-40]

From the fibre diffraction data a triple helical structure has been proposed in the solid state for both linear and branched β(1-3) glucans as well as anhydrous and hydrated forms.[32-37] The fibre diffraction data are supplemented by energy calculations which found the most likely structure to be a parallel right handed triple helix, with the three strands linked through triads of strong hydrogen bonds between the hydroxyl groups on carbon atom 2, with additional strong hydrogen

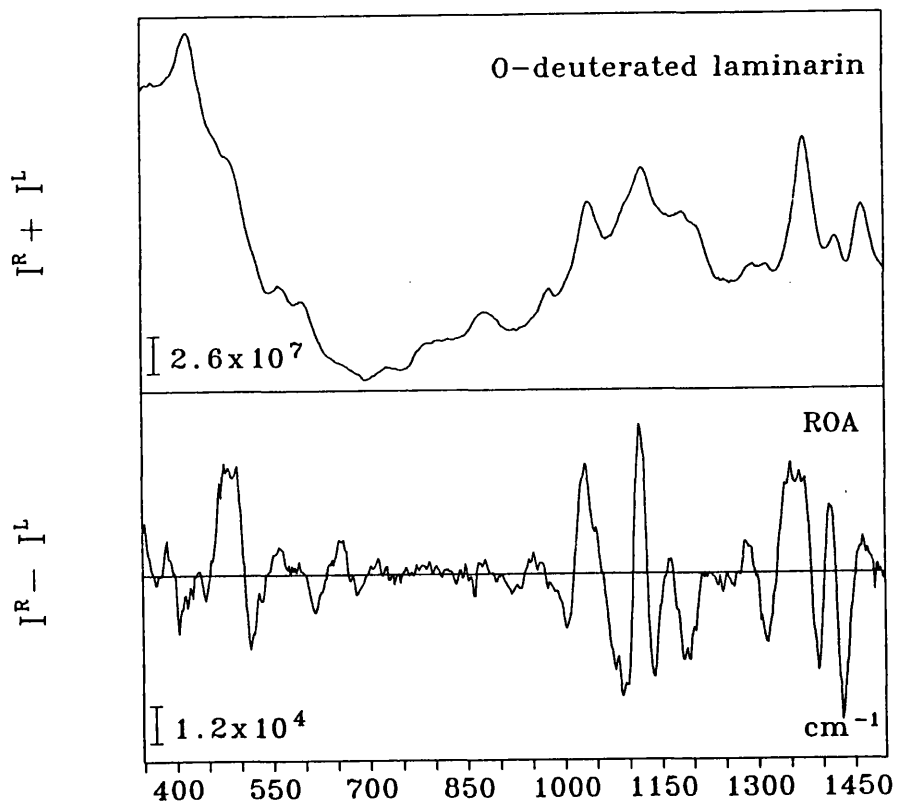

Figure 8.12 The backscattered Raman ($I^R + I^L$) and ROA ($I^R - I^L$) spectra of O-deuterated laminarin in deuterated tris buffer (pD=7.3, 50 mM).

bonds also forming within each helix between the hydroxyl groups on carbon atoms 4 and 6. This intramolecular hydrogen bond holds all the hydroxymethyl groups in the TG rotameric form. For the anhydrous form the φ and ψ glycosidic torsion angles are found to be 29^o and 10^o, respectively.[32] The hydrated form is found to be almost identical to the anhydrous form except that the hydroxymethyl groups are disordered and exist in all three rotameric forms.[33] Substitution of the hydroxyl group on carbon atom 6 was found not to hamper triple helix formation in the solid state as the substituents are situated on the periphery of the helix which makes lateral packing far more difficult.[34]

A left handed triple helical structure has also been calculated to have φ and ψ glycosidic torsion angles of -10^{o} and -40^{o}, respectively.

The crystal structure of D-laminaribiose, the dimer repeating unit of laminarin, was found to differ somewhat from that of the polymer, with an intramolecular hydrogen bond forming between the hydroxyl groups substituted at carbon atoms 4 and 5, only the GG and GT rotameric forms of the hydroxymethyl group being present and the φ and ψ glycosidic torsion angles being 28^{o} and -37^{o}, respectively.[36] Comparing the glycosidic torsion angles for a number of $\beta(1\text{-}3)$ linked dimers and polymers obtained from crystal structures revealed a much larger variation in the ψ than the φ torsion angle.[37]

From ^{13}C NMR experiments three main conformations have been characterised for $\beta(1\text{-}3)$ linked glucans: random coils, single helices and triple helices.[38-40] For chains with DP of between 14 and 130 the most likely conformation in the solid state is the triple helix which accounts for ~ 60% of the total with the remainder being of the random coil type conformation also adopted by low molecular weight oligomers.[38,39] For chains with DP of greater than 250 the amount of triple helix drops to ~ 10% and the majority of the chains adopt a single helical conformation.[38,39] (This single helical conformation is important in the formation of gels, but as laminarin is a non-gelling polysaccharide it is not expected to be present.) The branches that are present in laminarin promote triple helix formation as they prevent the close packing required for single helical chains. It was also noted that the C-3 chemical shift underwent much larger variation than the C-1 chemical shift which indicates that the ψ torsion angle is less restricted than the φ torsion angle in agreement with the x-ray data.[39]

In aqueous solution, ^{13}C NMR and optical rotation data reveal that both linear and branched β(1-3) linked glucans adopt ordered conformations.[34] A ^{1}H NMR relaxation study demonstrated that ~ 30% of a 10% w/w solution of laminarin adopts a triple helical structure, with the hydroxyl hydrogen atoms unexchanged after 2 hours in D_2O, while the remainder exists as random coils.[41] A recent optical rotation study of laminaribiose and β(1-3) linked glucans concluded that low molecular weight chains of DP less than ~ 20 adopt a conformation similar to that of the disaccharide but that changes in the optical rotation of longer chains were not characteristic of any single chain conformation but rather reflected chain association.[42]

When the Raman and ROA spectra of laminarin (Figure 8.11) are compared with those of D-laminaribiose (Figure 7.6), its dimer repeating unit, it is clear that, although the two Raman spectra are rather similar, there are some comprehensive differences in the ROA spectra. In particular, in the region between ~ 1050 and 1150 cm^{-1} the signs of the ROA signals are reversed, and above ~ 1200 cm^{-1} there are also distinct differences. In contrast, below ~ 1050 cm^{-1} the two ROA spectra are remarkably similar with the exception of a sign change at ~ 445 cm^{-1}. These changes indicate that there is some major conformational difference between the dimer and the polymer which is now discussed in more detail.

The region between ~ 1050 and 1150 cm^{-1} in D-laminaribiose has been assigned by normal coordinate analysis to C-O and C-C stretching coordinates with important contributions arising from the C-O stretches involving the glycosidic oxygen.[43] In this region there are some differences between the Raman spectra of D-laminaribiose and laminarin but the changes are far more distinct in the ROA spectra where four

signals at 1165 (+), 1128 (+), 1103 (-) and 1083 (+) in the dimer change sign in the polymer. These sign changes may be ascribed to triple helix formation in the polymer and the effect this has on the normal modes involving the glycosidic link. As discussed above in the solid state the dimer has $(\varphi,\psi)=(28^{O}, -37^{O})$, the right handed triple helical structure $(29^{O}, 10^{O})$ and the left handed triple helical structure $(-10^{O}, -40^{O})$. Both the x-ray diffraction and the ^{13}C NMR data provide evidence that the φ torsion angle is more resistant to change which implies that the right handed helical structure, which only involves a change in the ψ torsion angle relative to the dimer, is favoured with the ROA being sensitive to this change. In aqueous solution, there is probably a mixture of triple helix and random coil as evidenced by the NMR relaxation data of Hills *et al.*[41] Thus, the two types of laminarin chain present will tend to cancel out to a certain degree the ROA signal in this wavenumber range. Comparison of laminarin and its O-deuterated analogue (Figure 8.12) reveals that although the Raman spectra of the two in this range are quite different the ROA is basically the same but with small shifts to higher wavenumber. This means that although C-O-H deformations are involved significantly in the normal modes they contribute little to the associated ROA intensity. However, it is possible that the hydroxyl groups involved in hydrogen bonding in the triple helical conformation do not fully exchange[41] and may be making important contributions to the ROA intensity.

The region between ~ 1200 and 1500 cm^{-1} of the ROA spectrum of carbohydrates has, in the earlier chapters, been assigned to CH_2 and C-O-H deformations with some involvement from C-H related modes. Comparison of the ROA spectra of laminarin with D-laminaribiose reveals some distinct differences, in particular, the increase in intensity and shift to slightly higher wavenumber of the negative ROA signal at

~ 1431 cm^{-1} in the polymer. The other ROA signals in this region have the same sign in both the polymer and the dimer but are of much weaker relative intensity and are less distinct in the polymer. In chapter 7, the negative ROA signals at ~ 1407, 1410 and 1421 cm^{-1} in D-lactose, D-cellobiose and D-laminaribiose, respectively, were assigned to angle bending vibrations around the carbon atoms involved in the glycosidic link. This assignment is certainly consistent with the intensity increase, wavenumber shift and insensitivity to O-deuteration exhibited by this signal in the polymer. The other ROA signals in this region are known to be sensitive to hydroxymethyl group conformation and it is possible that the changes observed between the polymer and the dimer are due to the presence of the TG rotameric form. Although this rotamer is disfavoured in D-glucose residues it is observed in the crystal structures of both the anhydrous and hydrated forms of β(1-3) linked glucans as it forms stabilising intra-helix hydrogen bonds.

The O-deuterated laminarin undergoes a number of changes in this region including the appearance of a new ROA couplet, negative at low and positive at high wavenumber, centred at ~ 1400 cm^{-1}. This particular couplet may be attributable to the decoupling of the C-O-H deformation from the normal mode at this wavenumber which then produces this strong ROA signal. In addition, the weak positive and negative ROA signals at ~ 1260 and 1220 cm^{-1}, respectively, which were assigned to coupled C-O-H and CH_2 deformation in D-glucose are shifted to lower wavenumber and produce a new negative signal at ~ 1190 cm^{-1}.

Below ~ 1050 cm^{-1} there is little difference between the Raman and ROA spectra except for the Raman bands sensitive to anomeric configuration at 917, 888 and 846 cm^{-1}, which reflects the almost

negligible quantity of the α-anomeric form present in the polymer, and in the ROA where the sign is reversed at ~ 445 cm^{-1} in the polymer relative to the dimer. A couplet centred at ~ 427 cm^{-1} was assigned in the preceding chapter to the glycosidic link in diglucosides with the sign being dependent on the configuration of the link. It may be that the change in the sign at ~ 445 cm^{-1} reflects the difference in the glycosidic torsion angles in the triple helical structure. It has already been demonstrated in this chapter with the cyclodextrins that ROA signals in the anomeric region are sensitive to glycosidic linkage conformation for α-linked species but as with the β-linked disaccharides, laminarin lacks any ROA signals between ~ 700 and 890 cm^{-1}. There are some slight changes in the Raman bands on deuteration of the hydroxyl groups but the ROA is very similar to that of the undeuterated laminarin in the region below ~ 1050 cm^{-1}.

8.4 Glycoproteins

Since both carbohydrates and proteins[44-46] have now been fairly extensively examined by ROA it seems natural to enquire whether ROA can provide new information on glycoproteins, especially considering that intact glycoproteins are difficult to study using conventional physical methods. In this section the first ROA spectrum of a glycoprotein, orosomucoid, is presented and discussed briefly.

8.4.1 Experimental

A sample of orosomucoid (Cohn Fraction VI, 99%) from human blood serum was supplied by Sigma. The glycoprotein was made up as a 40 mg/ml solution in acetate buffer (pH=5.4, 200 mM), treated with charcoal and allowed to equilibrate. The sample was then filtered

through a 0.22 μm Millipore filter into a quartz microfluorescence cell and centrifuged for 15 min. It was found to have a very high fluorescent background and was required to be left in the beam overnight prior to ROA acquisition. The laser power was ~ 700 mW at the sample and the slit width was set for 120 μm corresponding to a spectral band pass of ~ 12 cm^{-1} at 514.5 nm. The acquisition time was 20 h.

8.4.2 Results and Discussion

The Raman and ROA spectra of orosomucoid (α_1-acid glycoprotein) in acetate buffer in the range ~ 700 to 1750 cm^{-1} is presented in Figure 8.13. This particular glycoprotein was chosen for its ready availability and high carbohydrate content of ~ 40%. It has a molecular weight of ~ 41,000 and consists of a single polypeptide chain of 181 amino acids with five hetero-oligosaccharides attached *via* N-glycosidic links to asparagine residues.[47]

We shall discuss first of all the signals in the ROA spectrum of orosomucoid that are characteristic of the protein segment of the molecule. A broad positive signal at ~ 1060 cm^{-1}, a strong sharp positive signal at ~ 1313 cm^{-1} and a couplet negative at low and positive at high wavenumber centred at ~ 1660 cm^{-1} indicate that the protein has a high β-sheet content.[45] This contrast with a recent study of orosomucoid that suggested that there may only be a small excess of β-sheet over α-helical structures.[48] There is also a strong sharp negative ROA signal at ~ 1245 cm^{-1} which also appears in insulin, ribonuclease A and lysozyme which may originate in dynamically disordered loops and end chains.

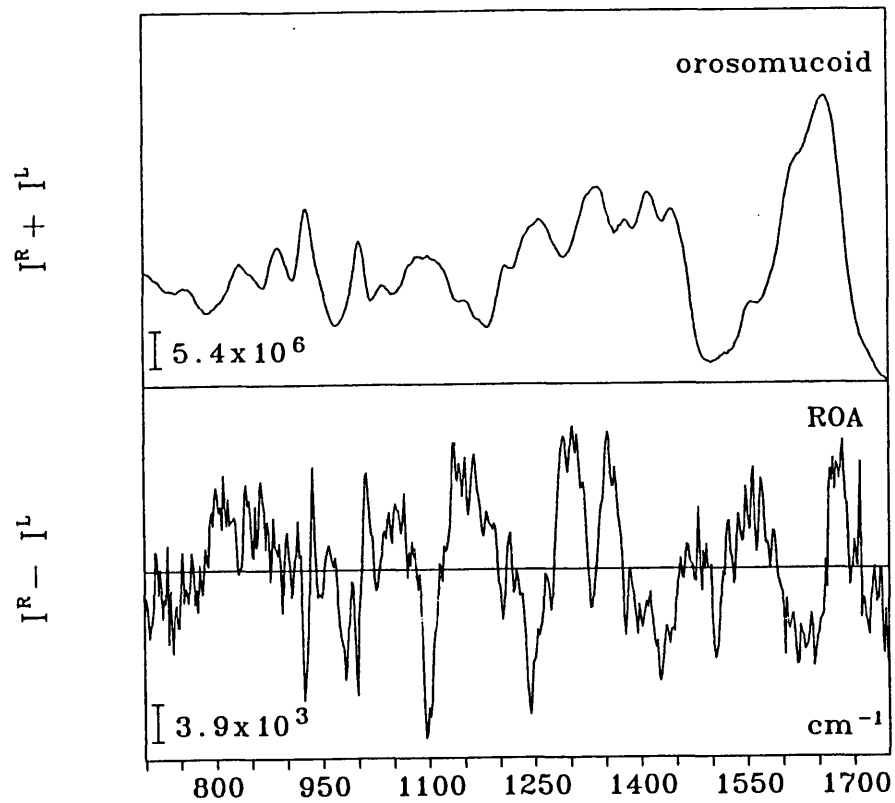

Figure 8.13 The backscattered Raman ($I^R + I^L$) and ROA ($I^R - I^L$) spectra of orosomucoid in acetate buffer (pH=5.4, 200 mM).

Although protein signals predominate, two striking ROA features which do not appear in any of the previous proteins studied to date could be specific to the carbohydrate and its association with the protein. The first of these new features is a large couplet, negative and sharp at lower wavenumber and positive at high, centred at ~ 1120 cm^{-1}. Early infrared studies[49] on a glycopeptide of orosomucoid identified contributions from the carbohydrate in the range ~ 1000 to 1200 cm^{-1}. The earlier discussion on β-linked disaccharides and laminarin revealed that these molecules exhibit ROA linkage features centred at ~ 1120 cm^{-1}. It seems likely then that this couplet may be assigned to the glycosidic links in the glycan chains having a β-configuration, which in the case of orosomucoid predominate over those with an

α-configuration. It is interesting to note that the couplet has the same sign in orosomucoid as in the β-linked disaccharides but is reversed relative to laminarin. This would seem to suggest that the conformation in the glycan chains is similar to that found in disaccharides and certainly unlike the triple helical structure proposed for laminarin.

The second new feature is a large sharp positive ROA signal at ~ 1360 cm^{-1}. In this region *negative* ROA signals have been identified in protein spectra that originate in β-turn vibrations.[46] It is interesting to note that the carbohydrates of the type present in orosomucoid are often attached at β-turns[50] so it seems possible that this positive ROA signal may be associated with the β-turns with glycan chains attached.

It does appear then that the ROA spectra of glycoproteins can contain information about both the carbohydrate and the protein and the mutual influence on each other's conformation and stability. An important aspect of future studies will be the use of linkage-specific endo-glycosidase enzymes to the cleave the glycan chains from the polypeptide so that a comparison can be made of the ROA spectrum of the complete glycoprotein with those of the separate carbohydrate and protein parts. Another valuable source of information on assignments should be forthcoming from deuteration studies on the glycoprotein.

Recently, Urbanova *et al.* applied vibrational circular dichroism (VCD) to the study of a glycoprotein, glucoamylase.[51] They found that the conventional electronic CD analysis of the protein secondary structure was quantitatively in error due to interference by sugar residues. The VCD analysis was thought to be more reliable because it avoids such interference, however, unlike ROA, it provides no information on the carbohydrate conformation.

References

1. J. Szejtli in *Cyclodextrins and their Inclusion Complexes,* Akedemiai Kiodo, Budapest, 1982.
2. W. Saenger in *Inclusion Compounds,* J. L. Atwood, J. E. D. Davies and D. D. MacNicol (Eds.), Academic Press, London, 1984, Vol. 2.
3. K. Harata in *Inclusion Compounds,* J. L. Atwood, J. E. Davies and D. D. MacNicol (Eds.), Academic Press, London, 1984, Vol 5.
4. W. Saenger, *Angew. Chem. Int. Ed.,* **19** (1980) 344-362.
5. P. R. Sundararajan and V. S. Rao, *Carbohydr. Res.,* **13** (1970) 351.
6. J. Szejtli in *Inclusion Compounds,* J. L. Atwood, J. E. Davies and D. D. MacNicol (Eds.), Academic Press, London, 1984, Vol. 2.
7. L. D. Barron, A. R. Gargaro, Z. Q. Wen, D. D. MacNicol and C. Butters, *Tetrahedron: Asymmetry,* **1** (1990) 513-516.
8. P. C. Manor and W. Saenger, *J. Am. Chem. Soc.,* **96** (1974) 3630.
9. K. Lindner and W. Saenger, *Carbohydr. Res.,* **99** (1982) 103.
10. K. Harata, *Bull. Chem. Soc. Jpn.,* **60** (1987) 2763.
11. K. K. Chako and W. Saenger, *J. Am. Chem. Soc.,* **103** (1981) 1708.
12. D. J. Wood, F. E. Hruska and W. Saenger, *J. Am. Chem. Soc.,* **99** (1977) 1735-1740.
13. J. E. H. Kohler, W. Saenger and W. F. van Gunsteren, *J. Mol. Biol.,* **203** (1988) 241-250.
14. K. B. Lipkowitz, *J. Org. Chem.,* **56** (1991) 6357-6367.
15. H. Dodziuk and K. Nowinski, *J. Mol. Structure,* **304** (1994) 61-68.
16. K. Harata, *Bull. Chem. Soc. Jpn.,* **61** (1988) 1939-1944.
17. K. Harata, K. Uekama, M. Otagiri and F. Hirayama, *Bull. Chem. Soc. Jpn.,* **56** (1983) 1732.
18. J. J. Cael, J. L. Koenig and J. Blackwell, *Biopolymers,* **14** (1975) 1885-1903.
19. I. Tvaroska, *Biopolymers,* **21** (1982) 1887-1897.

20. A. S. Shashkov, G. M. Lipkind and N. K. Kotchetkov,
21. E. S. Stevens, *Biopolymers*, **32** (1992) 1571-1579.
22. J. W. Brady and R. K. Schmidt, *J. Phys. Chem.*, **97** (1993) 958-966.
23. S. Perez, F. Taravel and G. Vergelati, *Nouv. J. Chem.*, **9** (1985) 561-564.
24. D. A. Rees and D. Thom, *J. Chem. Soc Perkins II*, (1977) 191-200.
25. R. L. Sidebotham, *Adv. in Carbohydr. Chem. Biochem.*, **30** (1974) 371-444.
26. C. T. Greenwood in *The Carbohydrates*, W. Pigman and D. Horton (Eds.), Academic Press, London, 1970, 471-509.
27. K. Nishinari, K. Kohyama, P. A. Williams, G. O. Phillips, W. Burchard and K. Ogino, *Macromolecules*, **24** (1991) 5590-5593.
28. D. A. Rees in *Polysaccharide Shapes*, Wiley, New York, 1977.
29. E. Percival and R. H. McDowell in *Biochemistry of Storage Carbohydrates in Green Plants*, P. M. Dey and R. A. Dixon (Eds.), Academic Press, London, 1985.
30. A. T. Bull and C. G. C. Chesters, *Adv. in Enzymology*, **28** (1966) 325-364.
31. T. E. Nelson, and B. A. Lewis, *Carbohydr. Res.*, **33** (1974) 63-74.
32. Y. Deslandes, R. H. Marchessault and A. Sarko, *Macromolecules*, **13** (1980) 1466-1471.
33. C. T. Chuah, A. Sarko, Y. Deslandes and R. H. Marchessault, *Macromolecules*, **16** (1983) 1375-1382.
34. T. L. Bluhm, Y. Deslandes, R. H. Marchessault, S. Perez and M. Rinaudo, *Carbohydr. Res.*, **100** (1982) 119-130.
35. T. L. Bluhm and A. Sarko, *Can. J. Chem.*, **55** (1977) 293-299.
36. H. Takeda, N. Yasuoka and N. Kasai, *Carbohydr. Res.*, **53** (1977) 137-152.
37. K. Noguchi, K. Okuyama, S. Kitamura and K. Takeo, *Carbohydr. Res.*, **237** (1992) 23-32.

38. H. Saito, M. Yokoi and Y. Yoshioka, *Macromolecules,* **22** (1989) 3892-3898.

39. H. Saito, R. Tabeta, T. Sasaki and Y. Yoshioka, *Bull. Chem. Soc. Jpn.,* **59** (1986) 2093-2101.

40. H. Saito, R. Tabeta, M. Yokoi and T. Erata, *Bull. Chem. Soc. Jpn.,* **60** (1987) 4259-4266.

41. B. P. Hills, C. Cano and P. S. Belton, *Macromolecules,* **24** (1991) 2944-2950.

42. C. A. Duda and E. S. Stevens, *Biopolymers,* **31** (1991) 1379-1385.

43. M. Dauchez, P. Derreumaux, M. Sekkal, P. Lagant, P. Legrand and G. Vergoten, *Spectrochim. Acta,* **50A** (1994) 87-105.

44. L. D. Barron and L. Hecht in *Advances in Spectroscopy, Vol 21, Biomolecular Spectroscopy Part B,* R. J. H. Clark and R. E. Hester (Eds.), Wiley, Chichester, 1993, 235.

45. Z. Q. Wen, L. Hecht and L. D. Barron, *J. Am. Chem. Soc.,* **116** (1994) 443.

46. Z. Q. Wen, L. Hecht and L. D. Barron, *Protein Science,* **3** (1994) 435.

47. K. Schmid, H. Kaufmann, S. Isemura, F. Bauer, J. Emura, T. Motoyama, M. Isihguro and S. Nanno, *Biochemistry,* **12** (1973) 2711.

48. V. Karpenko, L. Sinkorova and M. Kodicek, *Coll. Czech. Chem. Commun.,* **57** (1992) 641.

49. W. E. Marshall and J. Porath, *J. Biol. Chem.,* **240** (1965) 209.

50. J. J. Bentima, *Bioscience Reports,* **6** (1986) 709.

51. M. Urbanova, P. Pancoska and T. A. Keiderling, *Biochem. et Biophys. Acta,* **1203** (1990) 290.

Publications

A. Publications in Refereed Journals

1. **A. F. Bell, L. Hecht and L. D. Barron, *Journal of Raman Spectroscopy,* 24 (1993) 633-635.**
   "Low Wavenumber Vibrational Raman Optical Activity of Carbohydrates"

2. **A. F. Bell, L. D. Barron and L. Hecht, *Carbohydrate Research,* 257 (1994) 11-24.**
   "Vibrational Raman Optical Activity of Glucose"

3. **A. F. Bell, L. Hecht and L. D. Barron, *Journal of the American Chemical Society,* 116 (1994) 5155-5161.**
   "Disaccharide Solution Stereochemistry from Vibrational Raman Optical Activity"

4. **A. F. Bell, S. J. Ford, L. Hecht, G. Wilson and L. D. Barron, *International Journal of Biological Macromolecules,* in press.**
   "Vibrational Raman Optical Activity of Glycoproteins"

5. **A. F. Bell, L. Hecht and L. D. Barron, *Spectrochimica Acta.,* to be submitted.**
   "Vibrational Raman Optical Activity of Ketoses"

6. **L. D. Barron, L. Hecht and A. F. Bell in *Circular Dichroism: Conformational Analysis of Biomolecules,* G. D. Fasman (Ed.), Plenum, New York, to be published.**
   "Vibrational Raman Optical Activity of Biomolecules"

B. Conference Proceedings

1. L. D. Barron, L. Hecht, Z. Q. Wen, S. J. Ford, A. F. Bell and A. Cooper in: ***Proceddings of the Thirteenth International Conference on Raman Spectroscopy,*** W. Kiefer, M. Cardona, G. Schaack, F. W. Schneider and H. W. Schrotter (Eds.), Wiley, Chichester, 1992, 462-463.
   "Vibrational Raman Optical Activity of Biological Molecules"

2. L. D. Barron, L. Hecht, Z. Q. Wen, S. J. Ford and A. F. Bell in: ***Proceedings of the Fourth International Conference on Laser Applications in Life Sciences,*** J. E. I. Korppi-Tommola (Ed.) SPIE Proceedings Vol. 1922, 1992 2-11.
   "Vibrational Raman Optical Activity of Biological Molecules"

3. L. D. Barron, L. Hecht, S. J. Ford, A. F. Bell, Z. Q. Wen in: ***Lectures and Posters of the Fifth International Conference on Circular Dichroism,*** R. W. Woody, K. Nakanishi and N. Berova (Eds.), Colorado State University, Pingree Park, 1993, 158-163.
   "Vibrational Raman Optical Activity: From Small Organics to Biopolymers"

4. A. F. Bell, L. D. Barron, L. Hecht and Z. Q. Wen in: ***Lectures and Posters of the Fifth International Conference on Circular Dichroism,*** R. W. Woody, K. Nakanishi and N. Berova (Eds.), Colorado State University, Pingree Park, 1993, 218.
   "Vibrational Raman Optical Activity of Carbohydrates"

5. L. D. Barron, L. Hecht, S. J. Ford, A. F. Bell and G. Wilson in: ***Proceedings of the Fourteenth International Conference on Raman Spectroscopy,*** N. T. Yu (Ed.), Wiley, Chichester, 1994, 1056-1057.
   "Vibrational Raman Optical Activity of Biopolymers"

6. L. D. Barron, A. F. Bell, S. J. Ford, L. Hecht, G. Wilson and A. Cooper in: *Faraday Discussions Vol. 99,* The Royal Society of Chemistry, London, 1995, in press.
"Vibrational Raman Optical Activity of Biopolymers"

7. L. D. Barron, L. Hecht, S. J. Ford, A. F. Bell and G. Wilson in: *Proceedings of the Twenty-second European Congress on Molecular Spectroscopy,* B. Schrader (Ed.), Elsevier, Amsterdam, 1995, *J. Mol. Struct.,* in press.
"Vibrational Raman Optical Activity of Biopolymers"

8. A. F. Bell, L. Hecht and L. D. Barron in: *Proceedings of the Twenty-second European Congress on Molecular Spectroscopy,* B. Schrader (Ed.), Elsevier, Amsterdam, 1995, *J. Mol. Struct.,* in press.
"Vibrational Raman Optical Activity of Carbohydrates"